NACA TN 3857

NATIONAL ADVISORY COMMITTEE FOR AERONAUTICS

TECHNICAL NOTE 3857

EXPERIMENTAL INVESTIGATION AT LOW SPEED OF THE EFFECTS OF WING POSITION ON THE STATIC STABILITY OF MODELS HAVING FUSELAGES OF VARIOUS CROSS SECTION AND UNSWEPT AND 45° SWEPTBACK SURFACES

By William Letko

Langley Aeronautical Laboratory
Langley Field, Va.

Washington

November 1956

NATIONAL ADVISORY COMMITTEE FOR AERONAUTICS

TECHNICAL NOTE 3857

EXPERIMENTAL INVESTIGATION AT LOW SPEED OF THE EFFECTS OF WING POSITION ON THE STATIC STABILITY OF MODELS HAVING FUSELAGES OF VARIOUS CROSS SECTION AND UNSWEPT AND 45° SWEPTBACK SURFACES

By William Letko

SUMMARY

An experimental investigation was made to determine the effects of wing position on the low-speed static longitudinal and static lateral stability derivatives of airplane models having fuselages of square and rectangular cross sections and unswept and 45° sweptback surfaces. The horizontal tail of each model was located on the fuselage center line.

The results of the investigation indicated that at low angles of attack the complete unswept models with the wing in the high position were more stable or least longitudinally unstable; whereas, for the swept models there was little change in longitudinal stability with changes in wing position. For both the swept and unswept complete configurations the low-wing position was generally the least stable in the medium angle-of-attack range; whereas, at high angles of attack there was little significant difference in the stability of the models due to wing position. The results also showed that in the low and medium angle-of-attack range moving the wing from the low to the high position generally causes a decrease in the directional stability for both the swept and unswept configurations. The low-wing configuration was indicated to have the smallest detrimental effects caused by sidewash on the tail contribution to the static lateral stability derivatives for almost the entire test angle-of-attack range.

The results also showed that wing-fuselage interference causes an increase in effective dihedral angle when the wing is moved from the low to the high position as occurred for the circular-cross-section fuselage reported on in previous investigations.

INTRODUCTION

Pitch-up and loss in directional stability at high angles of attack have been encountered in some high-speed airplanes and have led to the consideration of changes in various airplane components in an attempt to alleviate or to eliminate these difficulties. Some of the changes under consideration are in wing position, fuselage cross-sectional shape, and horizontal-tail position. Several systematic investigations have been made to determine the effects of these changes on the stability characteristics of models with fuselages of circular cross section (refs. 1 and 2, for example) and the effects of fuselage cross-sectional shape on the static stability characteristics of midwing models having unswept and 45° sweptback surfaces (ref. 3).

The same models used in the investigation of reference 3 were used in the present investigation which was concerned with the effects of varying the wing position on the static stability characteristics of models having fuselages of square and rectangular cross sections and having interchangeable unswept and 45° sweptback wing and tail surfaces. For the present investigation the horizontal tail was located on the fuselage center line, as was the case in the investigation of reference 3.

SYMBOLS

The data are referred to the stability system of axes with the origin on the fuselage center line; the longitudinal location is at the projection of the wing aerodynamic center on the fuselage center line. Positive directions of forces, moments, and angular displacements are shown in figure 1. The coefficients and symbols are defined as follows:

C_L lift coefficient, F_L/qS_W

C_D' drag coefficient, F_D'/qS_W

C_Y lateral-force coefficient, F_Y/qS_W

C_l rolling-moment coefficient, $M_X/qS_W b_W$

C_m pitching-moment coefficient, $M_Y/qS_W \bar{c}_W$

C_n yawing-moment coefficient, $M_Z/qS_W b_W$

F_L lift

F'_D drag (approximate)

F_Y lateral force

M_X rolling moment

M_Y pitching moment

M_Z yawing moment

q dynamic pressure, $\frac{1}{2}\rho V^2$

V free-stream velocity

ρ mass density of air

A aspect ratio, b^2/S

b span, measured perpendicular to fuselage center line

S plan-form area

c chord, measured parallel to plane of symmetry

c_r root chord

c_t tip chord

$\bar{c}$ mean aerodynamic chord; for example, $\bar{c}_W = \frac{2}{S_W}\int_0^{b_W/2} c_W^2 dy$

y coordinate along Y-axis, measured from plane of symmetry

l_V or l_H tail length, distance parallel to fuselage center line from mounting point to $\bar{c}_V/4$ or $\bar{c}_H/4$

h' average fuselage height at wing root

w' average fuselage width at wing root

h perpendicular distance from fuselage center line to $\bar{c}_V/4$ (tail root chord coincides with fuselage center line)

Δh wing height, perpendicular distance from fuselage center line to wing chord plane (positive when wing is above fuselage center line)

R local radius of circular fuselage

r fuselage corner radius, $R/3$

w local half-width of square or rectangular fuselage

d local half-depth of square or rectangular fuselage; for square fuselage, $d = w$

x longitudinal distance along fuselage center line measured from fuselage nose

Γ effective dihedral angle, deg

λ taper ratio, c_t/c_r

Λ angle of sweep of quarter-chord line

β angle of sideslip

ψ azimuth angle

α angle of attack

$$C_{Y_\beta} = \frac{\partial C_Y}{\partial \beta}$$

$$C_{n_\beta} = \frac{\partial C_n}{\partial \beta}$$

$$C_{l_\beta} = \frac{\partial C_l}{\partial \beta}$$

$\Delta C_{Y_\beta}, \Delta C_{l_\beta}, \Delta C_{n_\beta}$ contribution of the tail group to derivatives; that is, for the wing on, $\Delta C_{Y_\beta} = \left(C_{Y_\beta}\right)_{WFVH} - \left(C_{Y_\beta}\right)_{WF}$,

for the wing off, $\Delta C_{Y_\beta} = \left(C_{Y_\beta}\right)_{FVH} - \left(C_{Y_\beta}\right)_{F}$, and

for a wing-tail configuration, $\Delta C_{Y_\beta} = \left(C_{Y_\beta}\right)_{WVH} - \left(C_{Y_\beta}\right)_{W}$

Subscripts and abbreviations:

W wing; used with subscripts 1, 2, and 3 to denote wing position relative to fuselage (see fig. 2)

F fuselage; used with subscripts 1 to 4 to denote various fuselages (see fig. 3)

H horizontal tail; used with subscripts 1 and 2 to denote unswept and swept configurations, respectively (see fig. 4)

V vertical tail; used with subscripts 1 and 2 to denote unswept and swept configurations, respectively (see fig. 4)

APPARATUS AND MODELS

The tests were conducted in the 6- by 6-foot test section of the Langley stability tunnel. The models used were designed to permit tests of the wing alone, the wing-tail combination, the fuselage alone, the wing-fuselage combination (with the wing at several different positions), or the fuselage with any tail configuration with or without the wings. The relative locations of the wing, fuselage, and tail surfaces are shown in figure 2.

Fuselages of square and rectangular cross sections having rounded corners were tested. A side view and cross section of each fuselage are given in figure 3 together with the designation by which the fuselages are identified. The coordinates of the square and rectangular fuselages were so determined that the variation of the cross-sectional area of each fuselage along the longitudinal axis was the same as that of the circular-cross-section fuselage (F_1) discussed in reference 3. The coordinates of the fuselage with circular cross section are given in table I.

The configurations tested had both swept and unswept wing and tail surfaces. The quarter-chord lines were swept back 0° and 45° for the unswept and swept surfaces, respectively. The wings had a taper ratio of 0.6 and an aspect ratio of 4. The tail surfaces also had a taper ratio of 0.6. The aspect ratio and other geometric characteristics of the various tail surfaces as well as those of the wings are given in table II. The geometric characteristics of the various tail surfaces are shown in figure 4 together with the designation chosen to identify each surface. The wings were tested at the midwing location and also at positions one-third of the maximum body depth above and below the fuselage center line. All lifting surfaces were set at 0° incidence with respect to the fuselage center line.

The models were mounted on a single strut support at a point on the fuselage center line, located for the swept and unswept configurations as shown in figure 2. A photograph of the swept configuration with fuselage 2 and with the wing in the middle location is given as figure 5.

For the wing-tail configurations the tail was mounted on a steel tube of small diameter which was fastened to the wing or wing mounting bracket. The locations of the wing and tail corresponded to the locations of the wing and tail when tested in combination with a fuselage. The isolated tail was mounted on the same tube which was then attached to the model support strut. For the wing-tail and isolated-tail tests, the tail area included the portion normally enclosed in the fuselage.

Forces and moments were measured by means of a conventional six-component balance system.

TESTS AND CORRECTIONS

Tests were made at a dynamic pressure of 24.9 pounds per square foot which corresponds to a Mach number of about 0.13 and a Reynolds number of about 0.71×10^6 based on the mean aerodynamic chord of the wings. The models were tested through an angle-of-attack range from -4 up to and beyond maximum lift (of wings alone) at angles of sideslip of 0° and $\pm 5^\circ$. Tests of the complete configurations were also made at angles of attack of 0°, 10°, 20°, and 26° through a range of sideslip angle from -20° to 20°.

Approximate corrections based on unswept-wing theory for the effects of jet boundaries (ref. 4) have been applied to the lift, drag, and pitching-moment coefficients. No corrections for the effects of support-strut interference have been applied to the data; however, some data are presented to show the support-strut interference for several complete-model configurations.

RESULTS AND DISCUSSION

Presentation of Results

The static longitudinal stability characteristics of the models are given in figures 6 to 13 and the static lateral stability characteristics are presented in figures 14 to 26. A summary of the configurations investigated and of the figures that present the basic data for these configurations is given in table III.

Static Longitudinal Stability Characteristics

Complete models.- The effects of wing position on the static longitudinal stability characteristics of the complete models are given in figure 6. In the low angle-of-attack range for the unswept configurations, the models with the wing in the high position were the most stable or least longitudinally unstable. For all wing positions the configurations with the shallow fuselage were unstable in the low angle-of-attack range due to the large instability of fuselage 4. Wing position had little effect on the longitudinal stability of the swept-wing models in the low angle-of-attack range. Although differences in the tare values, shown in figure 8, caused some change in trim for the swept-wing models, the stability in this range was unchanged by neglecting the tare data. For both the swept and unswept models the low-wing model was generally the least stable in the medium angle-of-attack range. At the high angles of attack there was little significant difference in the stability of the models due to wing position. For angles of attack just below the stall, the unswept configuration with the low wing and the swept configuration with the high wing appear to have slightly better longitudinal characteristics than the other configurations.

Both the unswept and swept models showed a pitch-up tendency; however, for the unswept model the angle for pitch-up was above the stall angle of attack and the effect for an actual airplane would not be as important as that for the swept models which showed this tendency at an angle of attack below stall. Wing position had little effect on pitch-up tendency of the models. As a matter of interest and in order to give an indication of the changes in trim that may occur with angle of sideslip, changes in pitching-moment coefficient with angle of sideslip for the complete models at several different angles of attack are presented in figure 7.

The data of figure 6 show that for both the swept and unswept configurations changes in wing position cause little change in drag coefficient at low angles of attack. At the high angles of attack changes in wing position generally cause a larger change in drag coefficient for the swept models than for the unswept models with the low-wing models providing the lowest drag and the high-wing models the highest drag coefficient. The reason for the low values of drag coefficient up to an angle of attack of 8° for the unswept complete configuration with fuselage 3 is not clear since the data for the wing-fuselage configuration do not show this effect (see fig. 9(b)). For the unswept models the low-wing configurations generally have a slightly higher lift coefficient at low angles of attack than the midwing or high-wing configurations; whereas, for the swept models the low-wing configurations generally have a slightly lower lift coefficient than the models with other wing positions. At high angles of attack the effect of wing position is generally greater for the swept models than for the unswept models with the high wing position providing the highest lift and the low wing position the lowest.

In order to give an indication of the strut tare corrections to C_m, C_L, and C_D for the complete models, figure 8 has been prepared. Although the corrections have not been applied to the data, it appears from the figure that the general conclusions are not altered. In the application of the corrections the values of C_L and C_m shown in figure 8 should be added to the data, whereas the increments of C_D' should be subtracted from the data.

In general, the effects of wing position on the longitudinal characteristics of the models with the square and rectangular fuselages are similar to those obtained with the circular fuselage reported in reference 1.

Wing-fuselage configurations.- For the wing-fuselage configurations, changes in wing position had only a small effect on the longitudinal stability throughout the angle-of-attack range tested. (See fig. 9.) The midwing configuration generally was less unstable than the high- or low-wing configurations. There were only small changes in drag coefficient at low angles of attack due to wing position. As was the case for the complete models, changes in wing position caused a larger increase in drag coefficient for the swept models than for the unswept models at high angles of attack with the low-wing models having the lowest drag and the high-wing models having the highest drag. The effects of wing position on the lift coefficient for the wing-fuselage configurations were similar to those noted for the complete models.

Fuselage and fuselage-tail configurations.- The data for the fuselage and fuselage-tail configurations have been presented in reference 3 but are also presented here for completeness. In figures 10 and 11 are presented the static longitudinal characteristics of the fuselage and fuselage-tail configurations, respectively. The pitch-up tendency shown for the fuselage—unswept-tail configuration at moderate angles of attack is, of course, due to stalling of the horizontal tail. There are two sets of pitching-moment data for the fuselage alone since the center of moments was slightly different depending on whether the fuselage was used in conjunction with swept or unswept wing-tail surfaces. This difference in center-of-moment location caused only a small difference in the longitudinal stability of the fuselages.

Wing, wing-tail, and isolated-tail configurations.- The longitudinal characteristics of the wing, wing-tail, and isolated-tail configurations are given in figures 12 and 13. Inasmuch as the characteristics of these swept and unswept wings have been reported in several other investigations, such as references 1, 5, and 6, they are not discussed herein.

As was mentioned in the section entitled "Apparatus and Models," the wing-tail and tail-alone configurations were tested with the tail

mounted at the appropriate tail length on a steel tube of small diameter which was fastened to the wing or wing mounting bracket. The locations of the wing and tail corresponded to the locations of the wing and tail when tested in combination with a fuselage. Since the effects of changes in wing position were the largest for the model with fuselage of deep rectangular cross section (F_3), only the results for the wing locations that correspond to those of fuselage 3 are presented in figures 12 and 13. Also in figure 13 are presented the longitudinal characteristics of the isolated tail. Figure 12 shows that there is little effect of wing location - that is, wing location with respect to the balance center - on the static longitudinal characteristics of the wings. A study of figure 13 shows that adding the wing to the isolated tail causes a decrease in longitudinal stability at low angles of attack which is much larger for the unswept wing than that obtained with the swept configuration. The decrease in longitudinal stability obtained is caused, of course, by downwash. Varying the wing position has only a small effect on the longitudinal stability of the swept wing-tail configurations in the low angle-of-attack range; however, for the unswept wing-tail configurations, raising or lowering the wing causes an increase in longitudinal stability at low angles of attack with little significant differences in stability at high angles of attack. For both the unswept and swept configurations the variation of pitching-moment coefficient with angle of attack is generally very similar to the variation obtained for the respective complete configurations.

Static Lateral Stability Characteristics

Complete models.- The effects of wing position on the static lateral stability characteristics for the complete models are given in figure 14. From the figure it can be seen that moving the wing from the low to the high position causes an increase in the negative value of C_{l_β} in the low angle-of-attack range, as was expected. The increase is greatest for the deep rectangular fuselage (F_3) for both the swept and unswept configurations. There is no consistent effect of wing position on C_{l_β} for either the unswept or swept configurations at high angles of attack. The value of C_{l_β}, however, becomes positive (negative dihedral effect) for all the swept configurations for a range of angle of attack below the angle of stall. This effect would not be expected to exist at higher Reynolds numbers. (See ref. 7, for example.)

In the low and medium angle-of-attack ranges for both the swept and unswept models moving the wing from the low to high position generally causes a decrease in the value of C_{n_β}. For the swept models the variation of C_{n_β} with angle of attack is such that C_{n_β} becomes negative

at the higher angles of attack. For the swept models the unstable values of C_{n_β} and the positive values of C_{l_β} in the range above about $\alpha = 10^\circ$ are factors which, together with the pitch-up tendencies noted before, can result in an airplane configuration that could have highly divergent characteristics at these high angles of attack. It should be pointed out, however, that the results of the present investigation have been obtained at a relatively low Reynolds number and that some changes in the derivatives obtained in the present investigation would probably not result at higher Reynolds numbers. For the unswept configurations with the square and shallow rectangular fuselages, C_{n_β} remains positive throughout the angle-of-attack range tested; whereas, for the deep-rectangular-fuselage configurations the values of C_{n_β} become negative at high angles of attack for the midwing and low wing position. However, for the high wing position small positive values of C_{n_β} are maintained throughout the angle-of-attack range tested. Moving the wing to either the high or low position generally causes C_{Y_β} to increase negatively. Part of the increase is due to the end-plate effect of the wing on the fuselage. This effect was also obtained with the circular fuselage in reference 1.

In general, the effects of wing position on the static lateral stability derivatives for models with square and rectangular fuselages are similar to those obtained with models having fuselages of circular cross section. In order to give an indication of the strut tare corrections to C_{l_β}, C_{n_β}, and C_{Y_β} for the complete configurations, figure 15 is presented. As was mentioned for the case of static longitudinal stability, the tare corrections were not applied to the data, but it appears from the figure that the general conclusions are not altered. In the application of the corrections the values of C_{l_β} shown in figure 15 should be added to the data, whereas the values of C_{n_β} and C_{Y_β} should be subtracted from the data.

The values of C_{l_β}, C_{n_β}, and C_{Y_β} discussed up to this point were obtained from the values of the coefficients at $\beta = \pm 5^\circ$. In order to show the range of sideslip angle for which these values would apply, figures 16 to 18 are presented to show the variation of C_l, C_n, and C_Y for angles of attack of 0°, 10°, 20°, and 26° for a range of sideslip angle β from -20° to 20°. Generally, the variation of C_l, C_n, and C_Y with angle of sideslip is nonlinear; however, the curves obtained for C_Y are more nearly linear than those for C_l and C_n. The range of sideslip angle for which C_{n_β} remains constant is decreased from $\pm 10^\circ$ at 0° angle of attack to roughly $\pm 5^\circ$ at 26° angle of attack. With few

exceptions which generally occur at 0° angle of attack, there is little effect of wing position on the range of linearity of the data.

The effects of wing position on the tail contribution to C_{l_β}, C_{n_β}, and C_{Y_β} can be seen from figure 19. This figure presents the increments ΔC_{l_β}, ΔC_{n_β}, and ΔC_{Y_β} due to the tail obtained by subtracting the values of C_{l_β}, C_{n_β}, and C_{Y_β} for the wing-fuselage configurations from the values of the derivatives for the complete configurations. For comparison purposes, the values of C_{l_β}, C_{n_β}, and C_{Y_β} for the isolated-tail group are also presented. The figure shows that at low angles of attack the interference (sidewash) of the wing-body combination on the tail contributions is small, whereas at the higher angles the interference is considerably greater. This condition is especially true for C_{n_β} and C_{Y_β}. The low-wing configuration generally has the smallest interference effects on ΔC_{l_β}, ΔC_{n_β}, and ΔC_{Y_β} for almost the entire test angle-of-attack range.

Wing-fuselage configurations.- The effects of wing position on C_{l_β}, C_{n_β}, and C_{Y_β} for the wing-fuselage configurations are given in figure 20. From the figure it can be seen that at low angles of attack changing the wing from the low to the high position changes the value of C_{l_β} from a positive to a negative value. This effect is true of course for both the swept and unswept configurations and is a result, as was pointed out in reference 1, of the crossflow about the yawed body which induces a positive angle of attack for the leading wing and a negative angle of attack for the trailing wing for the high wing arrangement and which induces the opposite effect for the low wing arrangement. The changes in effective dihedral angle with wing height at $\alpha = 0°$ for the configurations of the present investigation and also for the circular-fuselage configuration discussed in reference 3 are presented in figure 21. The values of C_{l_β} obtained in the present tests were converted into an effective dihedral angle by using the values of C_{l_β} caused by a unit change in dihedral angle as given in reference 8. The value of C_{l_β} per degree of geometric dihedral obtained from reference 8 was 0.00020 for the unswept configurations and 0.00018 for the swept configurations. Figure 21 shows that the effective dihedral angle varies from -3.5° to 4.0° for the circular-fuselage configuration and from -3.3° to 6.8° for the deep-rectangular-fuselage configuration when the unswept wing is raised from the low to the high position. For the swept configurations the effective dihedral varies from -4.1° to 4.5° for the circular-fuselage configuration and from -6.0° to 6.5° for the deep-rectangular-fuselage configuration when the wing is moved from the low to the high position.

The expression

$$\text{Increment in } C_{l_\beta} = \frac{1.2\sqrt{A}\left(\frac{\Delta h}{b}\right)\left(\frac{h' + w'}{b}\right)}{57.3}$$

obtained from reference 9 was used to estimate the increment in C_{l_β} at $\alpha = 0^\circ$ resulting from wing-body interference. The total measured increment resulting from moving the wing from the low to the high position was used in the comparison between measured and estimated values shown in figure 22, since for some cases equal increments were not obtained in the tests by moving the wing equal distances above and below the fuselage center line. Accordingly, the value obtained from the empirical relation was doubled. The comparison shows that the estimated values at $\alpha = 0^\circ$ are slightly lower than the measured values for the square- and rectangular-fuselage configurations. Figure 22 also shows that the increments in C_{l_β} measured for the swept configurations are slightly higher than those for the unswept configurations.

At low angles of attack near zero there is little or no effect of wing position on C_{n_β} for the wing-fuselage configurations. (See fig. 20.) At the higher angles of attack the effect of wing position is larger but the effect is not consistent.

As was the case with the complete configuration, adding the wing to the fuselage increases C_{Y_β} at low angles of attack because of the end-plate effect of the wing on the fuselage. The effect of wing position on C_{Y_β} is generally much larger at the high angles of attack for the square-fuselage and for the shallow-rectangular-fuselage configurations when tested with the unswept wing than for any of the other configurations tested (fig. 20). The configurations with the deep rectangular fuselage develop relatively large negative values of C_{Y_β} at high angles of attack.

Fuselage and fuselage-tail configurations.- The data for the fuselage and fuselage-tail configurations have been presented in reference 3 but are also presented here for completeness. The variations of C_{l_β}, C_{n_β}, and C_{Y_β} with α for the fuselage and fuselage-tail configurations tested are shown in figures 23 and 24, respectively. Data are presented for two center-of-moment locations; one corresponds to the center-of-moment position for the unswept configurations and the other to the center-of-moment position used for the swept configurations. The fuselage with the more rearward center of moments (used with the swept configurations) is slightly more directionally unstable than that with the forward center-of-moment location.

Wing, wing-tail, and isolated-tail configurations.- The lateral characteristics of the wings are given in figure 25. The location of the wings with respect to the mounting strut corresponded, of course, to the location of the wings when tested in combination with the other model components. Since the effects of changes in wing position were the largest for the model with F_3, only the results for the wing positions that correspond to those of fuselage 3 are presented in this figure. The results show little effect of wing location - that is, wing location with respect to the balance center - on the lateral characteristics of the wings. Inasmuch as the wing-alone characteristics have been reported in other investigations, such as those of references 1, 5, and 6, they are not discussed herein.

The results of the wing-tail and isolated-tail configurations are given in figure 26. From the figure it can be seen that the midwing reduces the dihedral effect of the vertical tail for the unswept midwing configuration at low angles of attack. The high and low wing positions, however, cause only a little change in dihedral effect of the tail. For the swept configurations near zero angle of attack there is little effect of wing on the tail dihedral effect caused by the midwing and low-wing configurations; however, the high wing causes an increased dihedral effect.

For the unswept wing-tail configuration raising the wing generally decreased the value of C_{n_β}, whereas there was little difference between the values for the midwing and low-wing configurations at low angles of attack. For the swept wing-tail configuration lowering the wing increased slightly the value of C_{n_β} obtained for the wing-tail configurations. An opposite effect to that obtained for C_{n_β} took place in regard to increases and decreases in the negative value of C_{Y_β}. A better indication of the interference effects of the wing on the tail contribution for the wing-tail configurations can be obtained from figure 27 which presents the tail contributions for the isolated tail and for the tail in the presence of the wing. The increments of ΔC_{n_β}, for example, contributed by the tail when tested in combination with the wing were obtained by subtracting the values of C_{n_β} obtained for the wing alone from the values of C_{n_β} obtained from tests of the wing-tail configurations. The difference between the values obtained with the isolated-tail and the wing-tail configurations can be attributed to interference effects. The interference effects of the wing on the tail generally are much larger at high angles of attack than they are at low angles of attack. For the unswept wing-tail configuration, the interference on the tail contribution to C_{l_β} is relatively large at low angles of attack for the midwing position and is considerably larger than the interference for either the high- or low-wing configuration. The high wing position causes the greatest interference

on the tail contribution to C_{n_β} at low angles of attack, whereas at angles of attack above the angle of wing-alone maximum lift the low-wing configuration has a considerably larger interference effect than either the high wing or midwing position for which the interference effects are nearly equal. The interference effects on C_{Y_β} are about the same as those for C_{n_β}. For the swept wing-tail configurations the interference of the wing on the tail contribution to C_{l_β}, C_{n_β}, and C_{Y_β} is the least at low angles of attack for the midwing configuration. At angles of attack above the angle of attack of wing-alone maximum lift the interference is generally much larger than that obtained at the low angles, but near an angle of attack of 32° the interference decreases with the high-wing configuration producing the lowest interference effects.

For easy comparison there are shown in figure 28 the increments in C_{n_β} and C_{Y_β} contributed by the tail when the tail was tested in combination with the wing and fuselage, with the wing (fuselage off), and with the fuselage (wing off). Also presented in the figure are the values of C_{n_β} obtained with the isolated tail. The approximate angle of maximum lift coefficient for each wing is also indicated in the figure. A study of figure 28 indicates that the separate effects of the wing and fuselage on the tail contributions to C_{n_β} and C_{Y_β} are not additive but are modified when the wing and fuselage are combined. The effects depend on wing sweep, wing position, and fuselage cross section.

CONCLUSIONS

The results of an experimental investigation to determine the effects of wing position on the low-speed static longitudinal and static lateral stability derivatives of airplane models having fuselages of square and rectangular cross sections and unswept and 45° sweptback surfaces indicate the following conclusions:

1. At low angles of attack the complete unswept models with the wing in the high position were most stable or least longitudinally unstable, whereas for the swept models there was little change in longitudinal stability with changes in wing position. For both the swept and unswept complete configurations the low wing position was generally the least stable in the medium angle-of-attack range, whereas at high angles of attack there was little significant difference in the stability of the models due to wing position.

2. In general, the effects of wing position on the longitudinal characteristics of the models with the square and rectangular fuselages are similar to those obtained with models having circular-cross-section fuselages.

3. In the low and medium angle-of-attack ranges, moving the wing from the low to the high position generally causes a decrease in the directional stability for both the swept and unswept configurations.

4. The low-wing configuration generally has the smallest detrimental effects, caused by sidewash, on the tail contribution to the static lateral stability derivatives for almost the entire test angle-of-attack range.

5. Wing-fuselage interference causes an increase in effective dihedral angle when the wing is moved from the low to the high position. This effect is similar to that obtained for a circular-cross-section fuselage in a previous investigation; however, for the deep-rectangular-fuselage configuration the change in dihedral is somewhat larger than that obtained with the circular fuselage.

Langley Aeronautical Laboratory,
National Advisory Committee for Aeronautics,
Langley Field, Va., August 10, 1956.

REFERENCES

1. Goodman, Alex: Effects of Wing Position and Horizontal-Tail Position on the Static Stability Characteristics of Models With Unswept and 45° Sweptback Surfaces With Some Reference to Mutual Interference. NACA TN 2504, 1951.

2. Goodman, Alex, and Thomas, David F., Jr.: Effects of Wing Position and Fuselage Size on the Low-Speed Static and Rolling Stability Characteristics of a Delta-Wing Model. NACA Rep. 1224, 1955. (Supersedes NACA TN 3063.)

3. Letko, William, and Williams, James L.: Experimental Investigation at Low Speed of Effects of Fuselage Cross Section on Static Longitudinal and Lateral Stability Characteristics of Models Having 0° and 45° Sweptback Surfaces. NACA TN 3551, 1955.

4. Silverstein, Abe, and White, James A.: Wind-Tunnel Interference With Particular Reference to Off-Center Positions of the Wing and to the Downwash at the Tail. NACA Rep. 547, 1936.

5. Letko, William, and Riley, Donald R.: Effect of an Unswept Wing on the Contribution of Unswept-Tail Configurations to the Low-Speed Static- and Rolling-Stability Derivatives of a Midwing Airplane Model. NACA TN 2175, 1950.

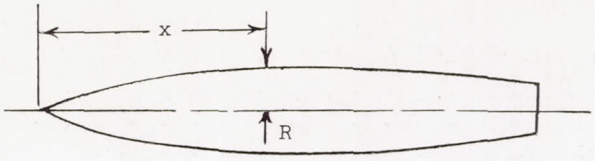
6. Brewer, Jack D., and Lichtenstein, Jacob H.: Effect of Horizontal Tail on Low-Speed Static Lateral Stability Characteristics of a Model Having 45° Sweptback Wing and Tail Surfaces. NACA TN 2010, 1950.

7. Neely, Robert H., and Conner, D. William: Aerodynamic Characteristics of a 42° Swept-Back Wing With Aspect Ratio 4 and NACA 64_1-112 Airfoil Sections at Reynolds Numbers From 1,700,000 to 9,500,000. NACA RM L7D14, 1947.

8. Bird, John D.: Some Theoretical Low-Speed Span Loading Characteristics of Swept Wings in Roll and Sideslip. NACA Rep. 969, 1950. (Supersedes NACA TN 1839.)

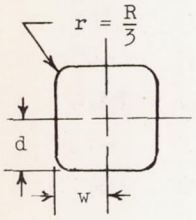
9. Campbell, John P., and McKinney, Marion O.: Summary of Methods for Calculating Dynamic Lateral Stability and Response and for Estimating Lateral Stability Derivatives. NACA Rep. 1098, 1952. (Supersedes NACA TN 2409.)

TABLE I.- COORDINATES OF THE CIRCULAR-CROSS-SECTION FUSELAGE AND EQUATIONS FOR COORDINATES OF THE SQUARE- AND RECTANGULAR-CROSS-SECTION FUSELAGES



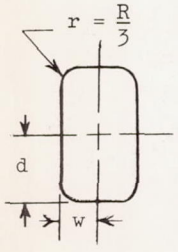
Circular-fuselage coordinates

x, in.	R, in.
0	0
2	.64
4	1.20
6	1.68
8	2.09
10	2.42
12	2.67
14	2.85
16	2.96
18	3.00
20	2.99
22	2.97
24	2.93
26	2.87
28	2.79
30	2.70
32	2.60
34	2.47
36	2.33
38	2.18
40	2.01
42	1.82
44	1.61
45	1.50



Equation for coordinates of square fuselage:

$$4w^2 - \left[4\left(\frac{R}{3}\right)^2 - \pi\left(\frac{R}{3}\right)^2\right] = \pi R^2$$



Equations for coordinates of rectangular fuselage:

$$4wd - \left[4\left(\frac{R}{3}\right)^2 - \pi\left(\frac{R}{3}\right)^2\right] = \pi R^2$$

$$w = \frac{2}{3}R$$

TABLE II.- PERTINENT GEOMETRIC CHARACTERISTICS OF MODEL

Wing:		
Aspect ratio, A_W	4.0	4.0
Taper ratio, λ_W	0.6	0.6
Quarter-chord sweep angle, Λ, deg	0	45
Dihedral angle, Γ, deg	0	0
Twist, deg	0	0
NACA airfoil section	65A008	65A008
Area, S_W, sq in.	324	324
Span, b_W, in.	36	36
Mean aerodynamic chord, $\bar{c}_W$, in.	9.19	9.19
Vertical tails:	V_1	V_2
Aspect ratio, A_V	2.00	1.40
Taper ratio, λ_V	0.6	0.6
Quarter-chord sweep angle, Λ, deg	0	45
NACA airfoil section	65A008	65A008
Area, S_V, sq in.	48.6	48.6
Span, b_V, in.	9.90	8.25
Mean aerodynamic chord, $\bar{c}_V$, in.	5.02	6.02
Tail length, l_V, in.	16.70	16.70
Distance from root chord to $\bar{c}_V/4$, h, in.	4.54	3.78
Horizontal tails:	H_1	H_2
Aspect ratio, A_H	4.00	2.77
Taper ratio, λ_H	0.6	0.6
Quarter-chord sweep angle, Λ, deg	0	45
NACA airfoil section	65A008	65A008
Area, S_H, sq in.	64.8	64.8
Span, b_H, in.	16.10	13.40
Mean aerodynamic chord, $\bar{c}_H$, in.	4.11	4.94
Tail length, l_H, in.	16.70	16.70

Fuselages:	F_1	F_2	F_3	F_4
Length, in.	45	45	45	45
Volume, cu in.	823	823	823	823
Side area, sq in.	206	186	250	136
Wing height-span ratio, $\Delta h/b$	± 0.0555	± 0.050	± 0.0627	± 0.037

TABLE III.- CONFIGURATIONS INVESTIGATED

Configuration	Basic data	Figure
Complete models	C_L C_D' C_m / C_{Y_β} C_{l_β} C_{n_β} plotted against α	6, 14
	C_m / C_Y C_l C_n plotted against β	7, 16 to 18
	Tare corrections to C_L C_D' C_m / Tare corrections to C_{Y_β} C_{l_β} C_{n_β} plotted against α	8, 15
Wing-fuselage	C_L C_D' C_m / C_{Y_β} C_{l_β} C_{n_β} plotted against α	9, 20
Fuselage	C_L C_D' C_m / C_{Y_β} C_{l_β} C_{n_β} plotted against α	10, 23
Fuselage-tail	C_L C_D' C_m / C_{Y_β} C_{l_β} C_{n_β} plotted against α	11, 24
Wing	C_L C_D' C_m / C_{Y_β} C_{l_β} C_{n_β} plotted against α	12, 25
Wing-tail and isolated-tail	C_L C_D' C_m / C_{Y_β} C_{l_β} C_{n_β} plotted against α	13, 26

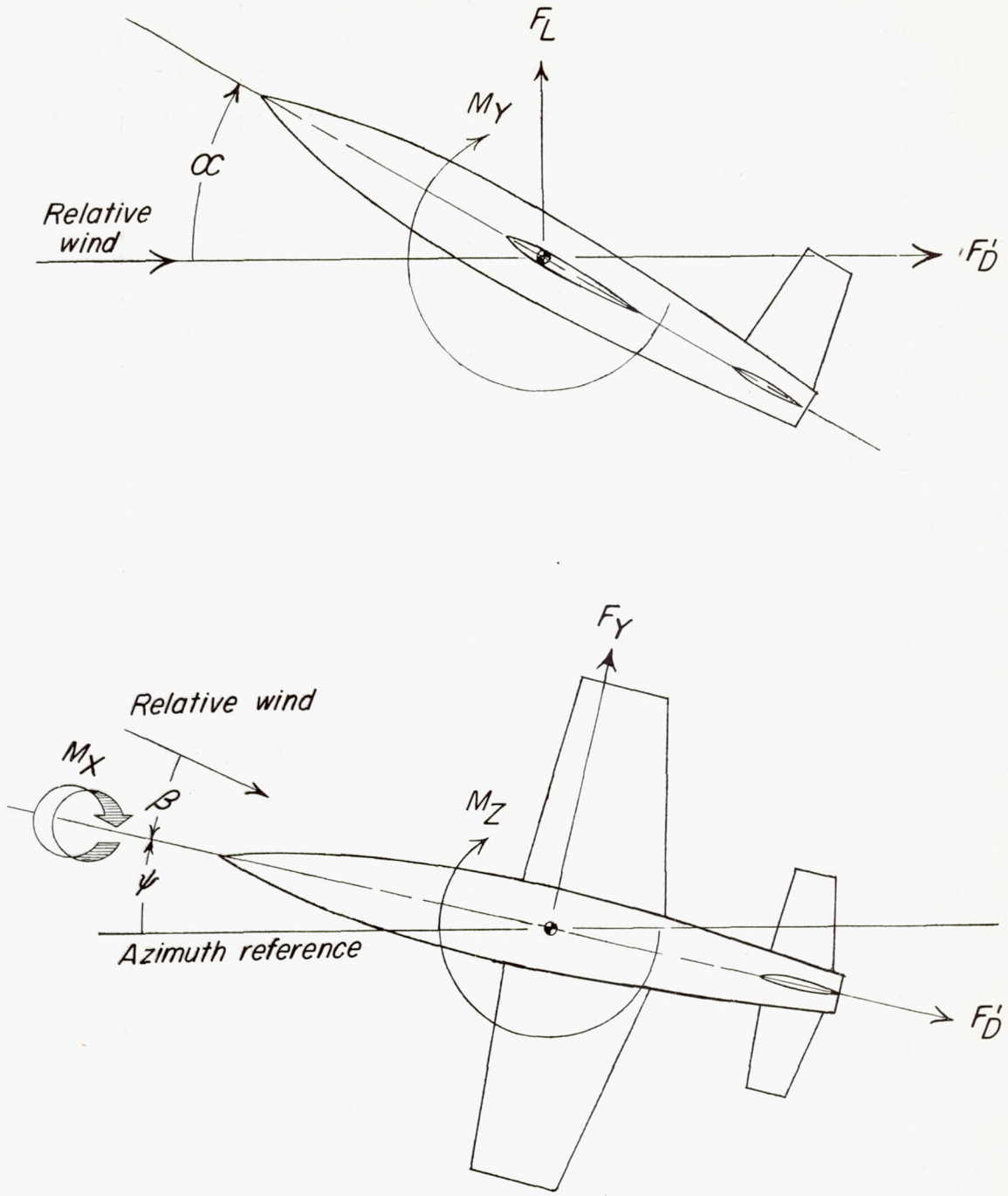
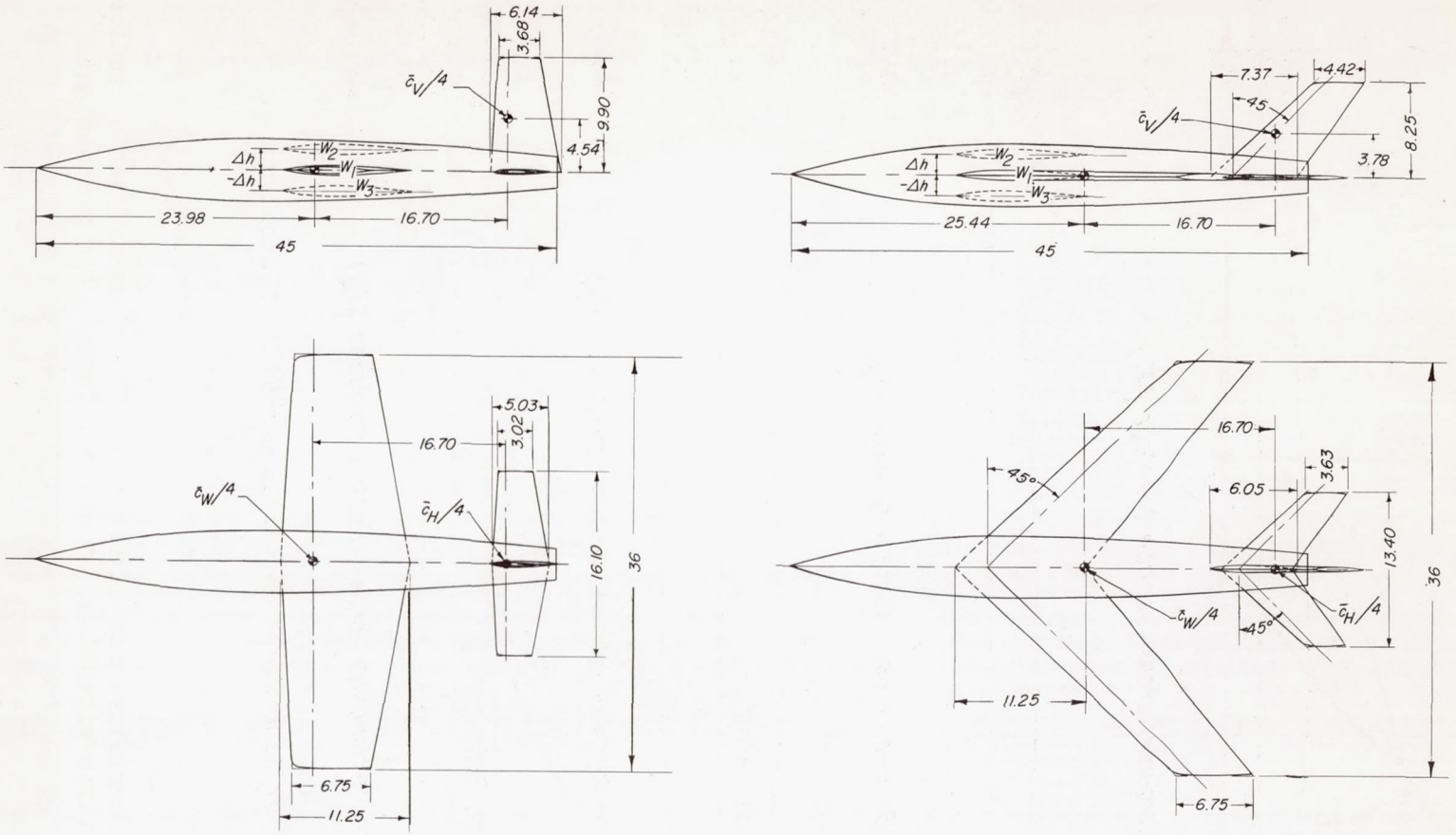


Figure 1.- Nomenclature for stability system of axes. Arrows indicate positive directions of angles, forces, and moments.



(a) Unswept surfaces.

(b) 45° swept surfaces.

Figure 2.- Dimensions of a complete model. (All dimensions are in inches unless otherwise stated.)

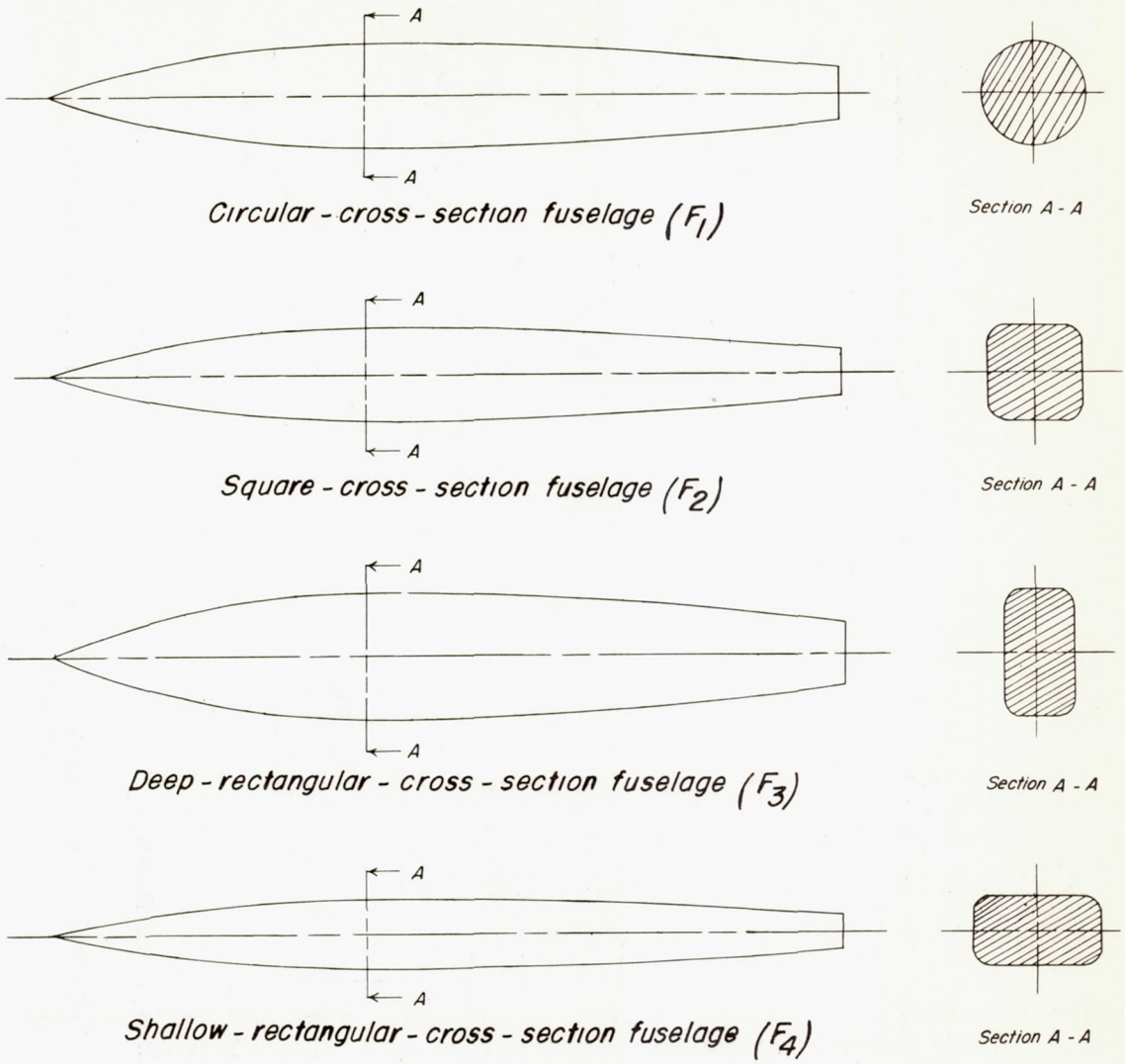


Figure 3.- Side views and cross sections of fuselages.

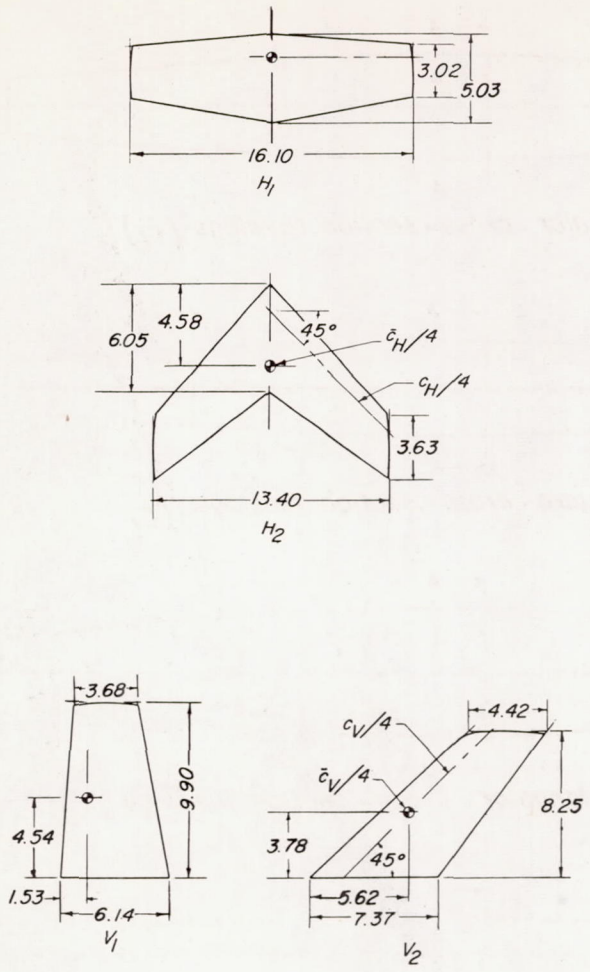


Figure 4.- Geometric characteristics of the horizontal and vertical tails. (All dimensions are in inches unless otherwise stated.)

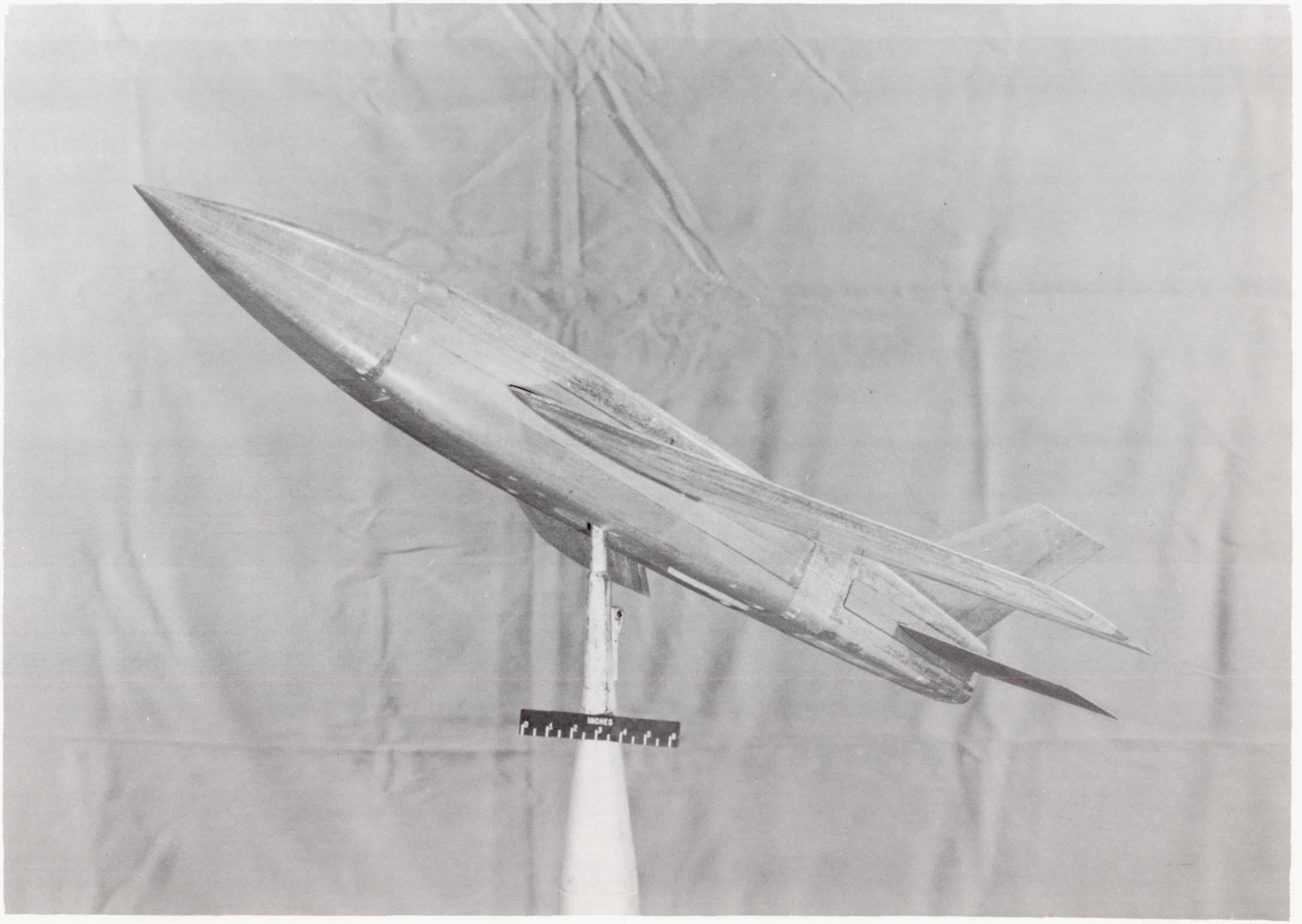
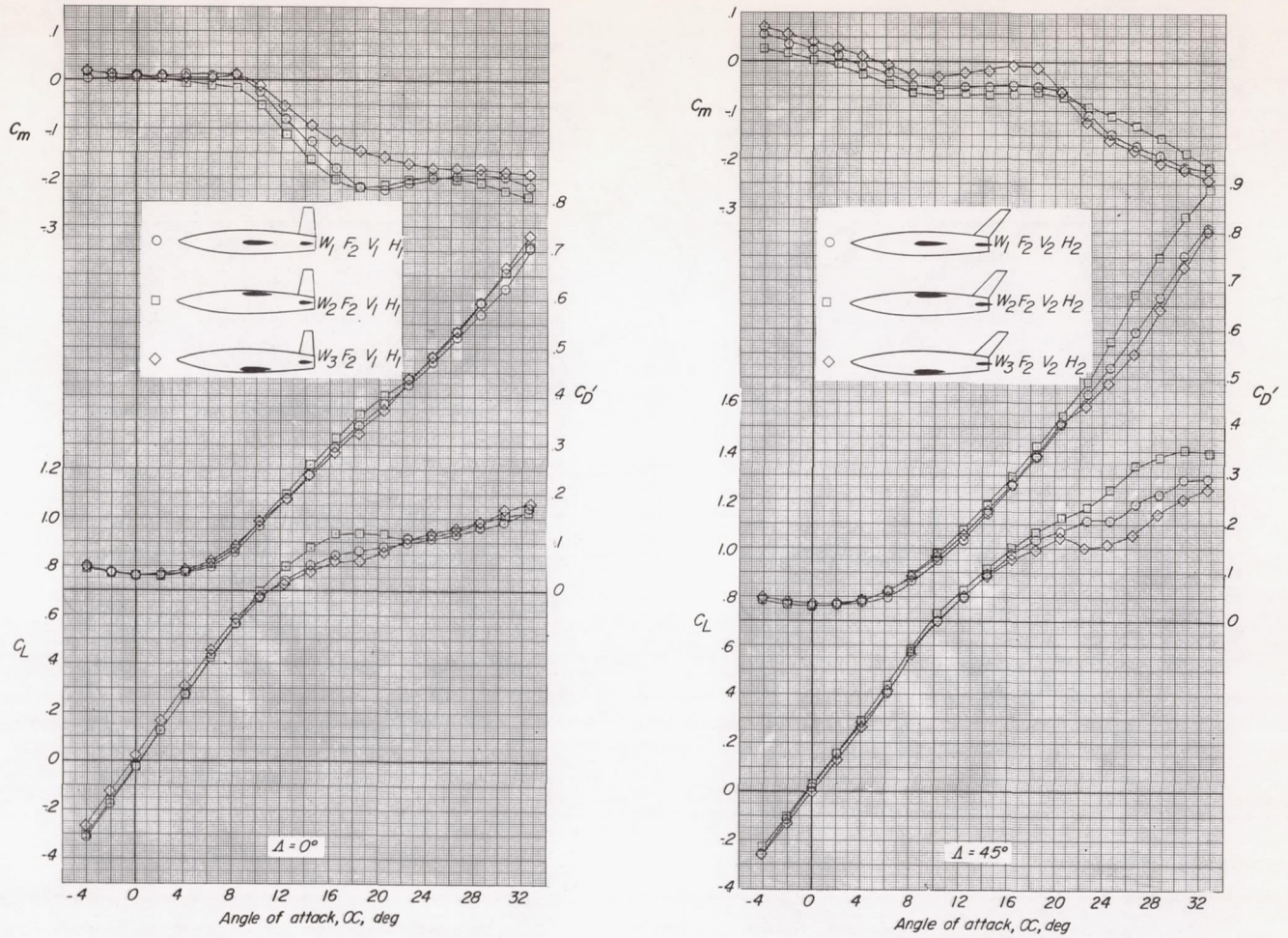
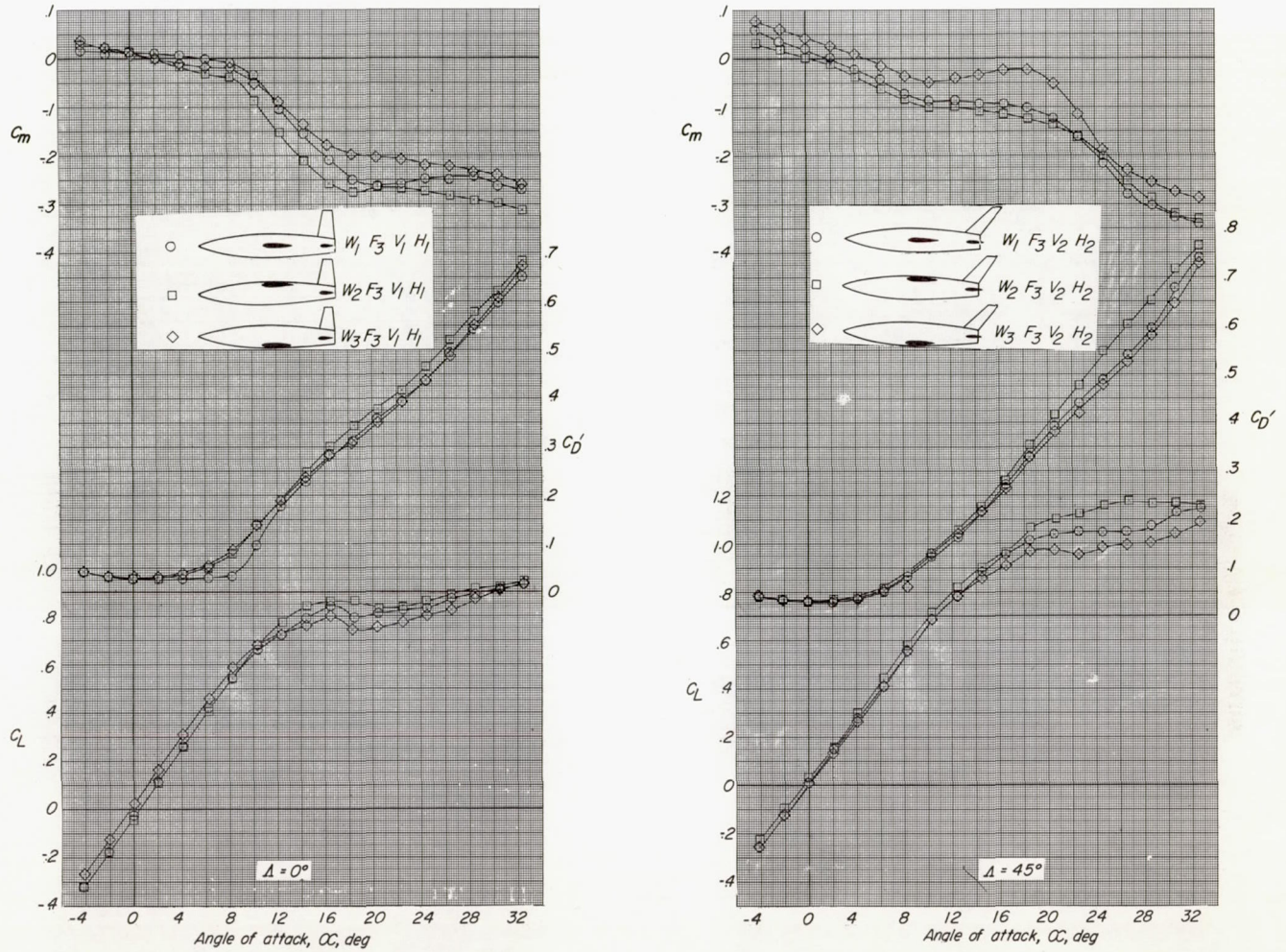


Figure 5.- View of 45° sweptback configuration. L-88741



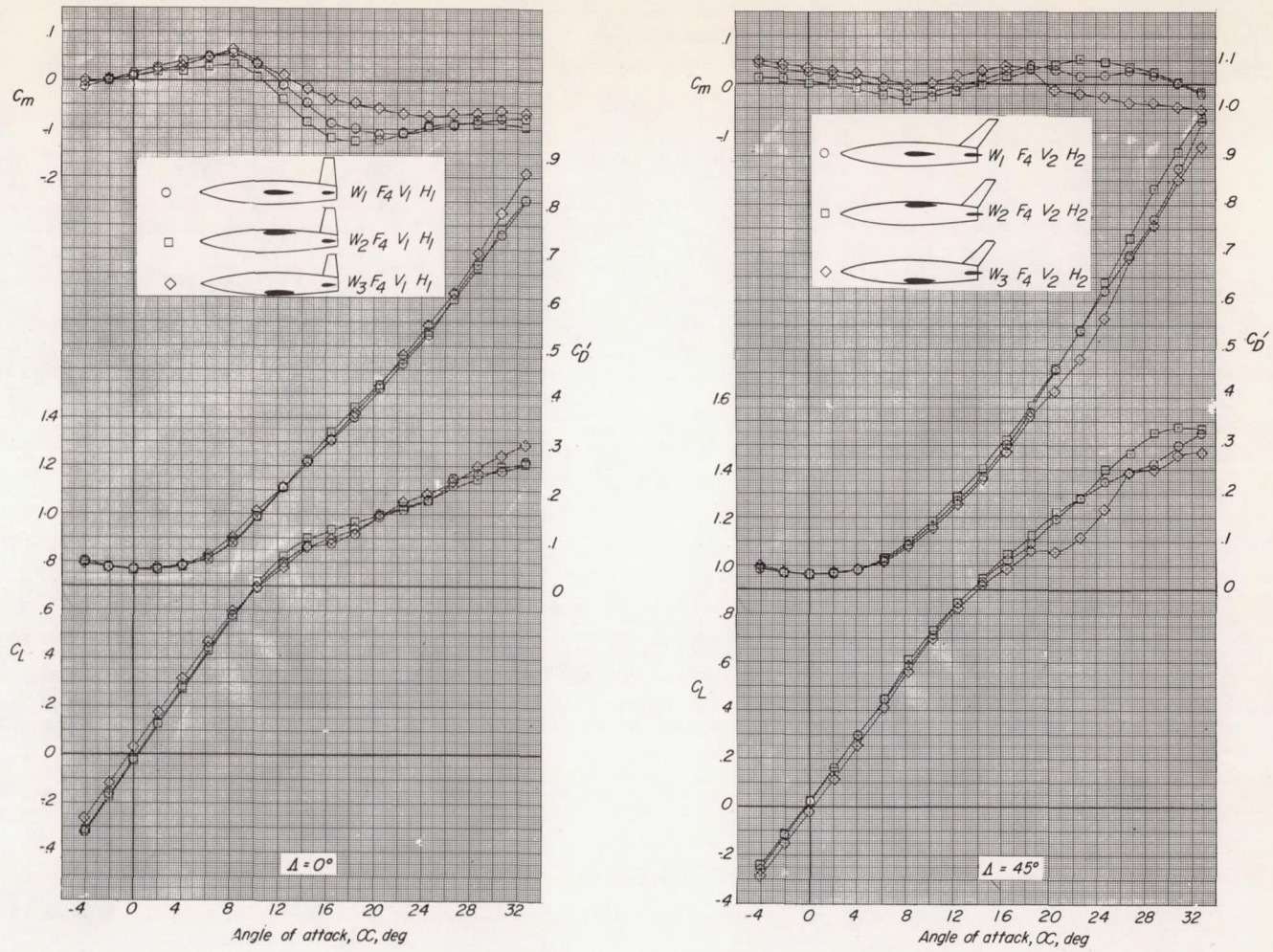
(a) Square fuselage, F_2.

Figure 6.- Effect of wing position on the static longitudinal stability characteristics of several unswept and 45° sweptback wing-fuselage-tail configurations.



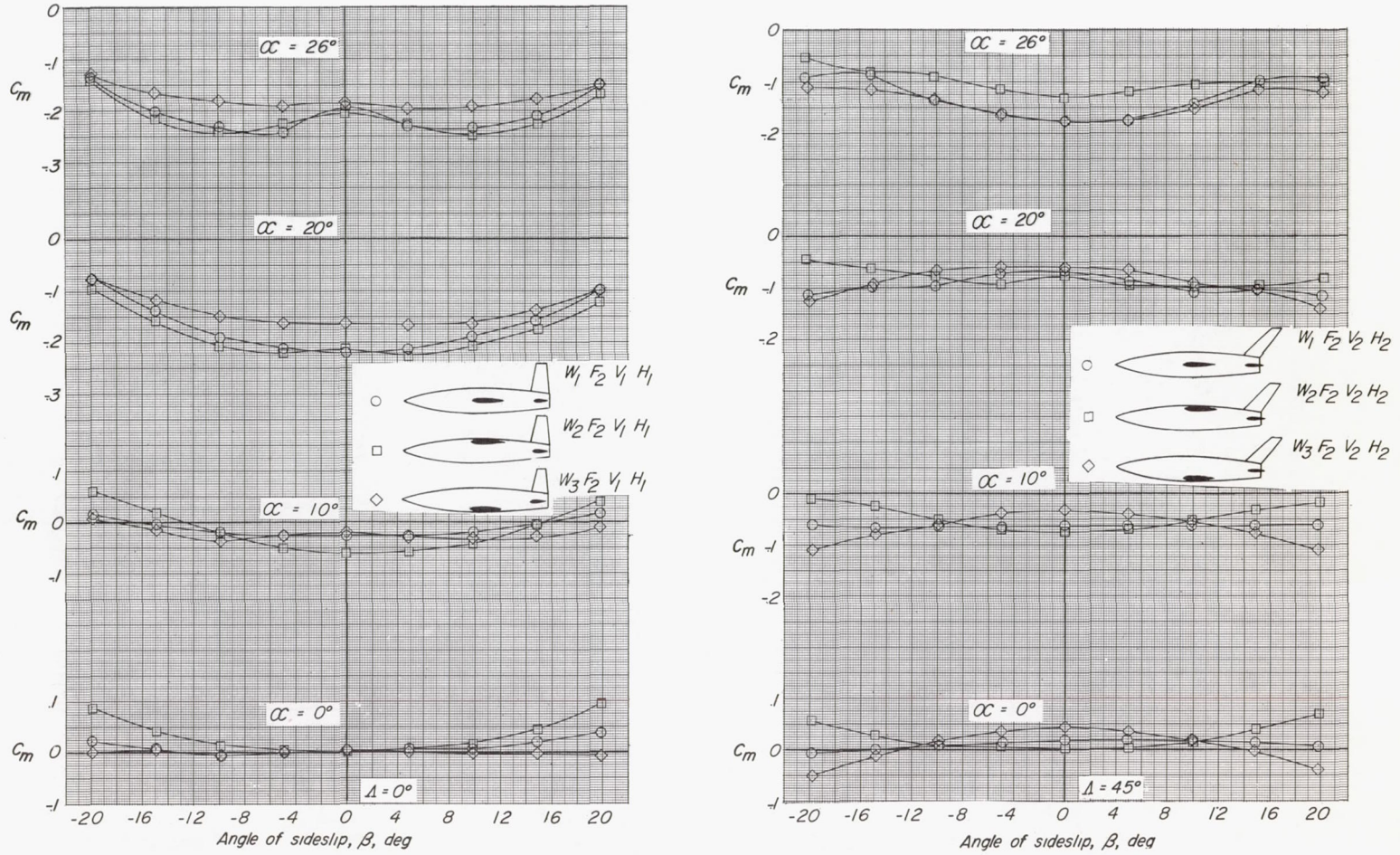
(b) Deep rectangular fuselage, F_3.

Figure 6.- Continued.



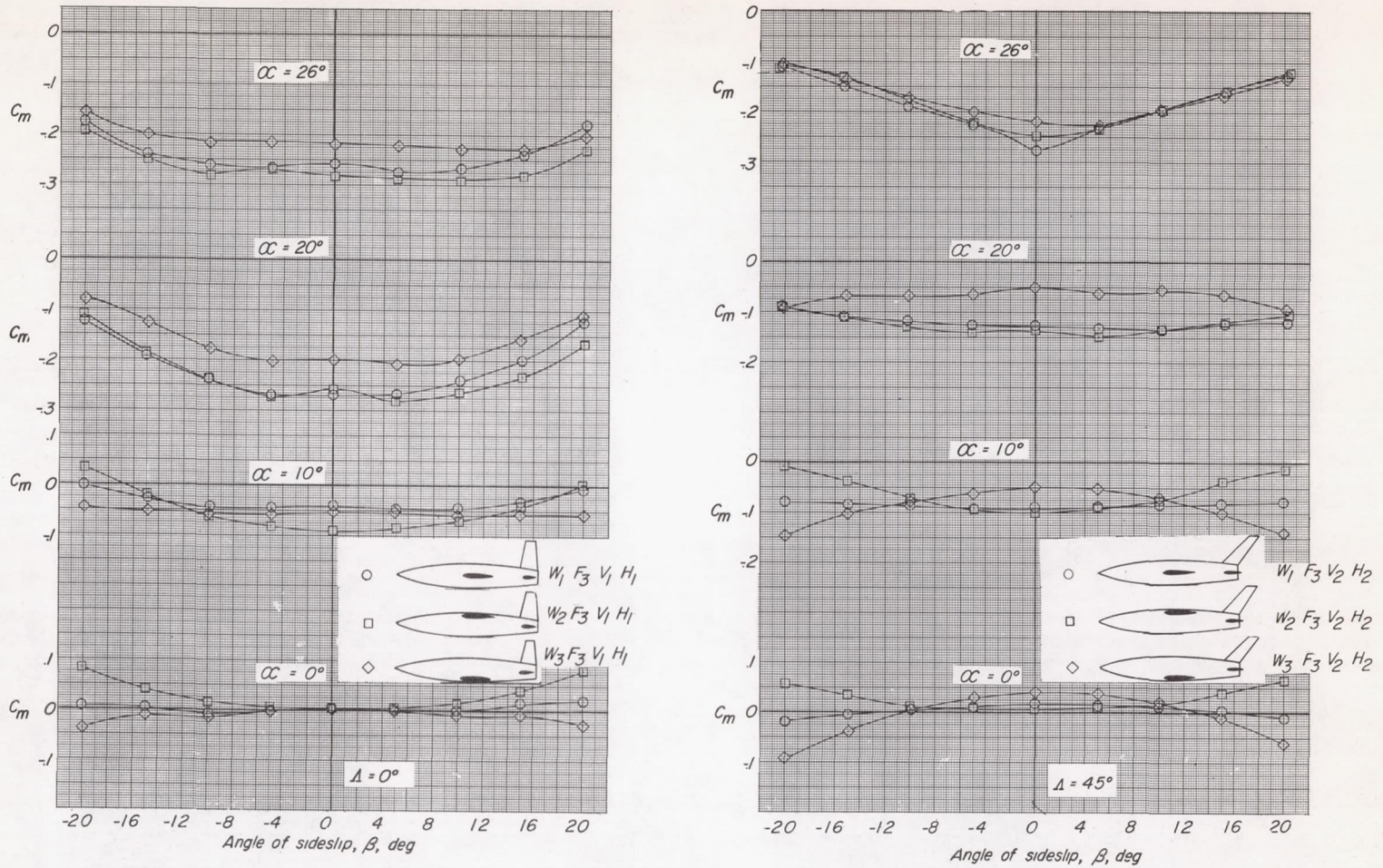
(c) Shallow rectangular fuselage, F_4.

Figure 6.- Concluded.



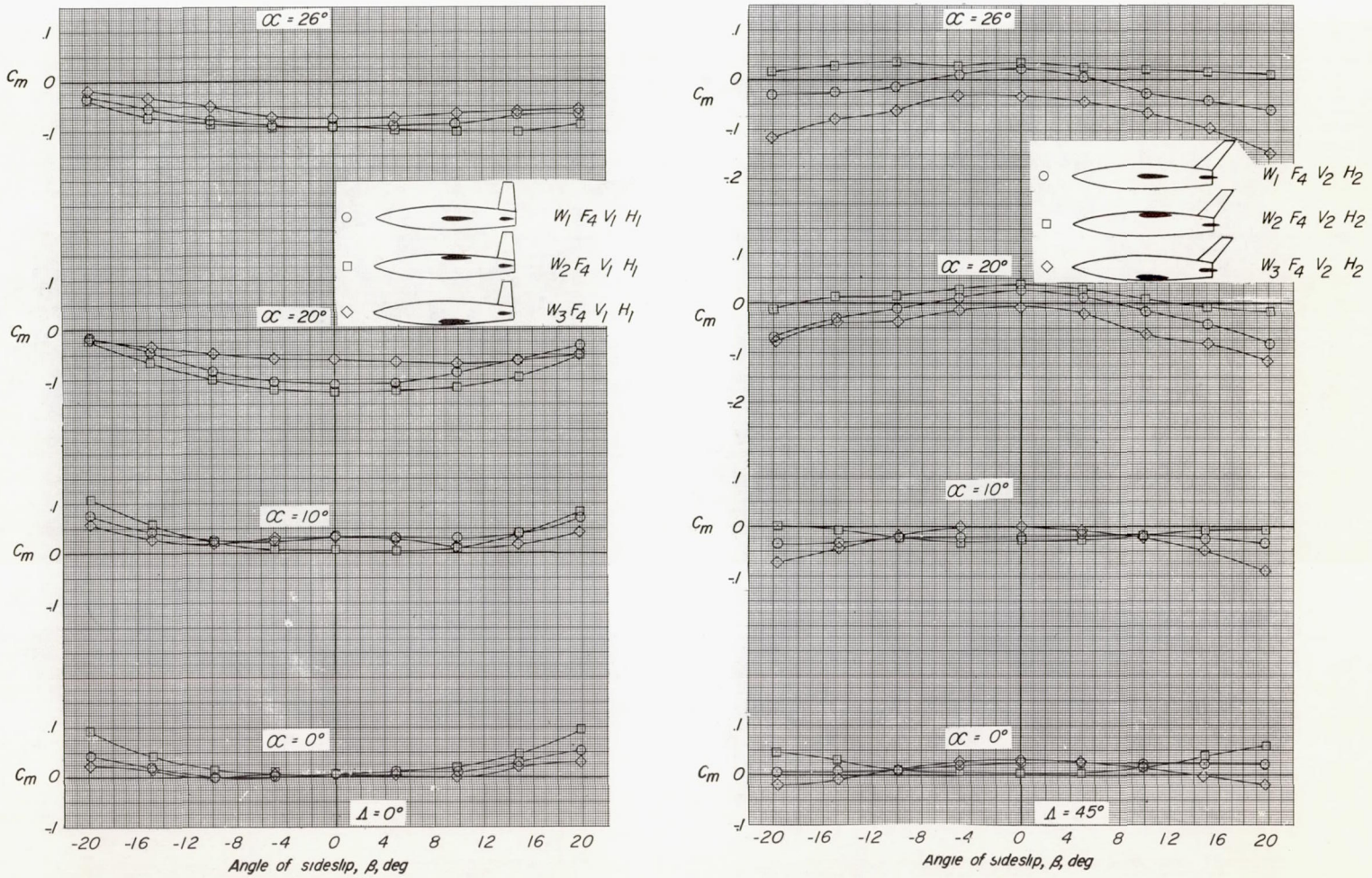
(a) Square fuselage, F_2.

Figure 7.- Effect of wing position on the pitching-moment coefficient of several unswept and 45° sweptback wing-fuselage-tail configurations through the sideslip range. $\alpha = 0°$, 10°, 20°, and 26°.



(b) Deep rectangular fuselage, F_3.

Figure 7.- Continued.



(c) Shallow rectangular fuselage, F_4.

Figure 7.- Concluded.

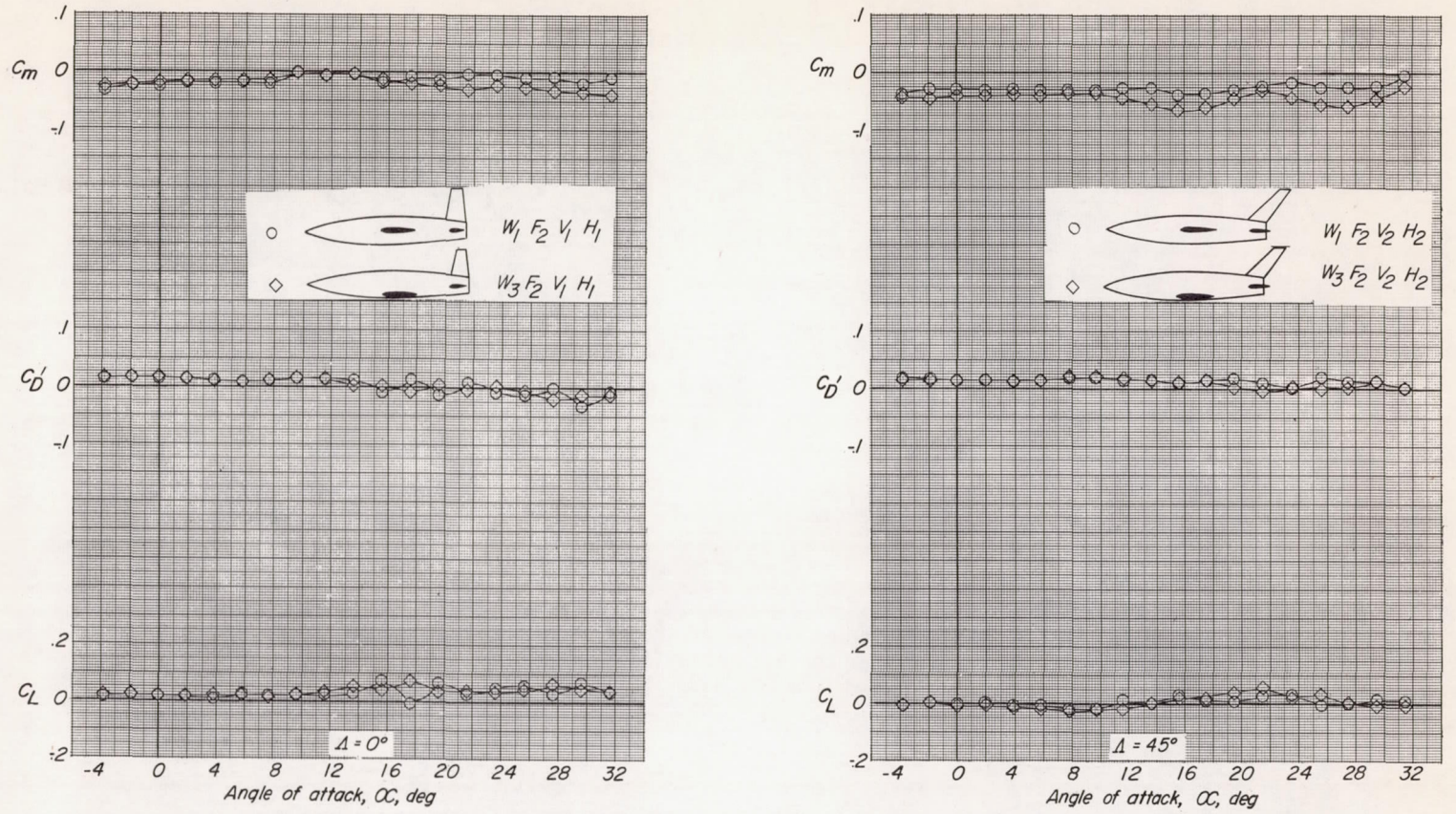
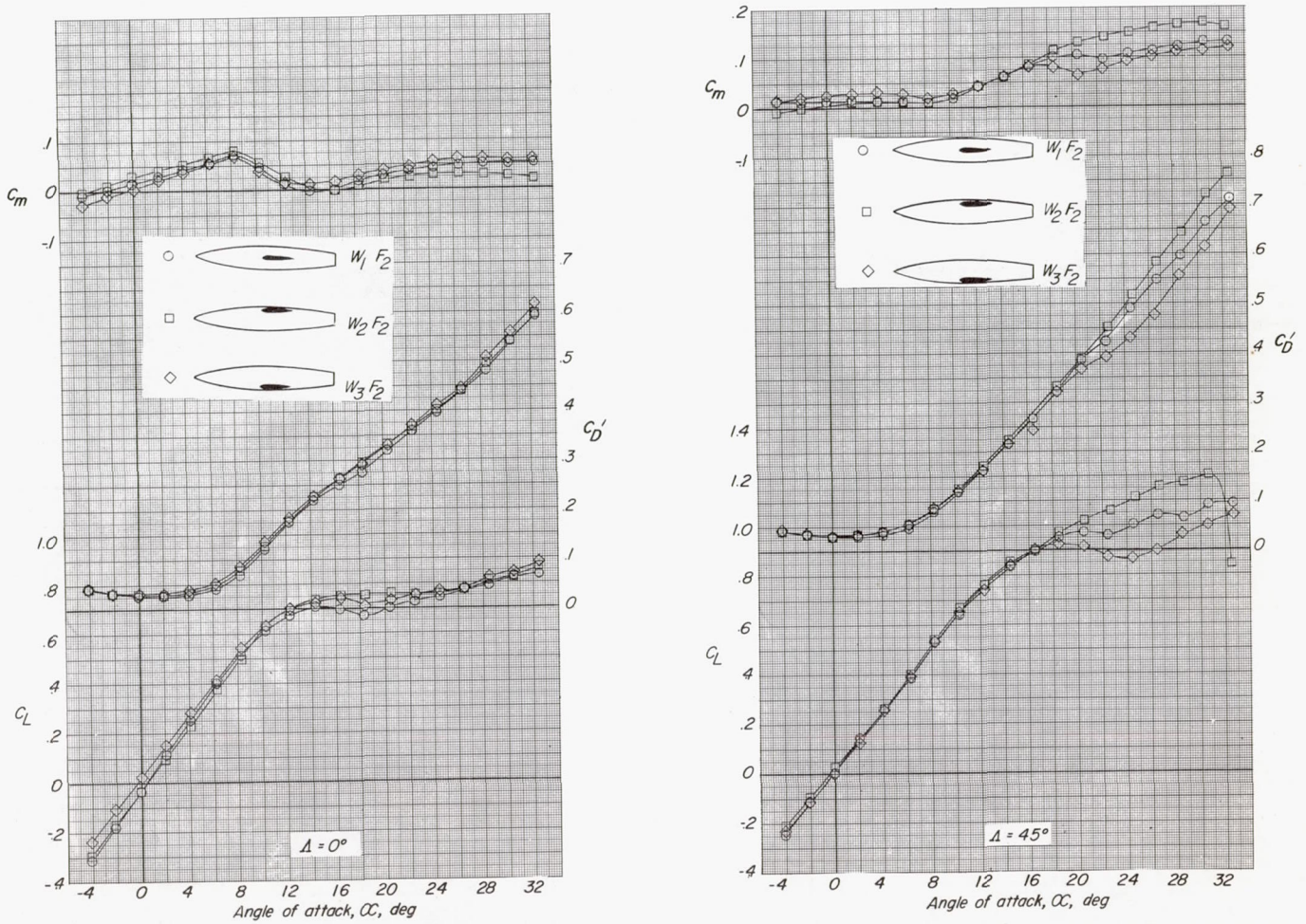
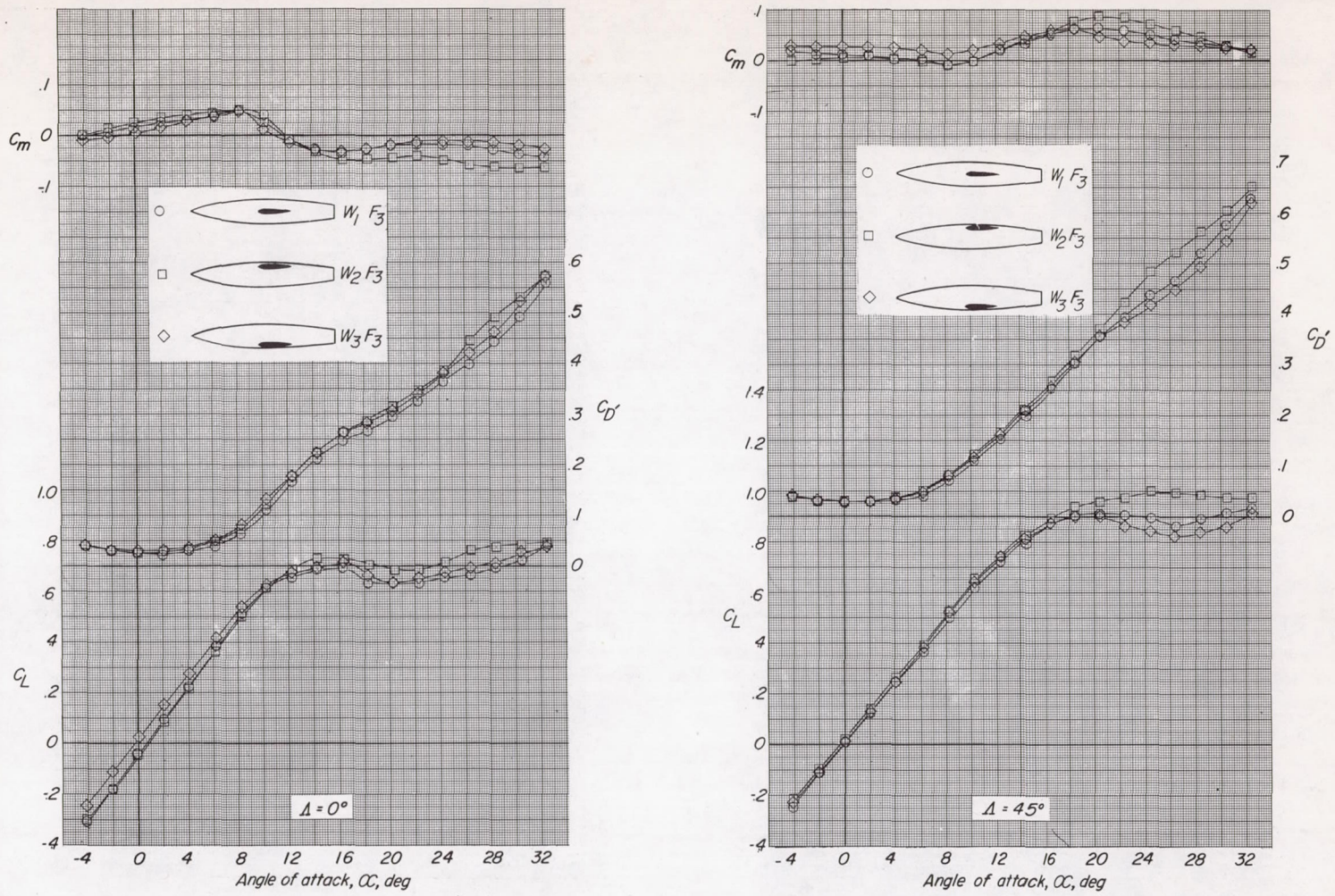


Figure 8.- Variation of the strut tare corrections to C_m, C_D', and C_L for several unswept and 45° sweptback wing-fuselage-tail configurations through the angle-of-attack range.



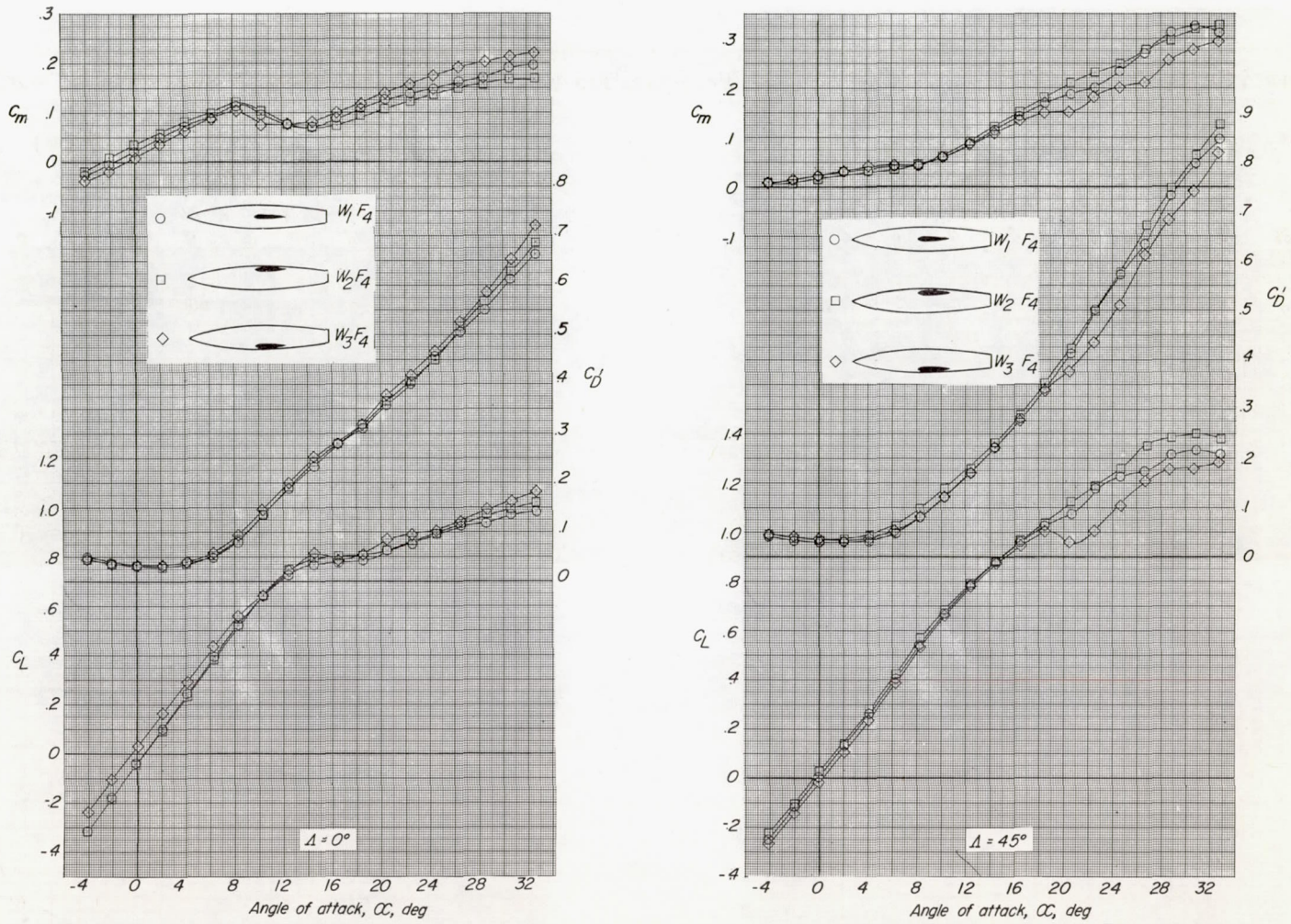
(a) Square fuselage, F_2.

Figure 9.- Effect of wing position on the static longitudinal stability characteristics of several unswept and 45° sweptback wing-fuselage configurations.



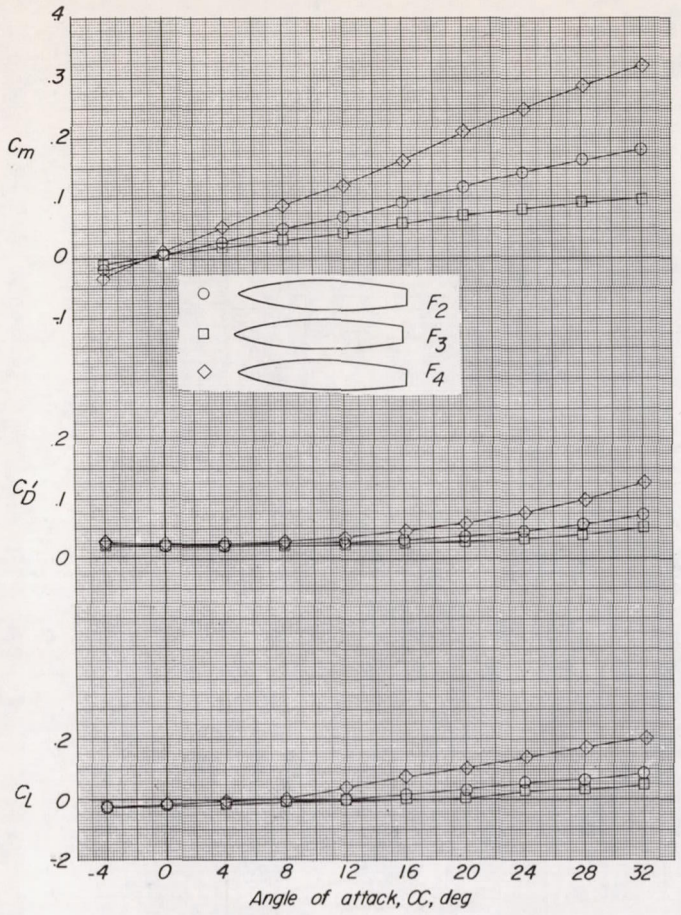
(b) Deep rectangular fuselage, F_3.

Figure 9.- Continued.

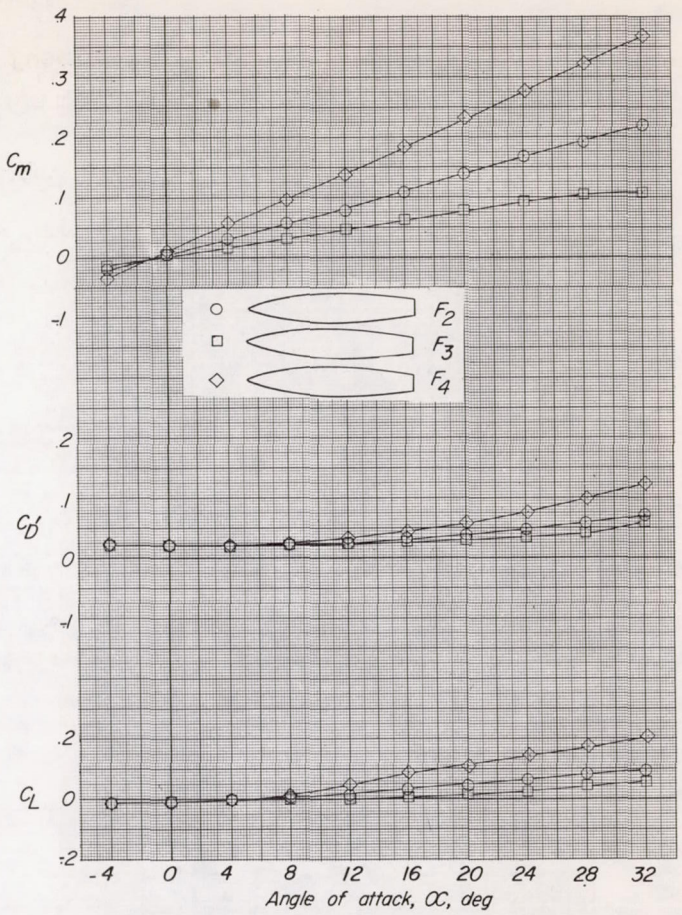


(c) Shallow rectangular fuselage, F_4.

Figure 9.- Concluded.



(a) Center of moments for $\Lambda = 0^\circ$.



(b) Center of moments for $\Lambda = 45^\circ$.

Figure 10.- Static longitudinal stability characteristics of several fuselage configurations with different center-of-moment locations.

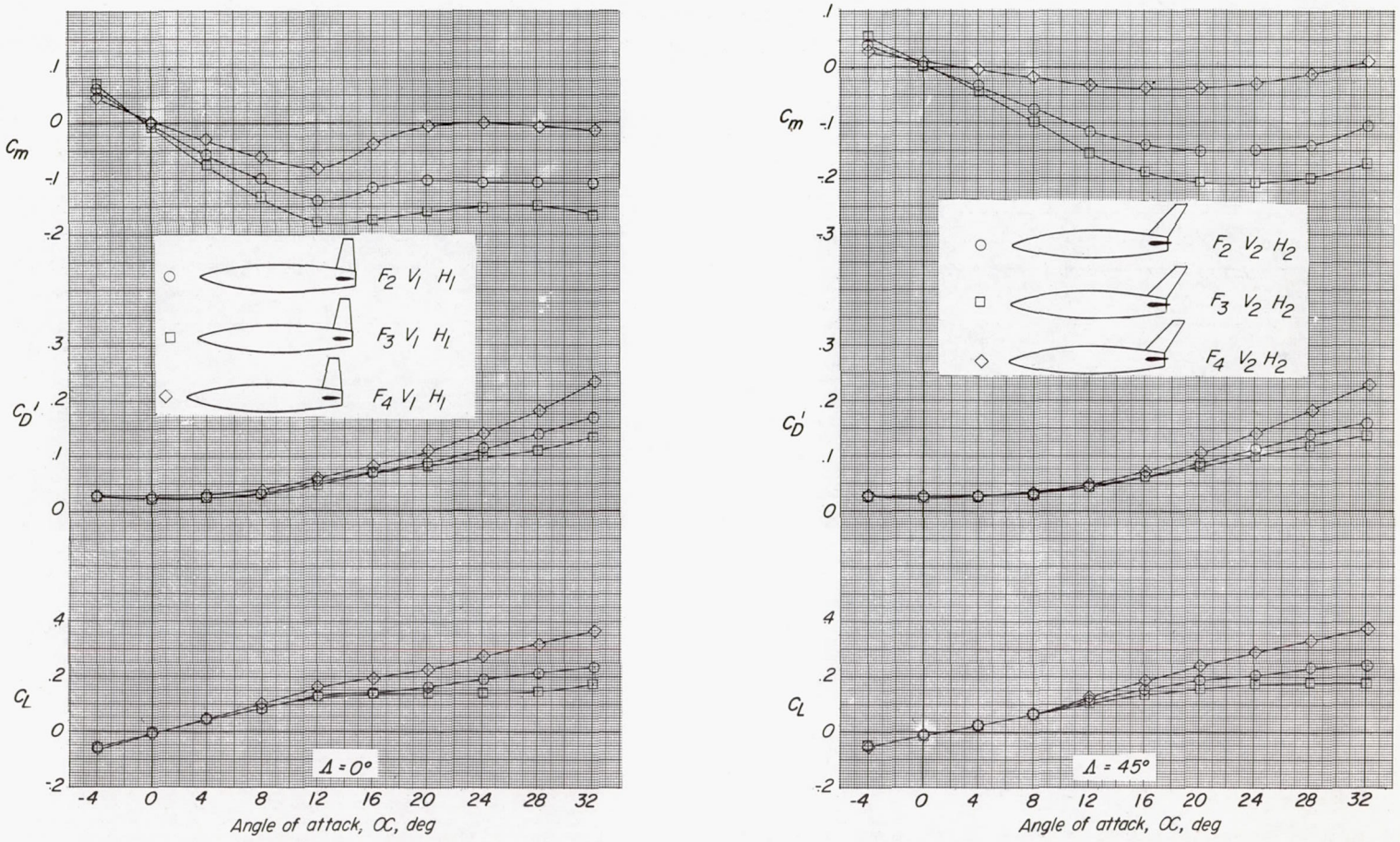


Figure 11.- Static longitudinal stability characteristics of several fuselages in combination with unswept- and 45° sweptback-tail configurations.

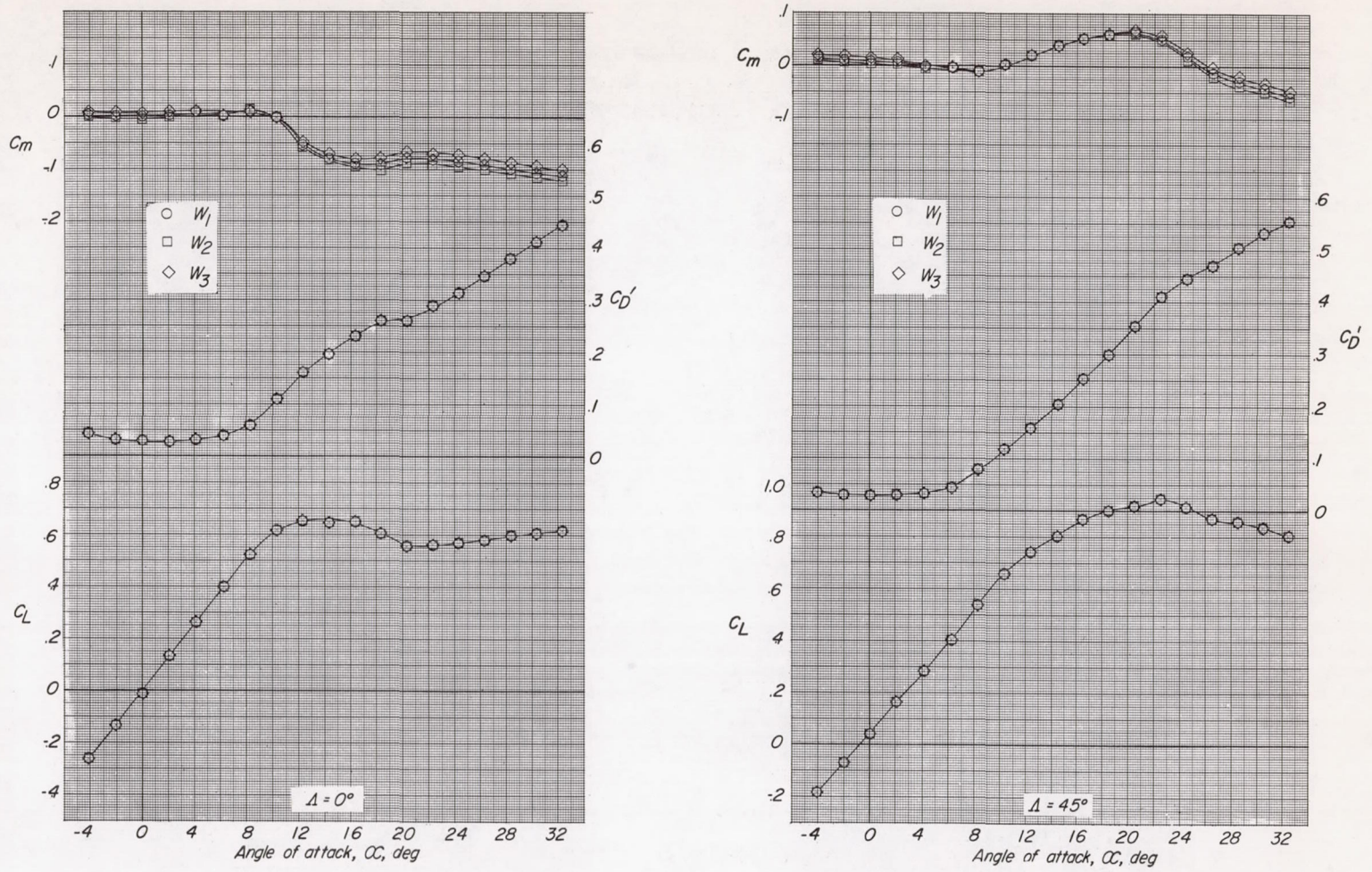


Figure 12.- Static longitudinal stability characteristics of the unswept and 45° sweptback wings. Wings located on balance center and at $\Delta h/b = 0.0672$ above and below balance center.

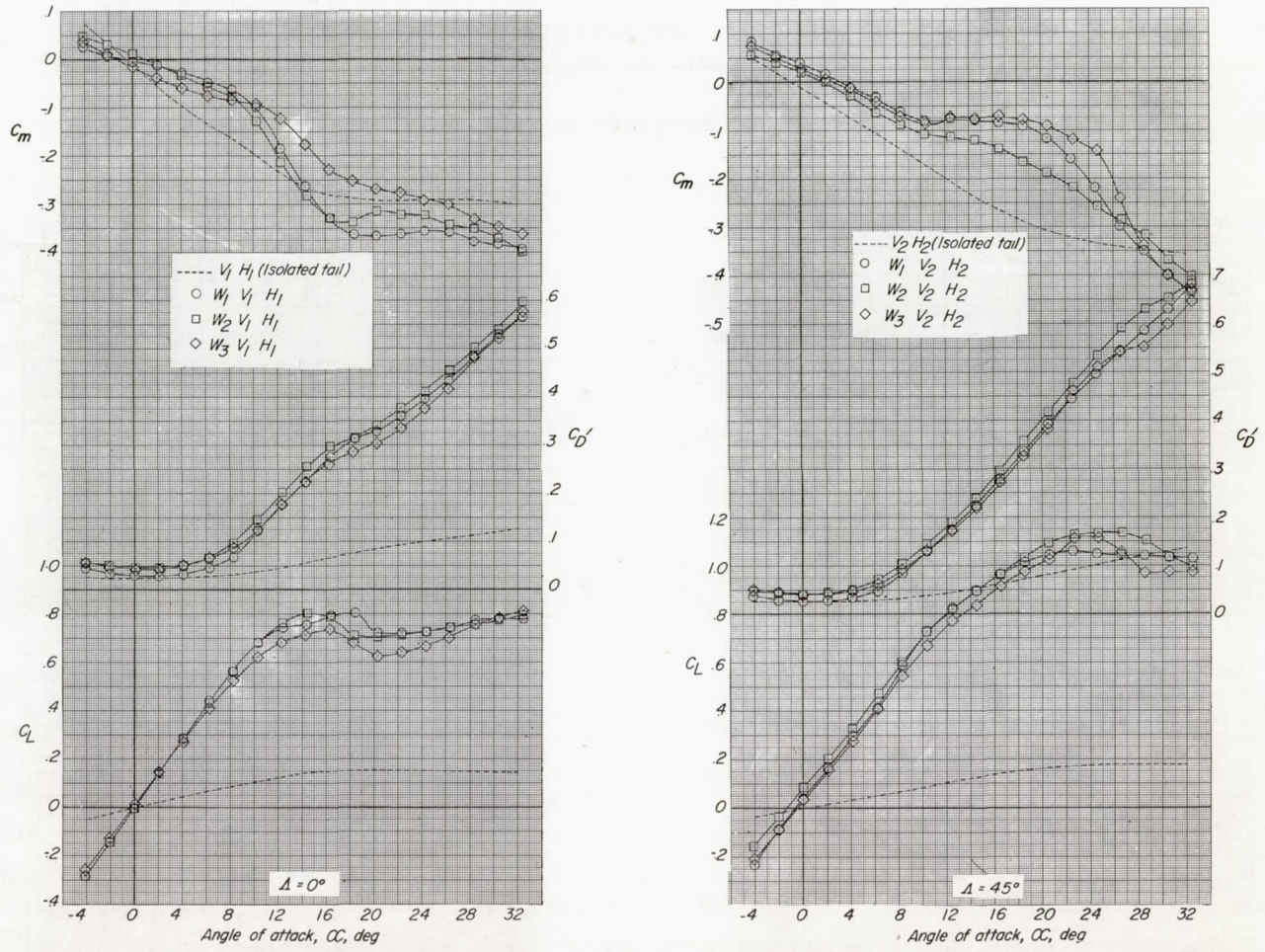
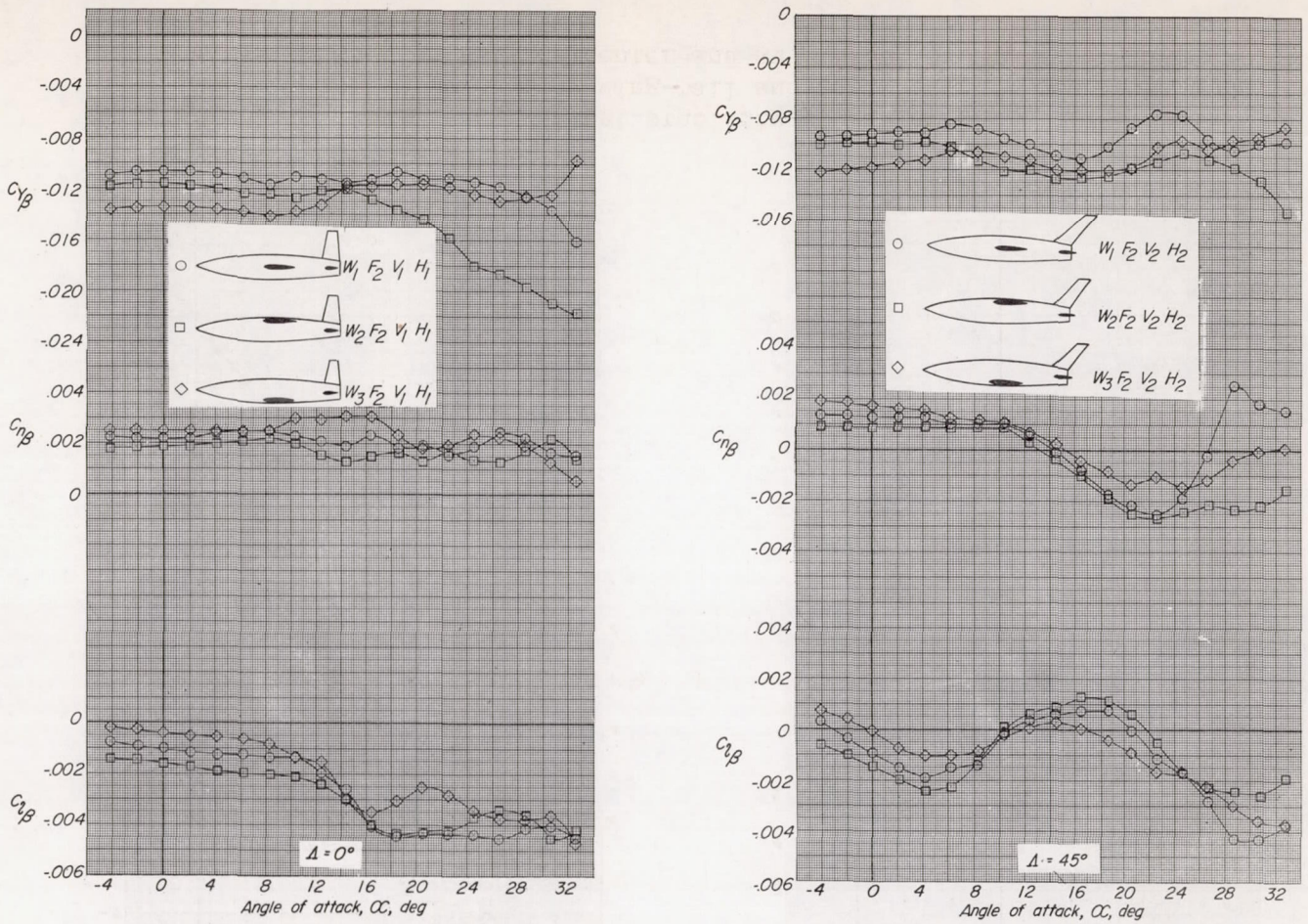
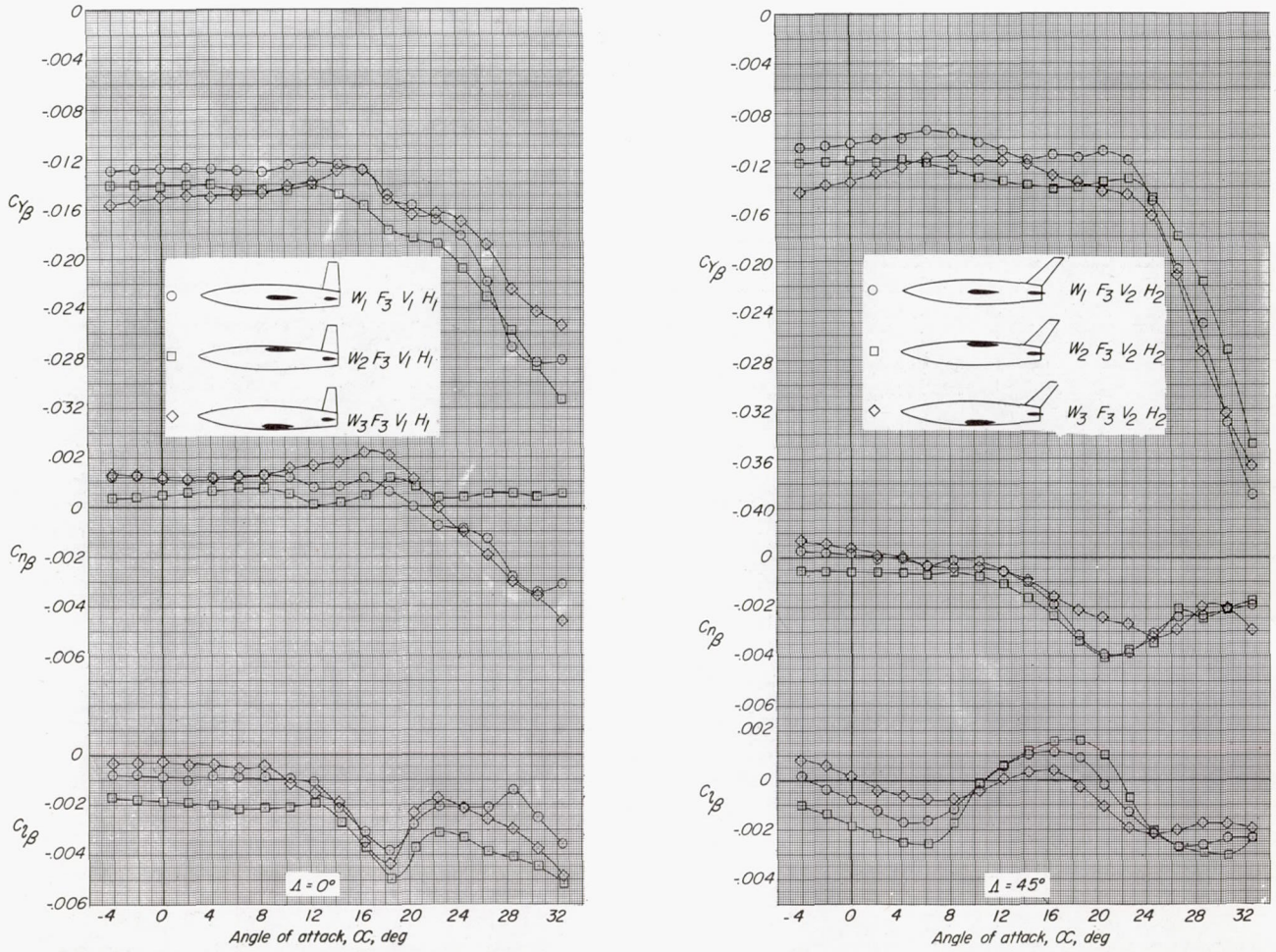


Figure 13.- Static longitudinal stability characteristics of several unswept and 45° sweptback wing-tail and isolated-tail configurations. Wings located on balance center and at $\Delta h/b = 0.0672$ above and below balance center.



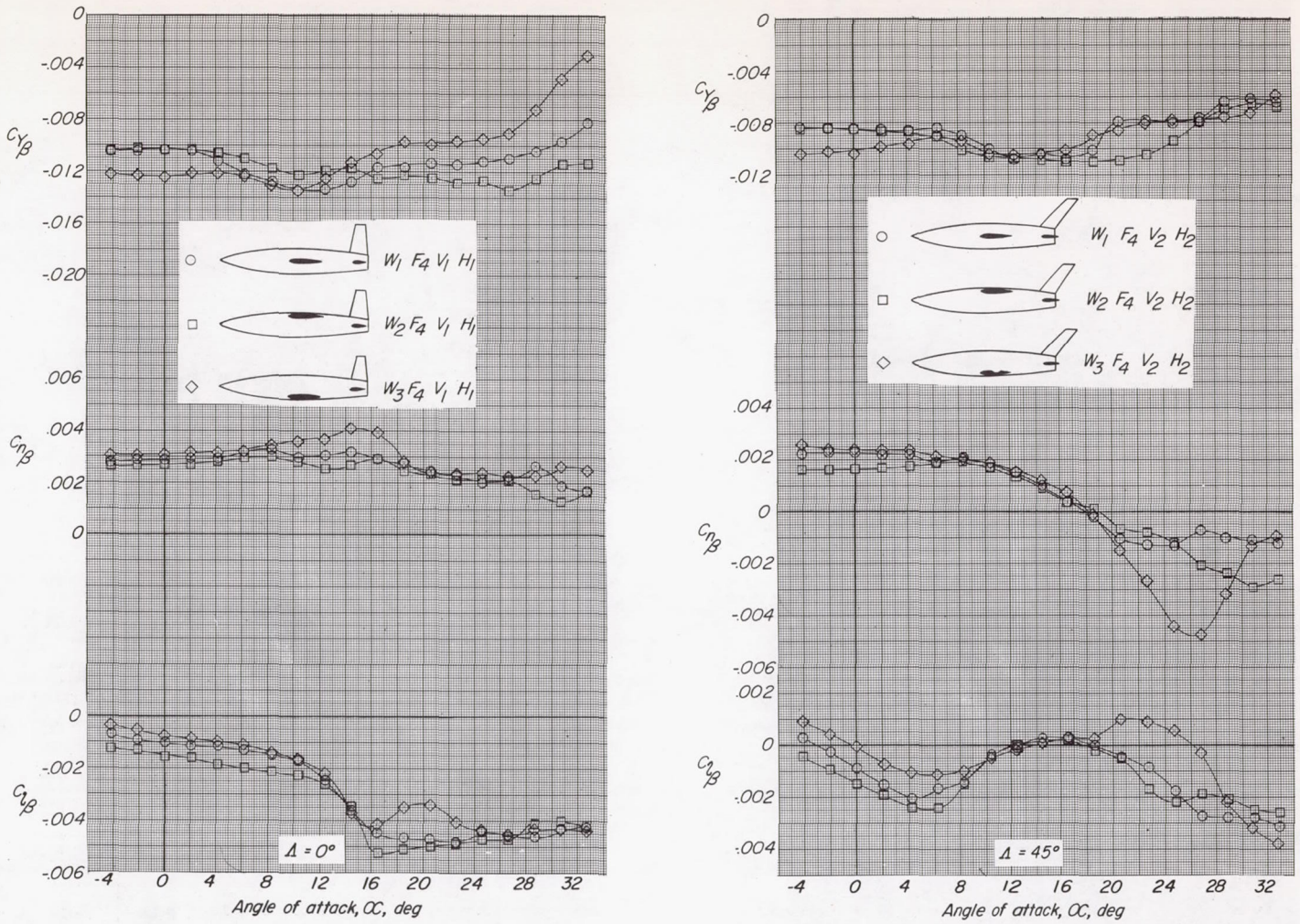
(a) Square fuselage, F_2.

Figure 14.- Effect of wing position on the static lateral stability characteristics of several unswept and 45° sweptback wing-fuselage-tail configurations.



(b) Deep rectangular fuselage, F_3.

Figure 14.- Continued.



(c) Shallow rectangular fuselage, F_4.

Figure 14.- Concluded.

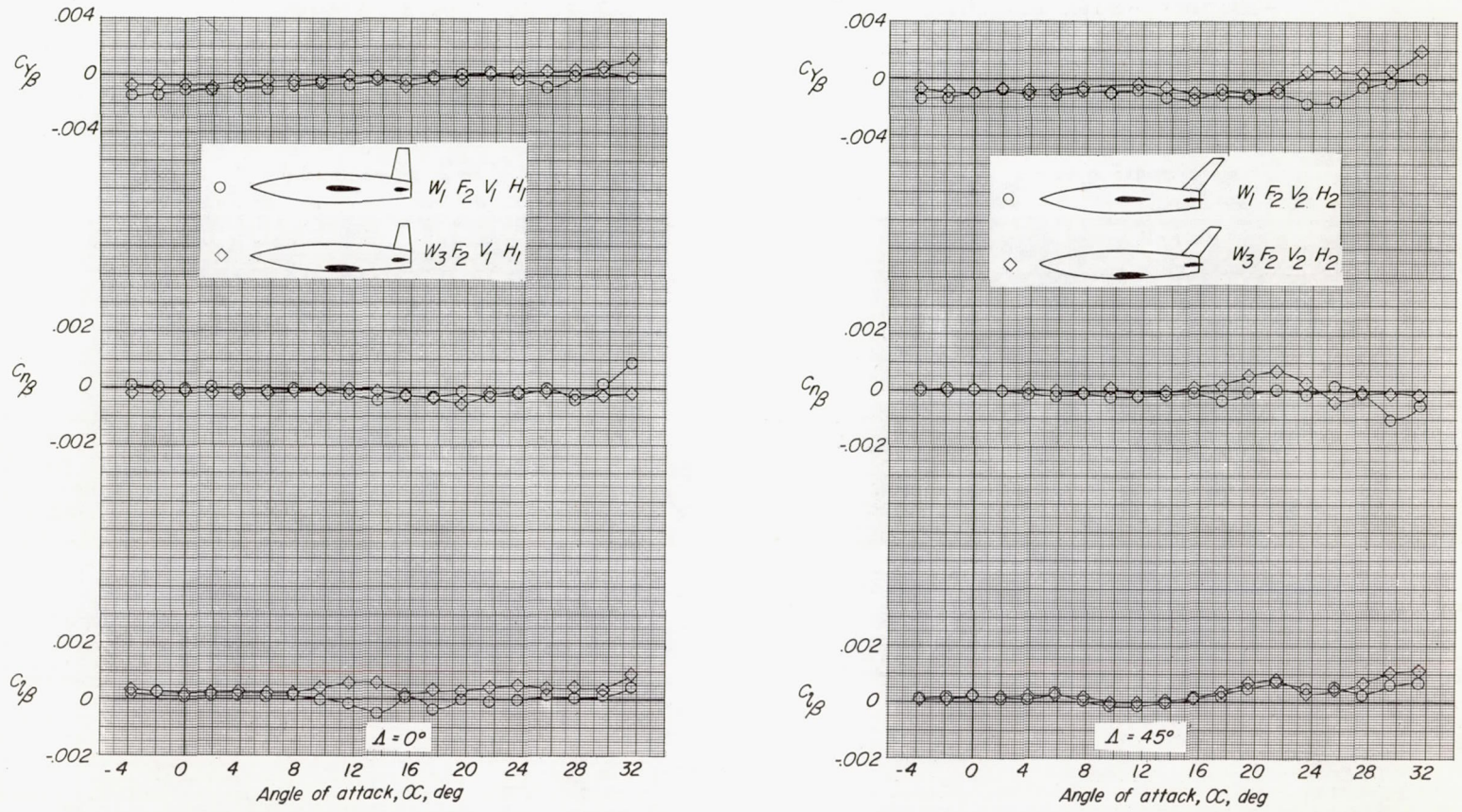
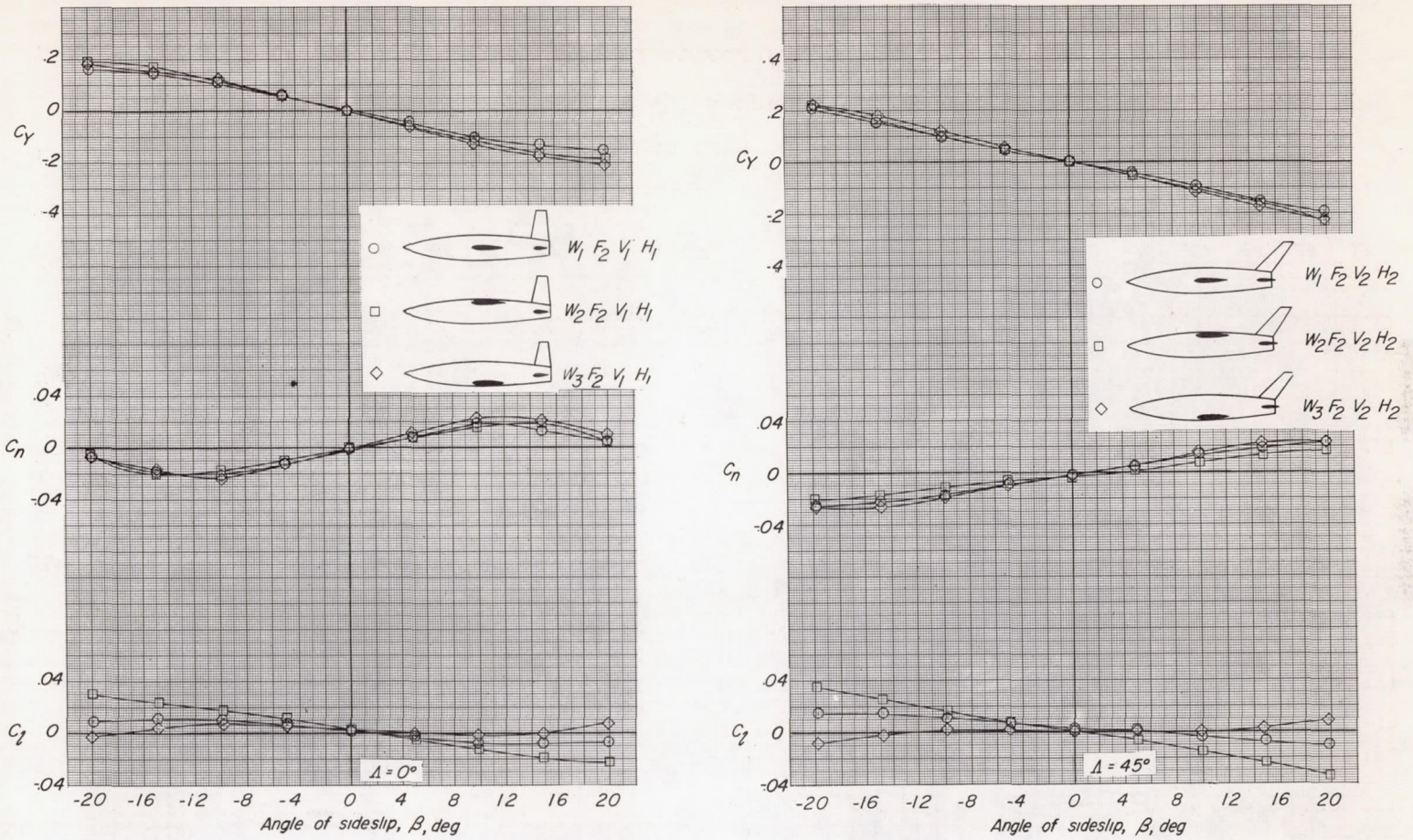
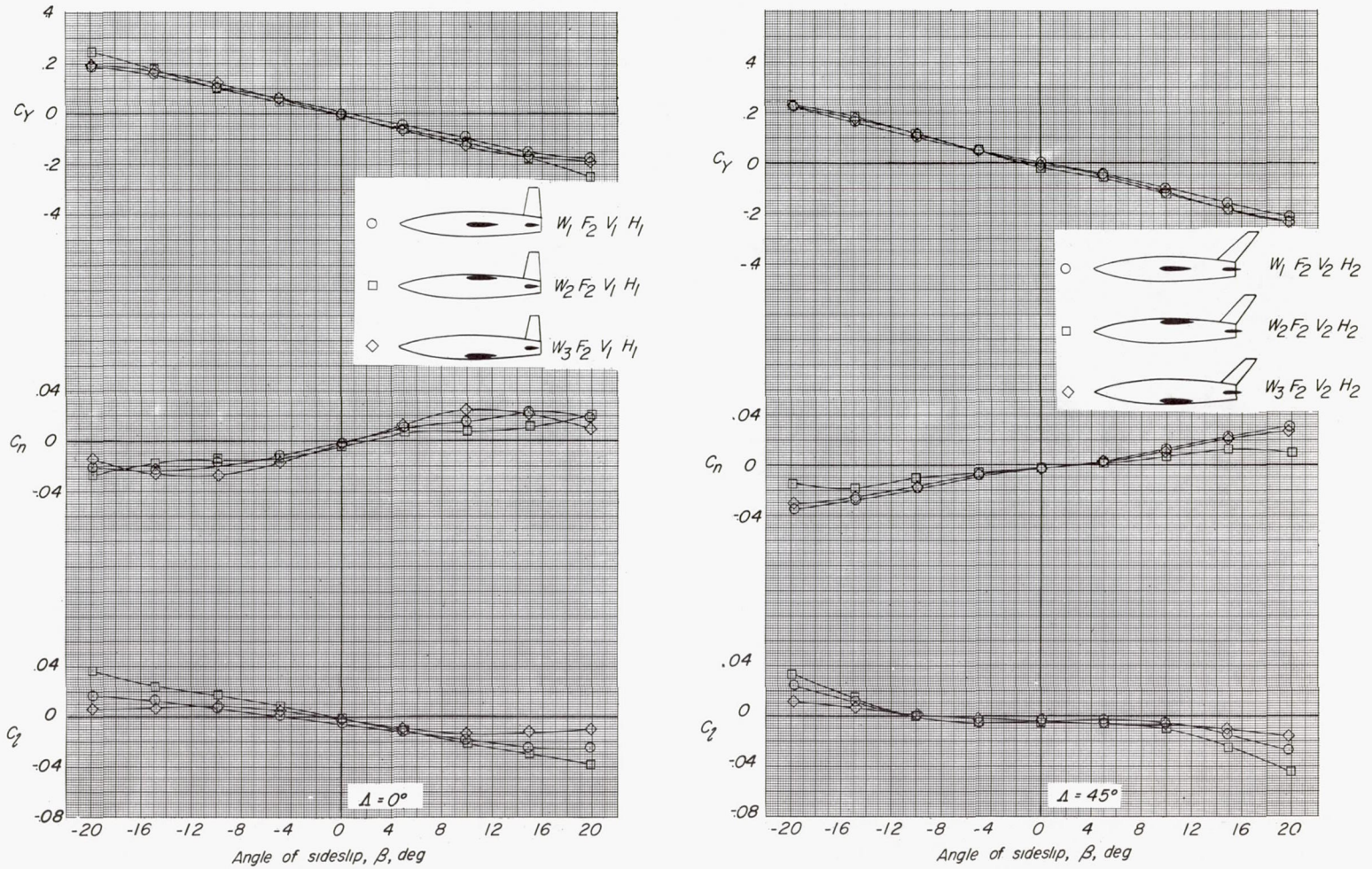


Figure 15.- Variation of the strut tare corrections to C_{Y_β}, C_{n_β}, and C_{l_β} for several unswept and 45° sweptback wing-fuselage-tail configurations through the angle-of-attack range.



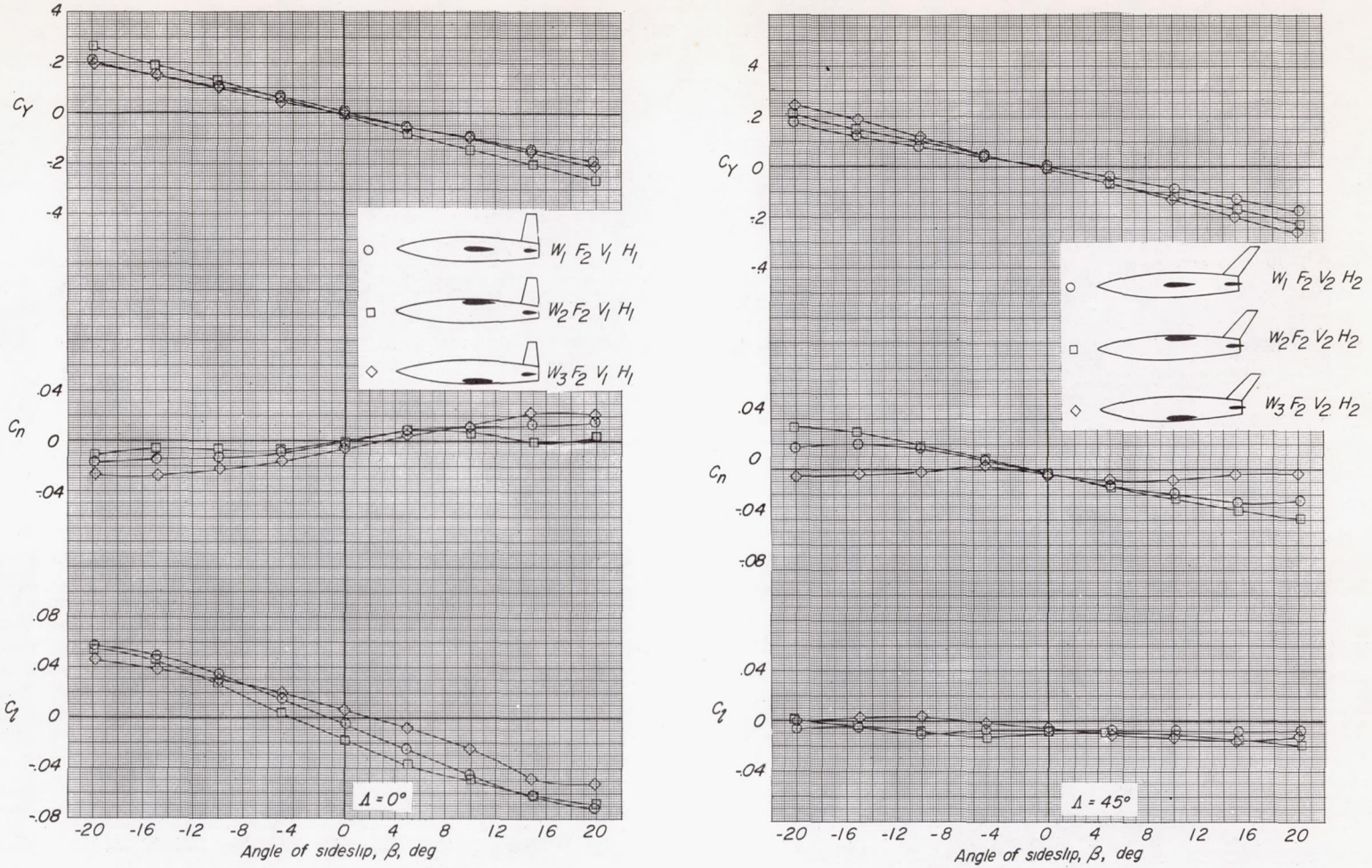
(a) $\alpha = 0°$.

Figure 16.- Effect of wing position on the static lateral stability characteristics of several unswept and 45° sweptback wing-fuselage-tail configurations. Square fuselage, F_2.



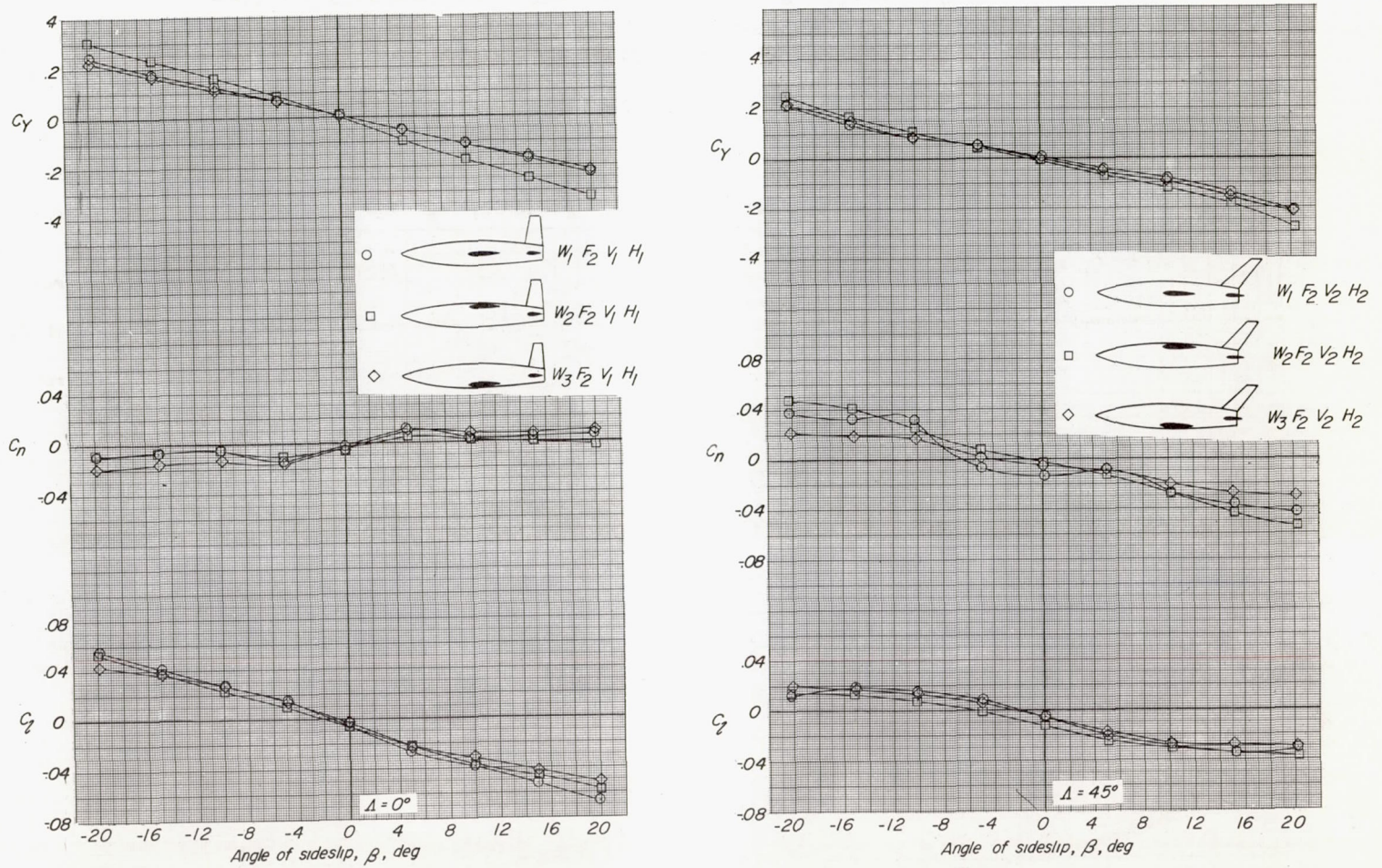
(b) $\alpha = 10°$.

Figure 16.- Continued.



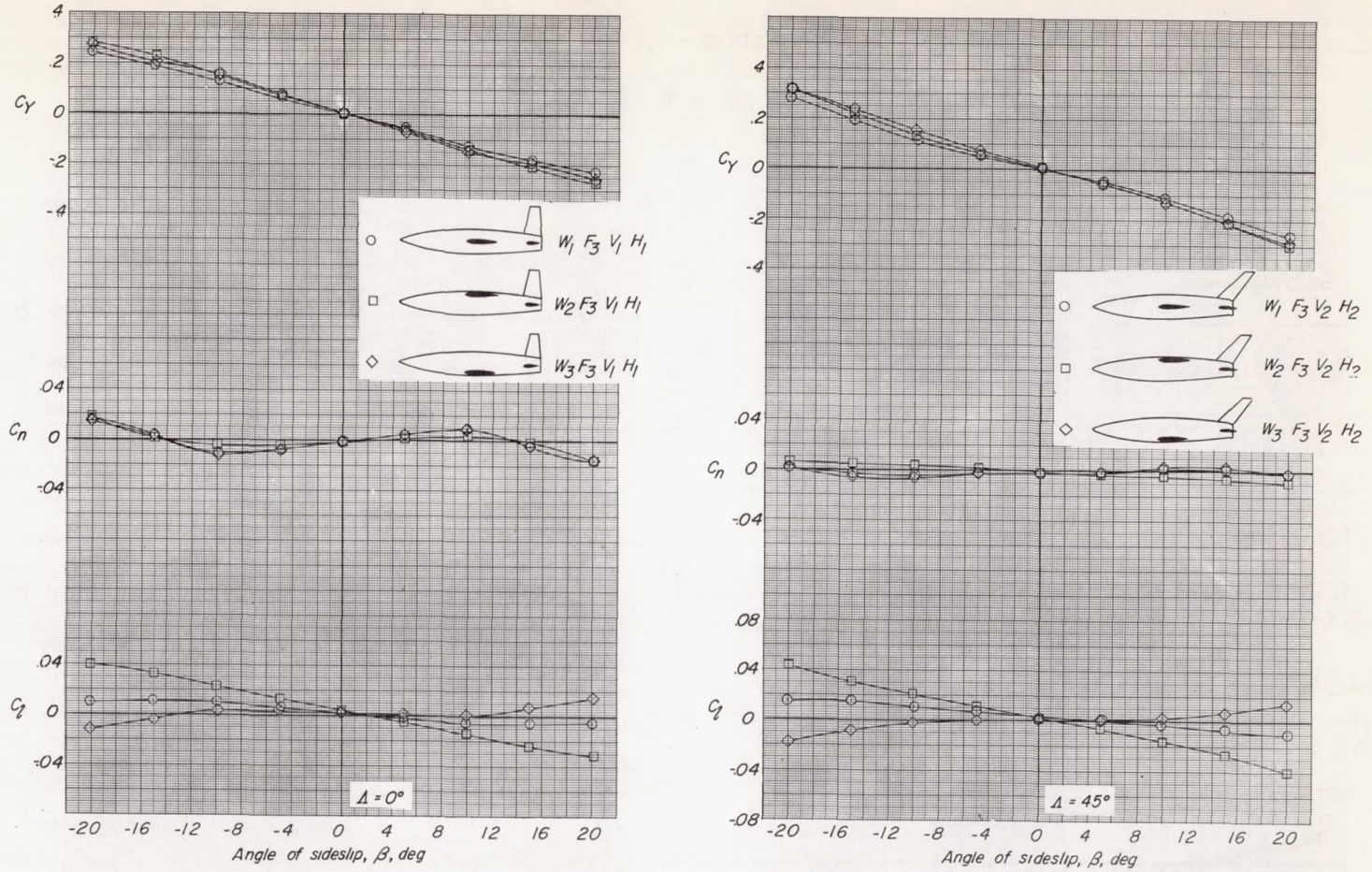
(c) $\alpha = 20^{\circ}$.

Figure 16.- Continued.



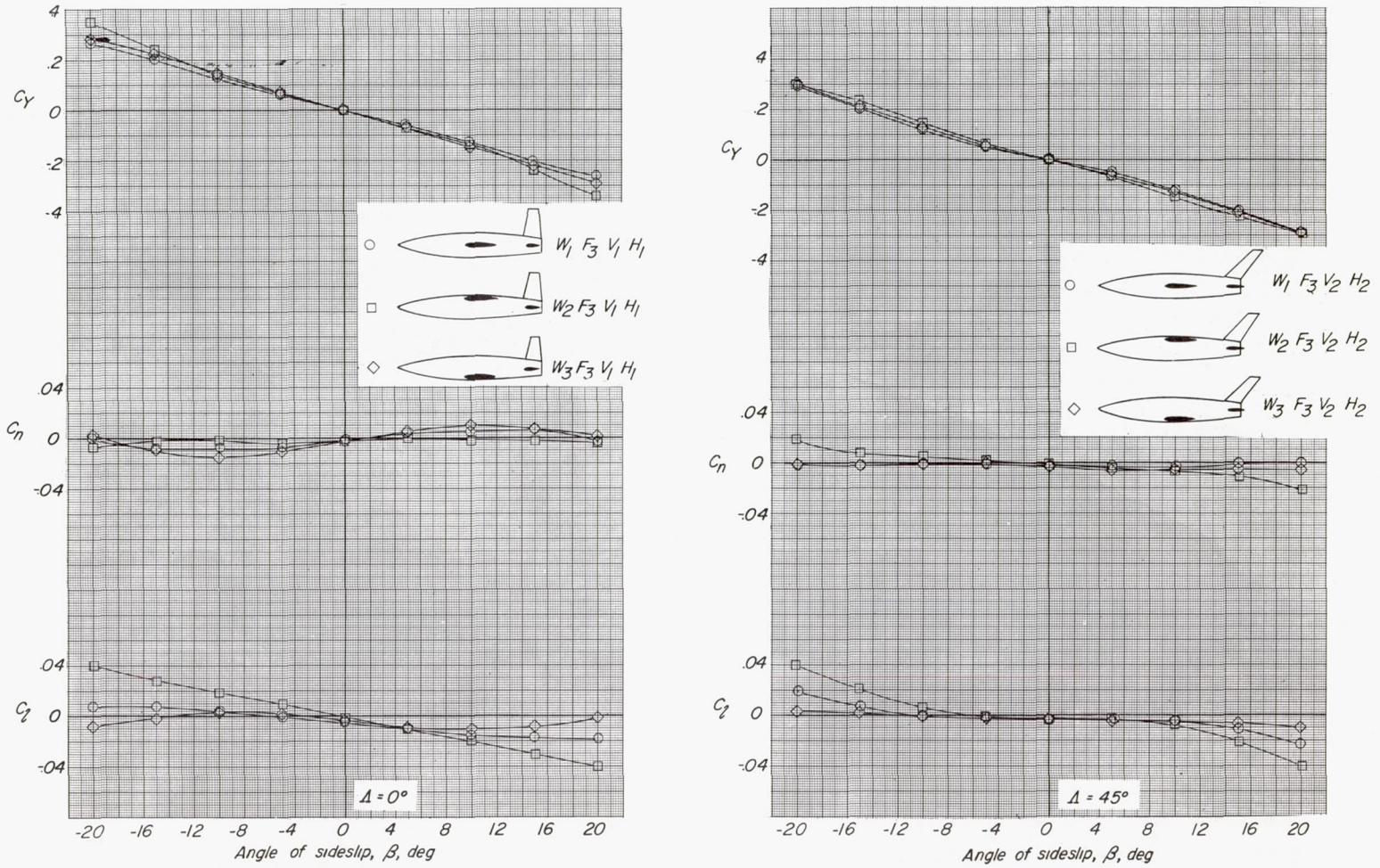
(d) $\alpha = 26^\circ$.

Figure 16.- Concluded.



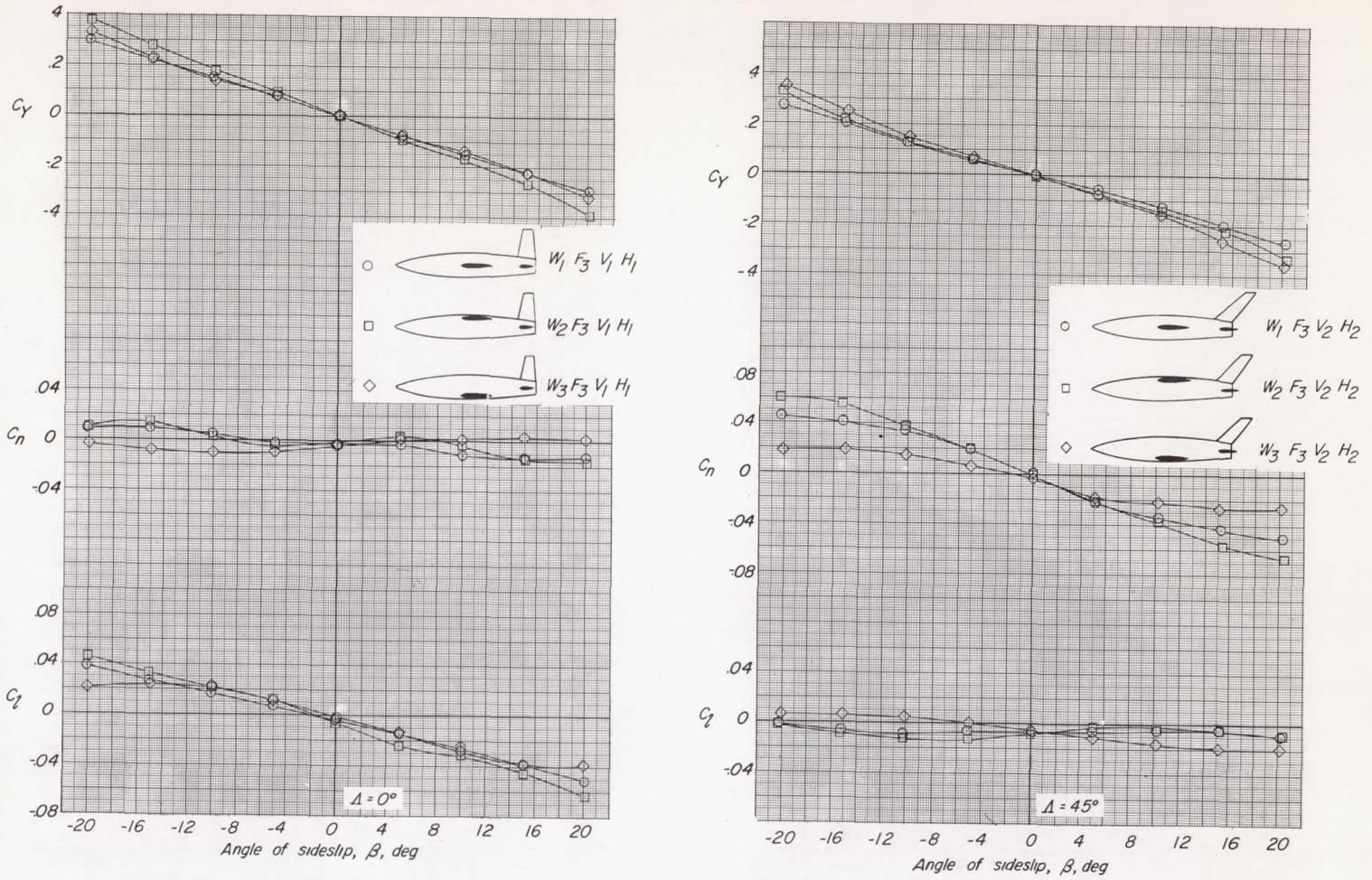
(a) $\alpha = 0°$.

Figure 17.- Effect of wing position on the static lateral stability characteristics of several unswept and 45° sweptback wing-fuselage-tail configurations. Deep rectangular fuselage, F_3.



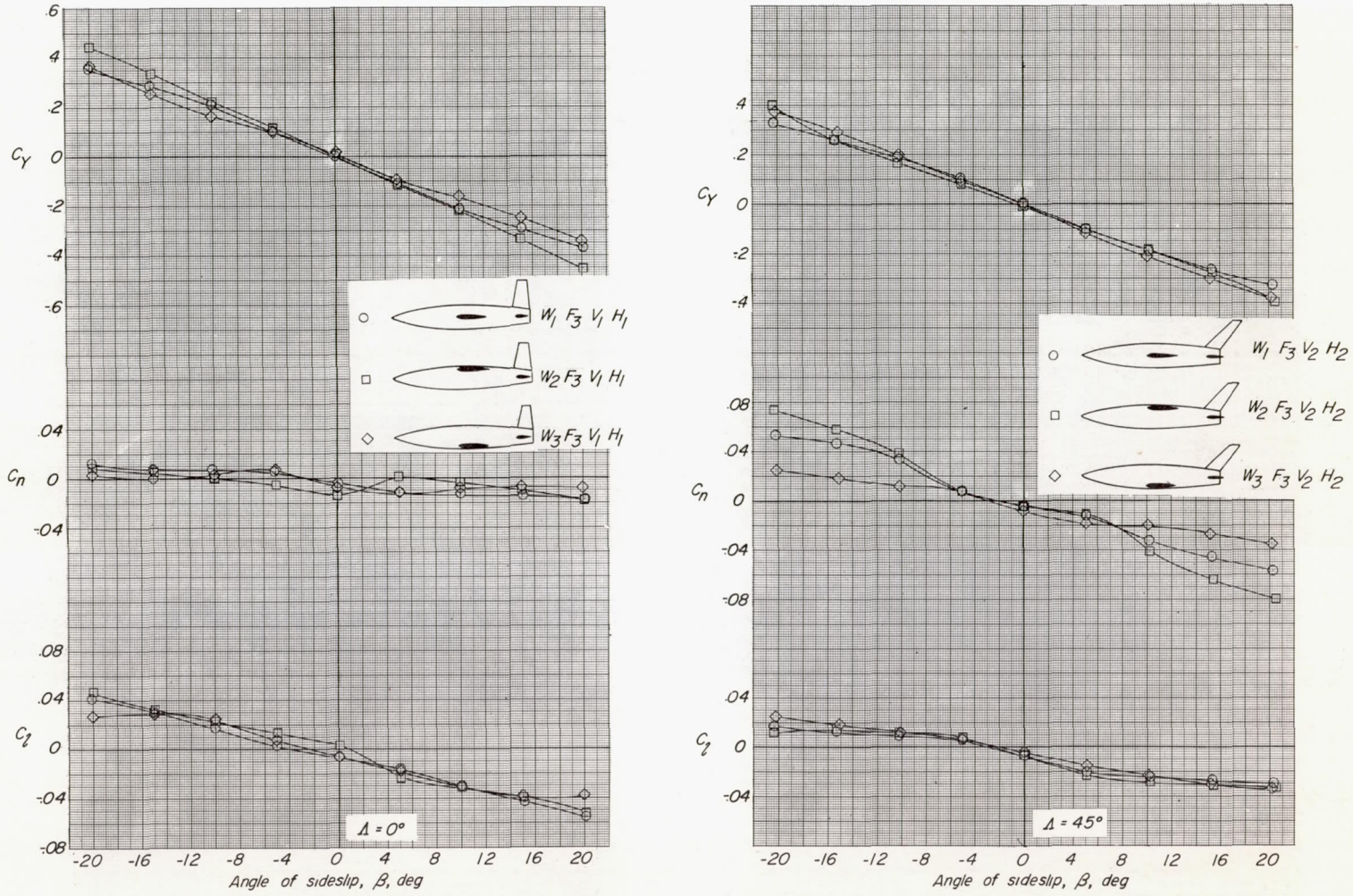
(b) $\alpha = 10^{\circ}$.

Figure 17.- Continued.



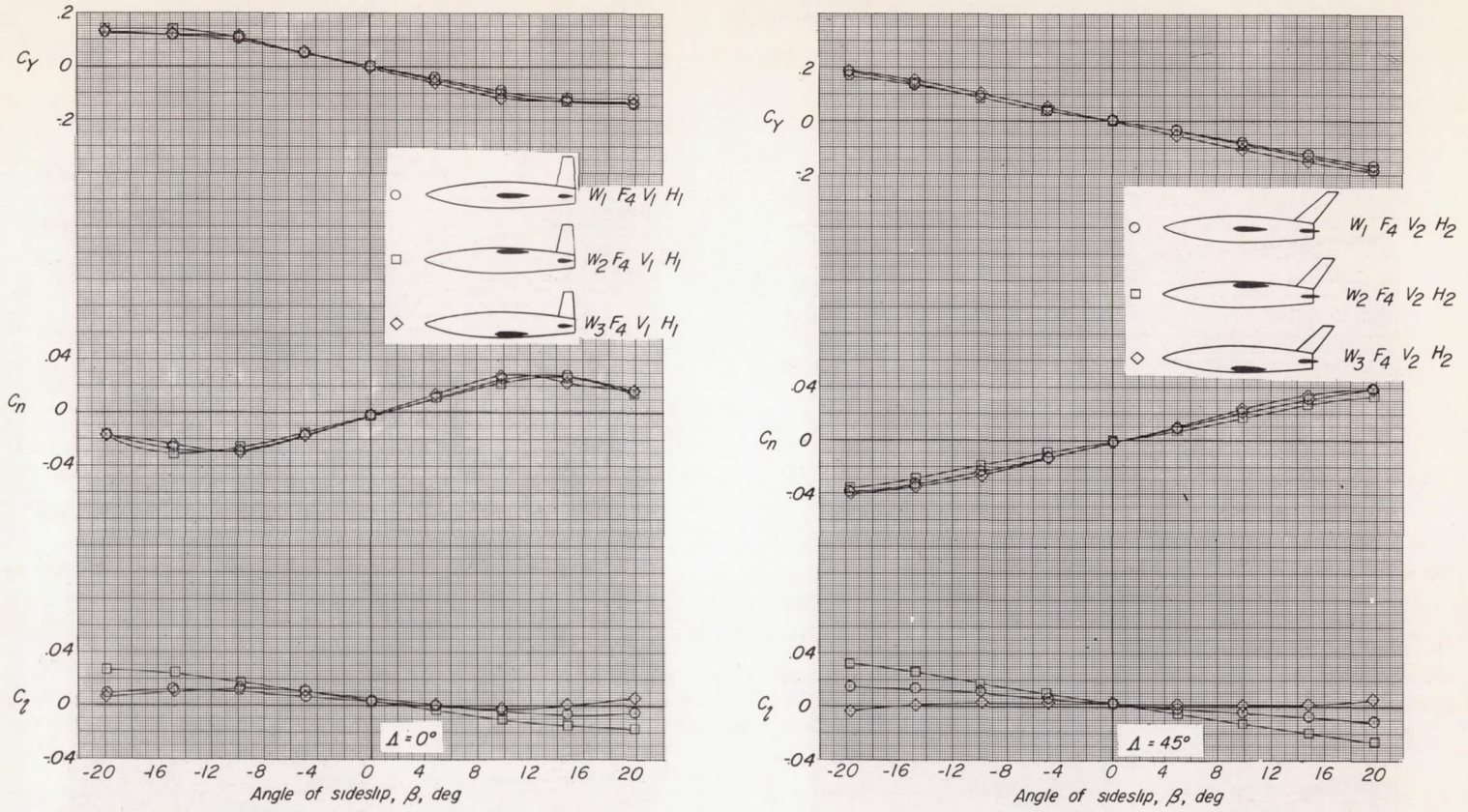
(c) $\alpha = 20^{\circ}$.

Figure 17.- Continued.



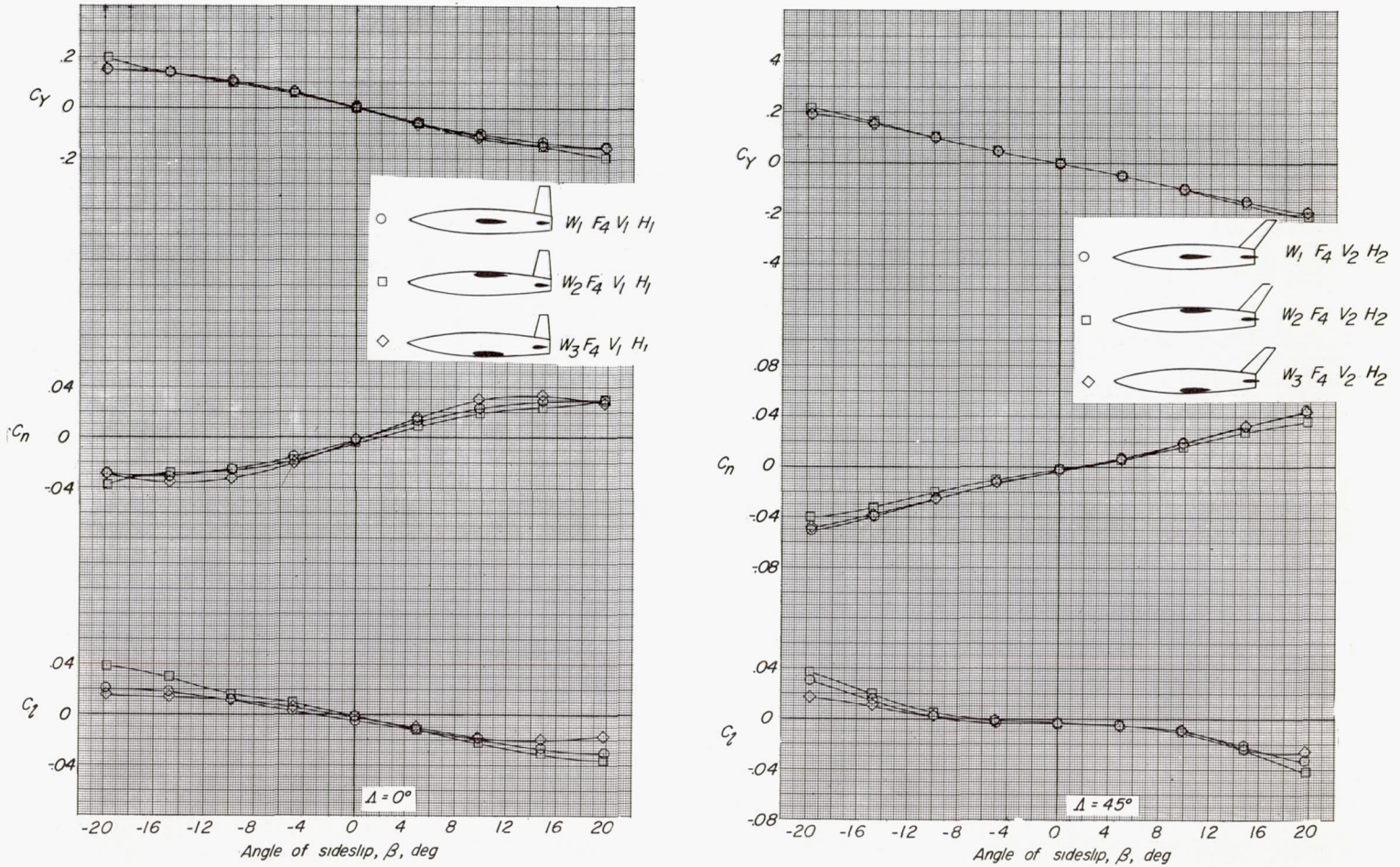
(d) $\alpha = 26°$.

Figure 17.- Concluded.



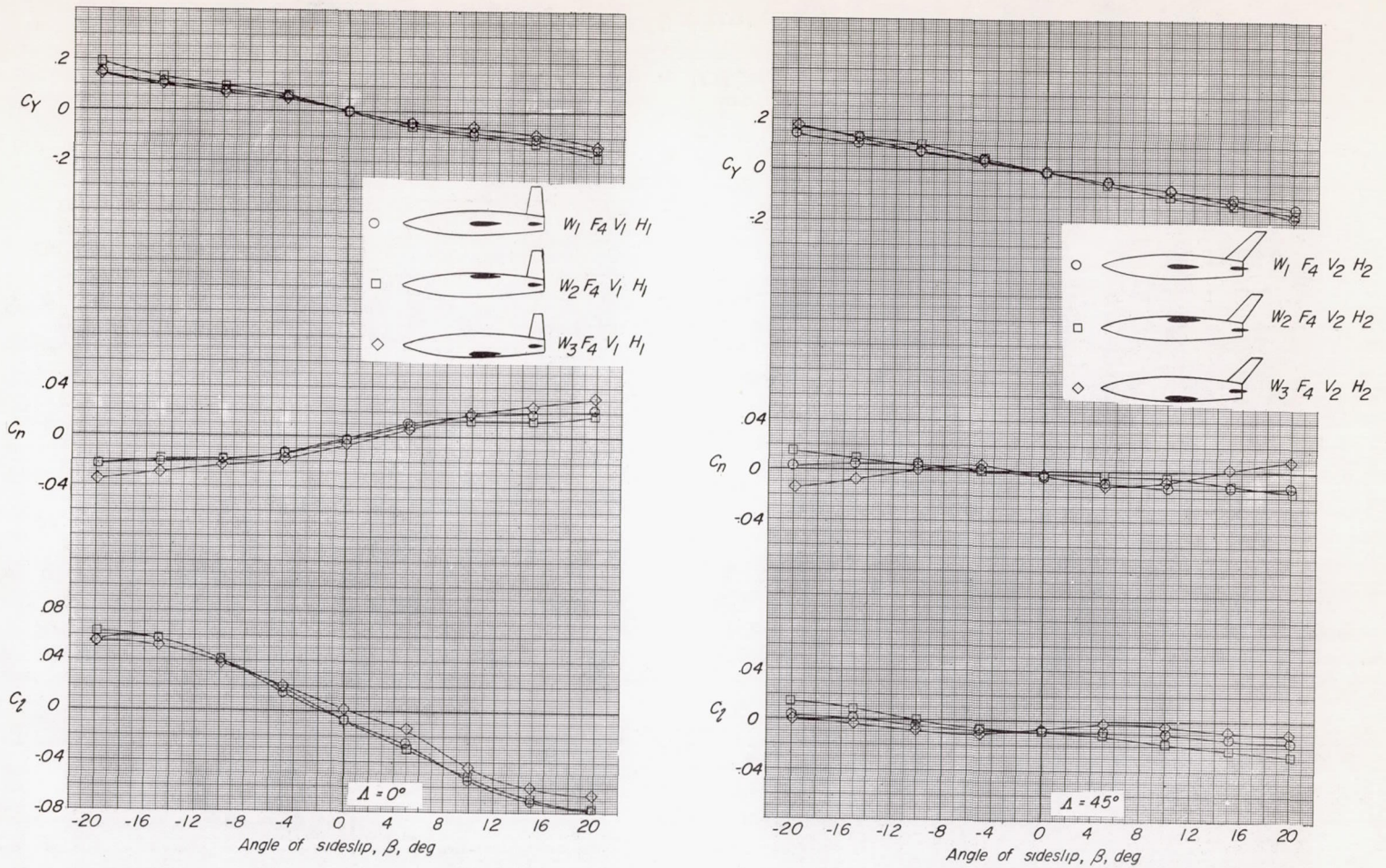
(a) $\alpha = 0^\circ$.

Figure 18.- Effect of wing position on the static lateral stability characteristics of several unswept and 45° sweptback wing-fuselage-tail configurations. Shallow rectangular fuselage, F_4.



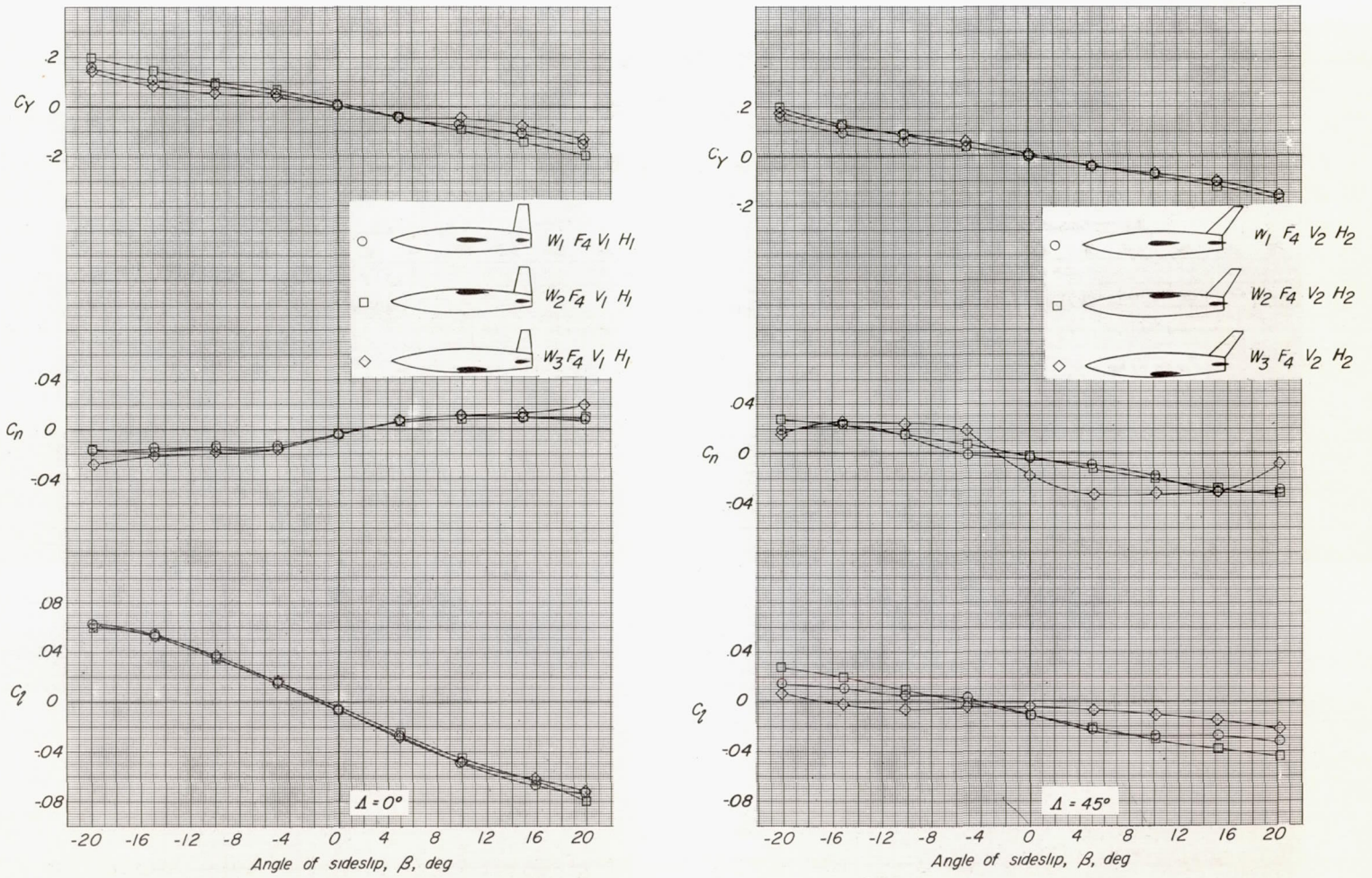
(b) $\alpha = 10^\circ$.

Figure 18.- Continued.



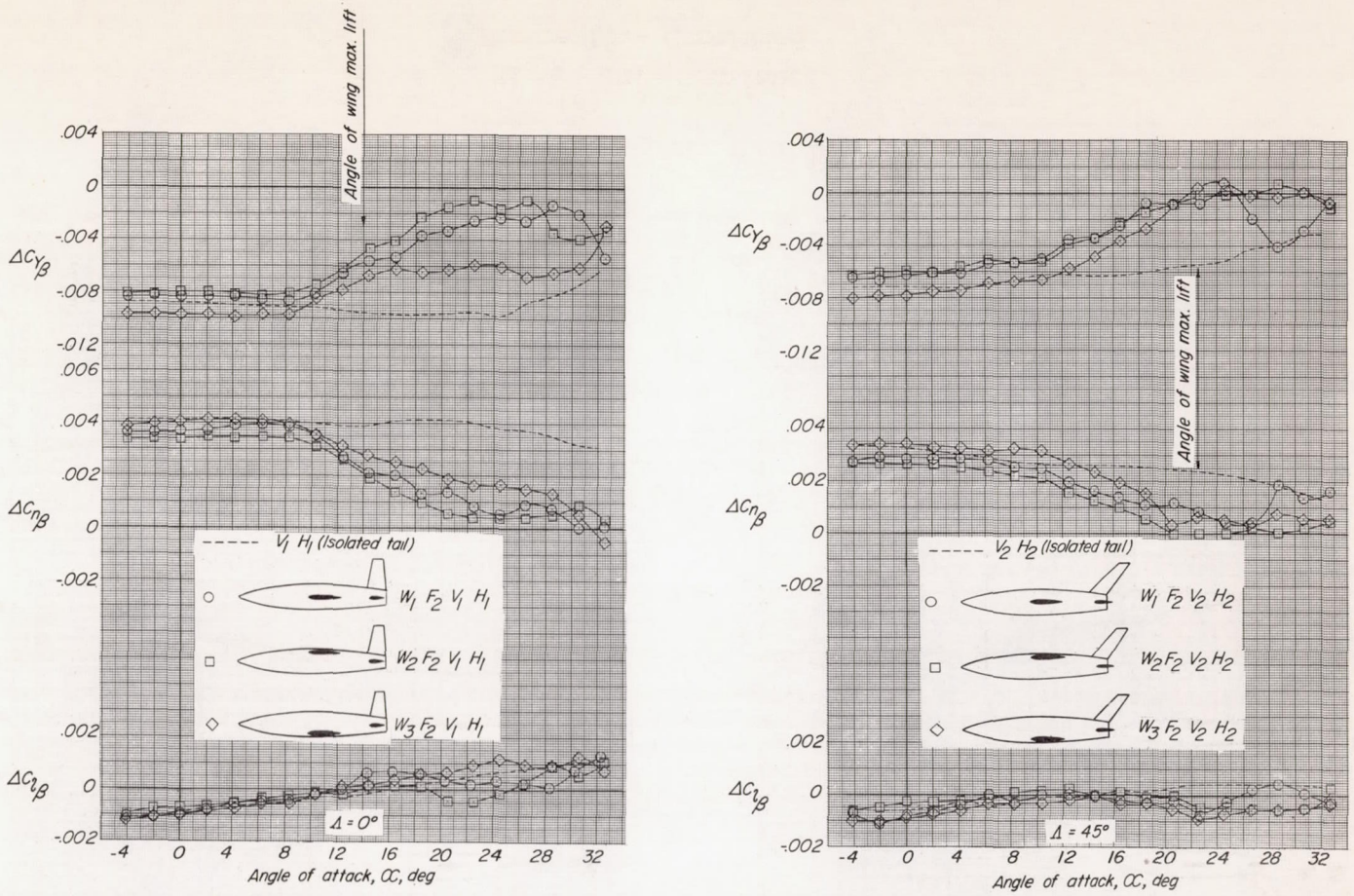
(c) $\alpha = 20°$.

Figure 18.- Continued.



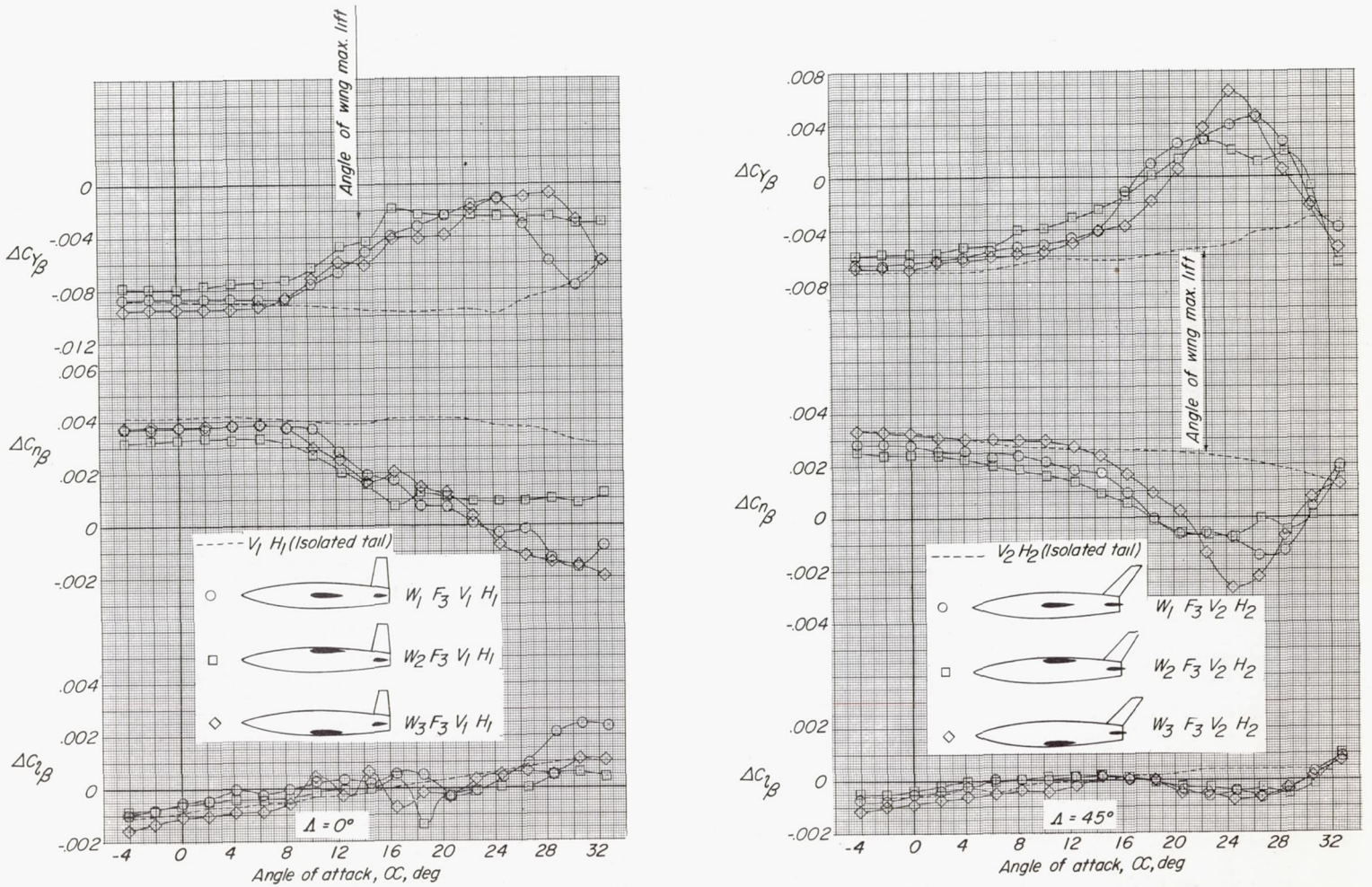
(d) $\alpha = 26°$.

Figure 18.- Concluded.



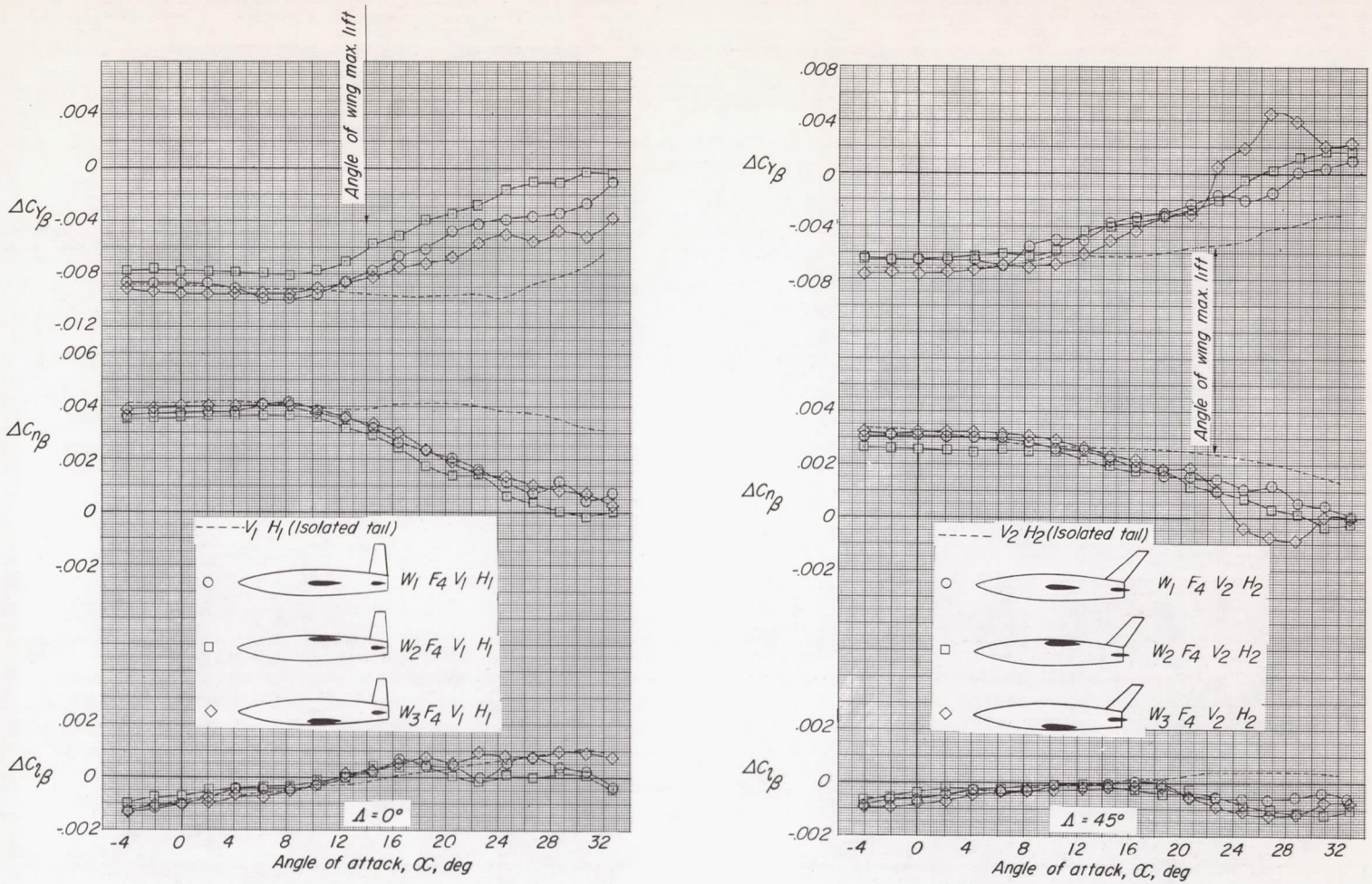
(a) Square fuselage, F_2.

Figure 19.- Effect of wing position on the tail contribution to C_{Y_β}, C_{n_β}, and C_{l_β} of several unswept and 45° sweptback wing-fuselage-tail configurations.



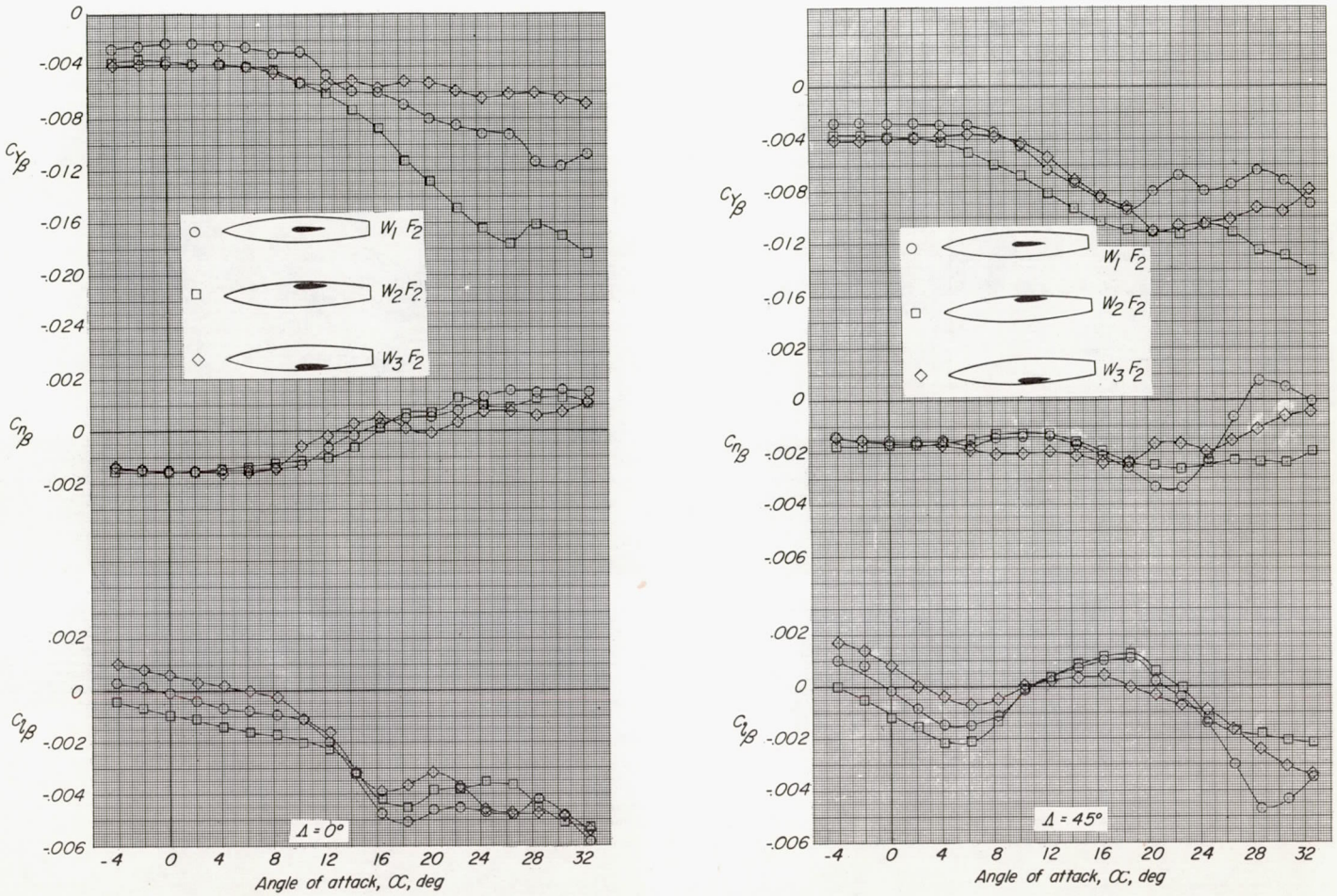
(b) Deep rectangular fuselage, F_3.

Figure 19.- Continued.



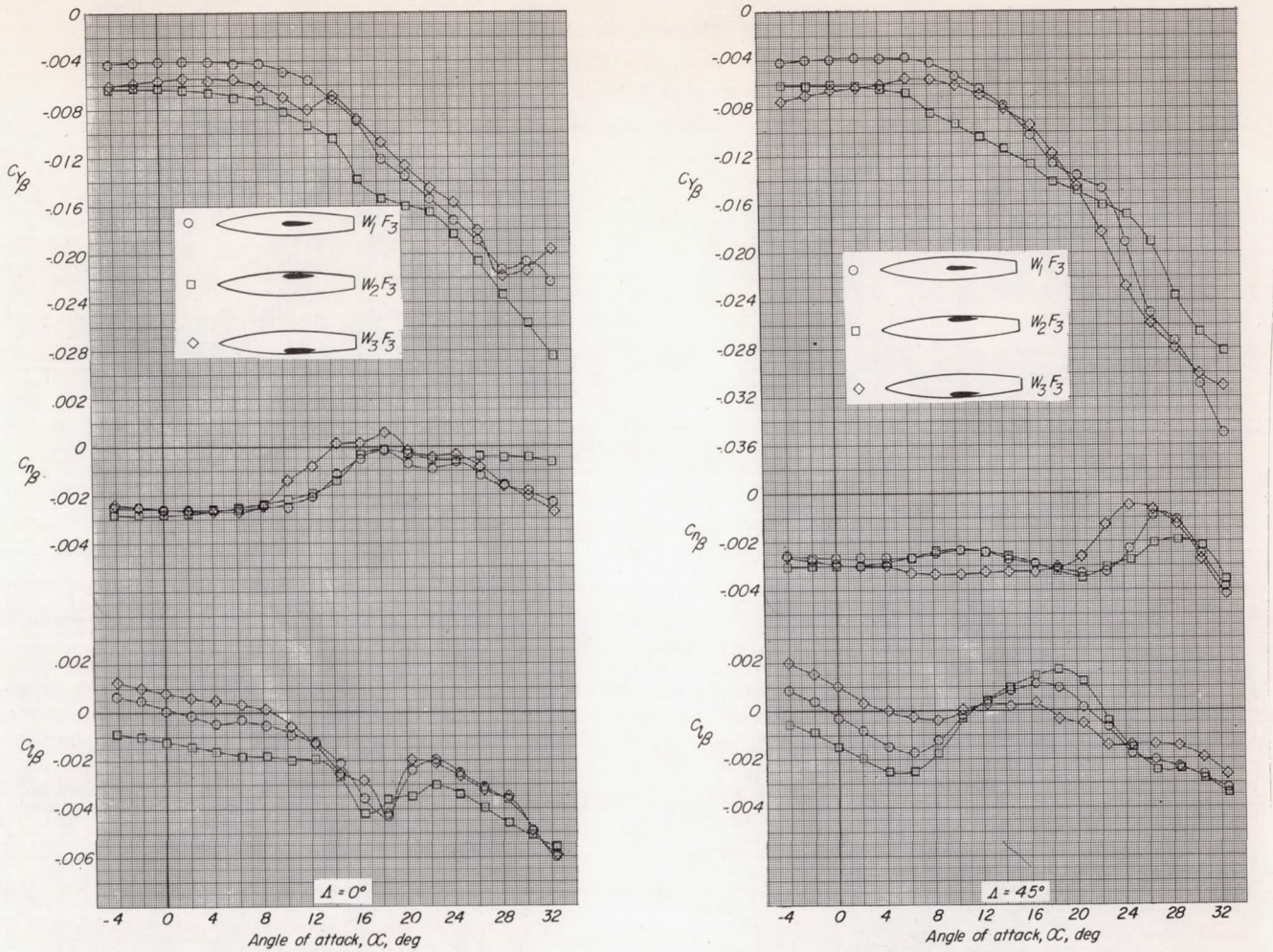
(c) Shallow rectangular fuselage, F_4.

Figure 19.- Concluded.



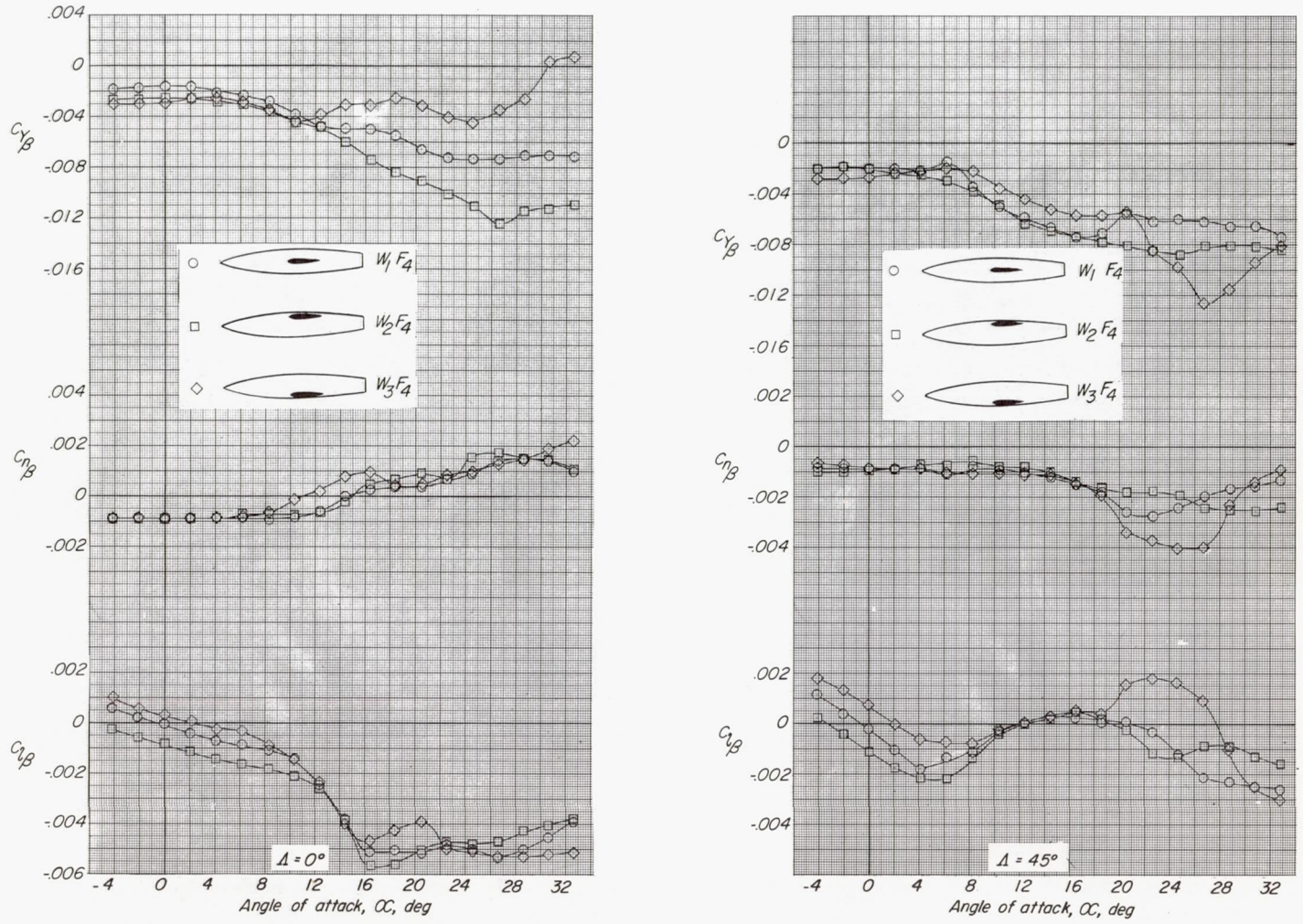
(a) Square fuselage, F_2.

Figure 20.- Effect of wing position on the static lateral stability characteristics of several unswept-wing and 45° sweptback-wing—fuselage configurations.



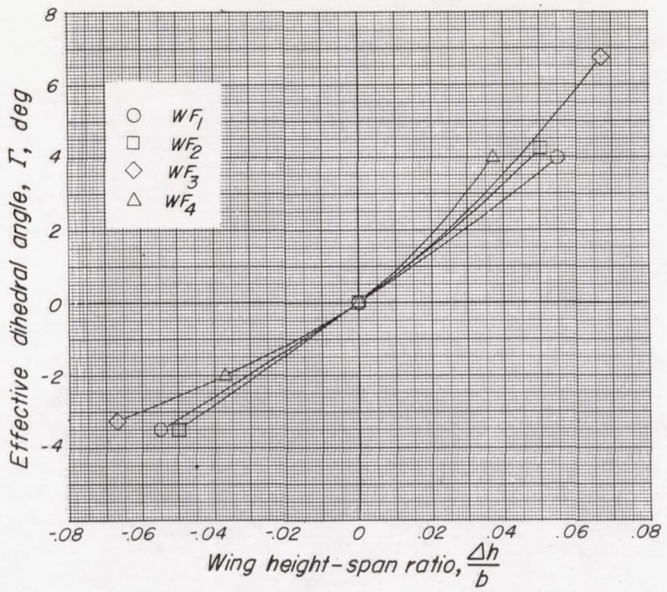
(b) Deep rectangular fuselage, F_3.

Figure 20.- Continued.

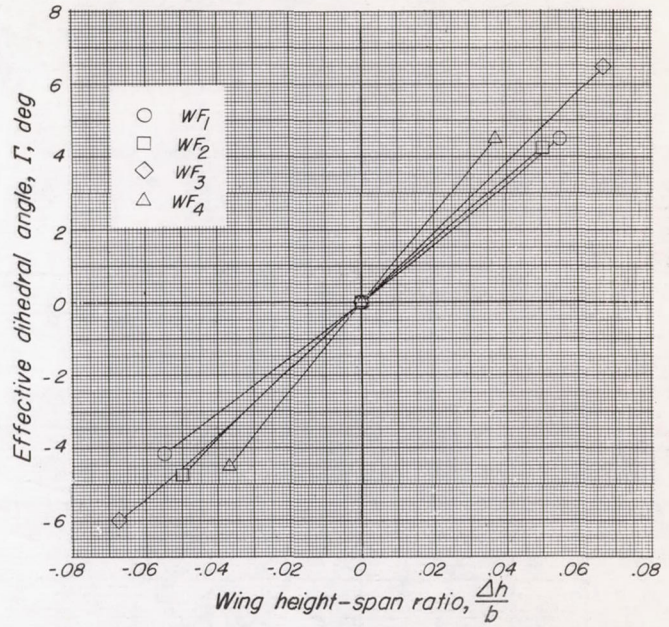


(c) Shallow rectangular fuselage, F_4.

Figure 20.- Concluded.



(a) $\Lambda = 0^\circ$.



(b) $\Lambda = 45^\circ$.

Figure 21.- Variation with wing height-span ratio of the effective dihedral angle due to wing-fuselage interference for several unswept-wing and 45° sweptback-wing—fuselage configurations. $\alpha = 0^\circ$.

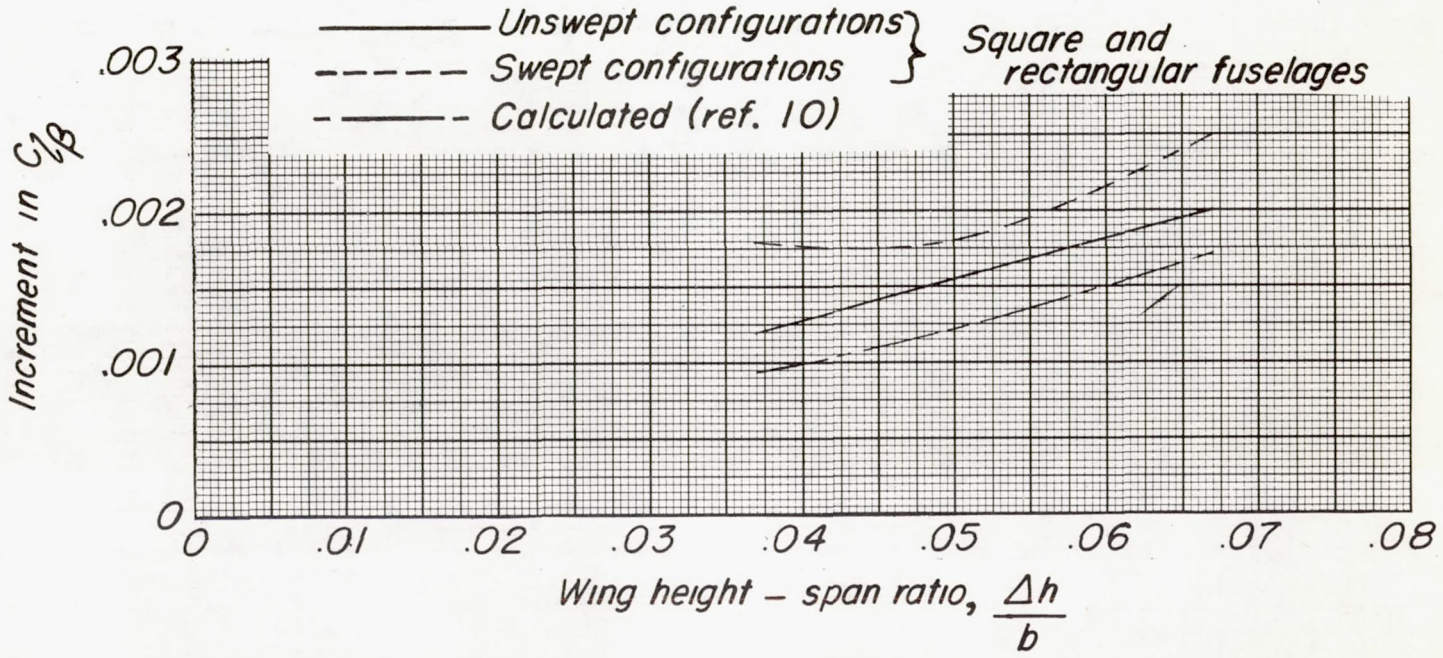
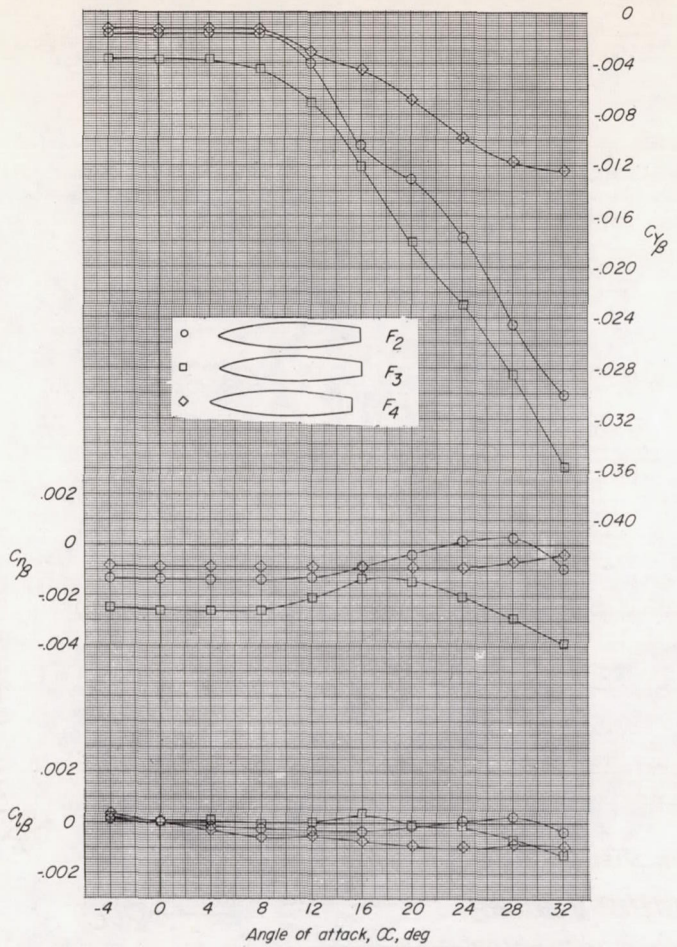
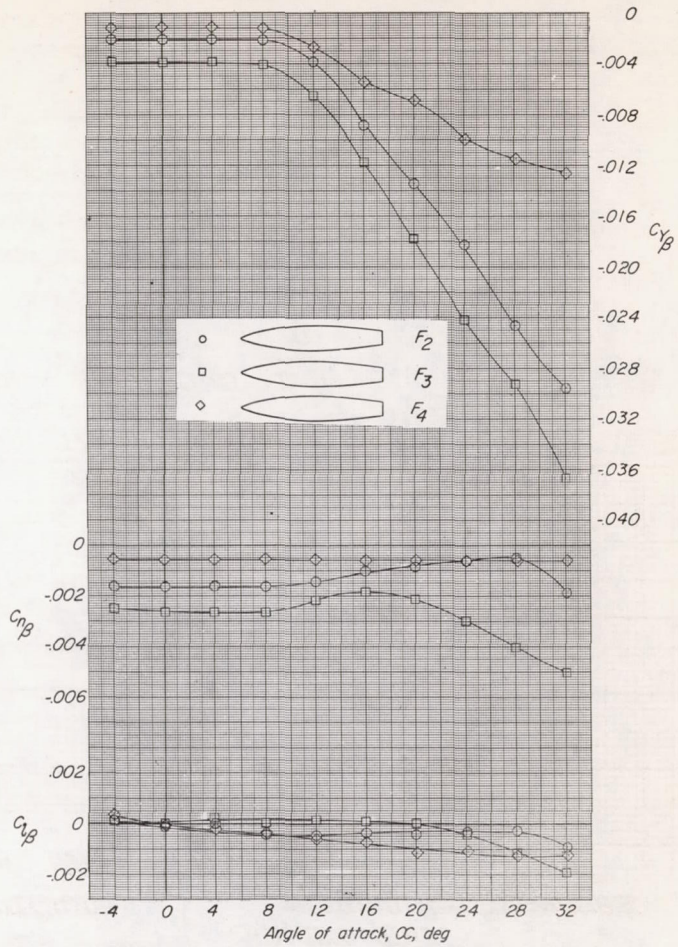


Figure 22.- Comparison of the measured and calculated variation of the total increment in C_{l_β} due to wing-fuselage interference for unswept-wing and 45° sweptback-wing—fuselage configurations caused by moving the wing from low to high position. $\alpha = 0°$.



(a) Center of moments for $\Lambda = 0^\circ$.



(b) Center of moments for $\Lambda = 45^\circ$.

Figure 23.- Static lateral stability characteristics of several fuselage configurations with different center-of-moment locations.

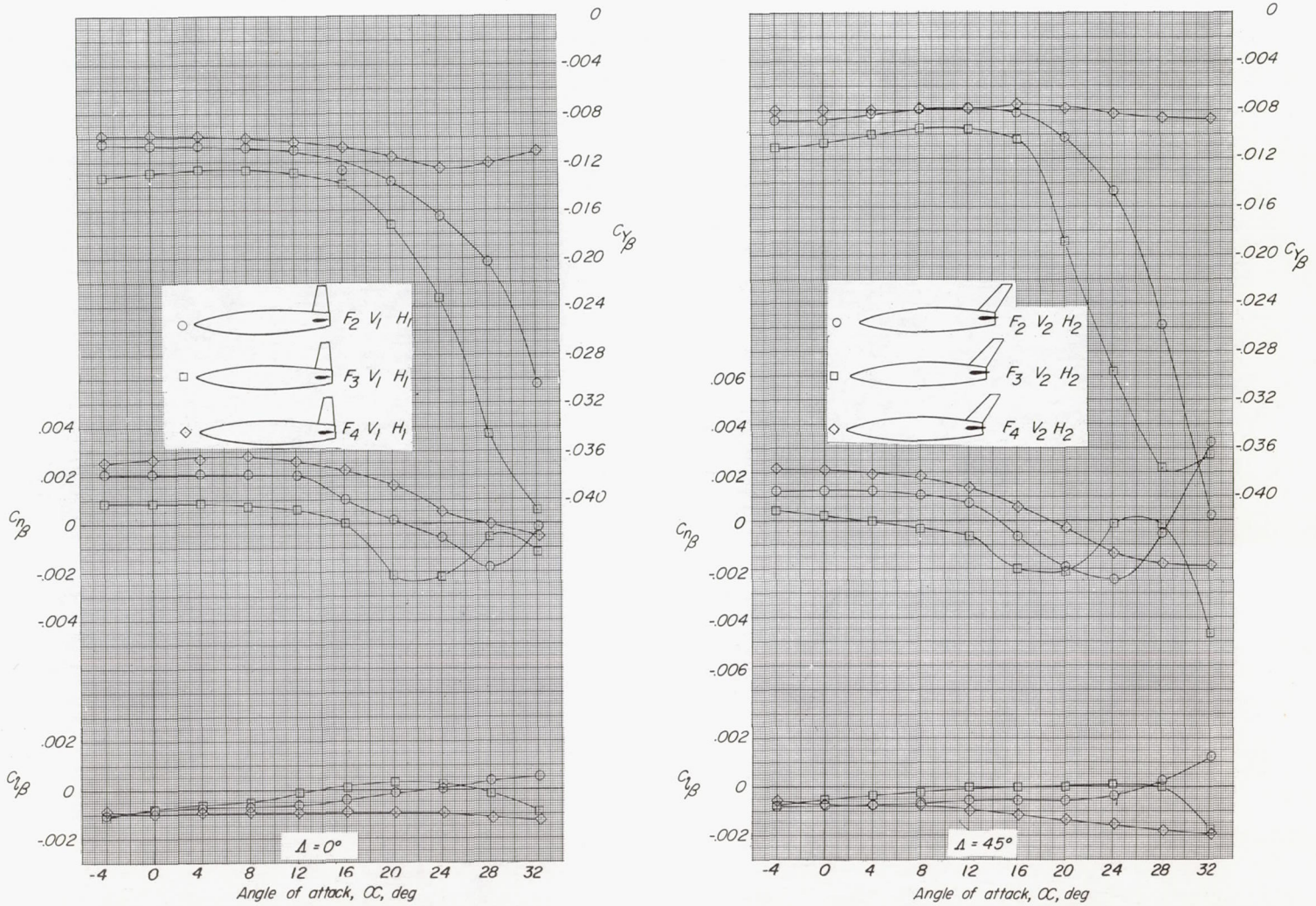


Figure 24.- Static lateral stability characteristics of several fuselages in combination with unswept- and 45° sweptback-tail configurations.

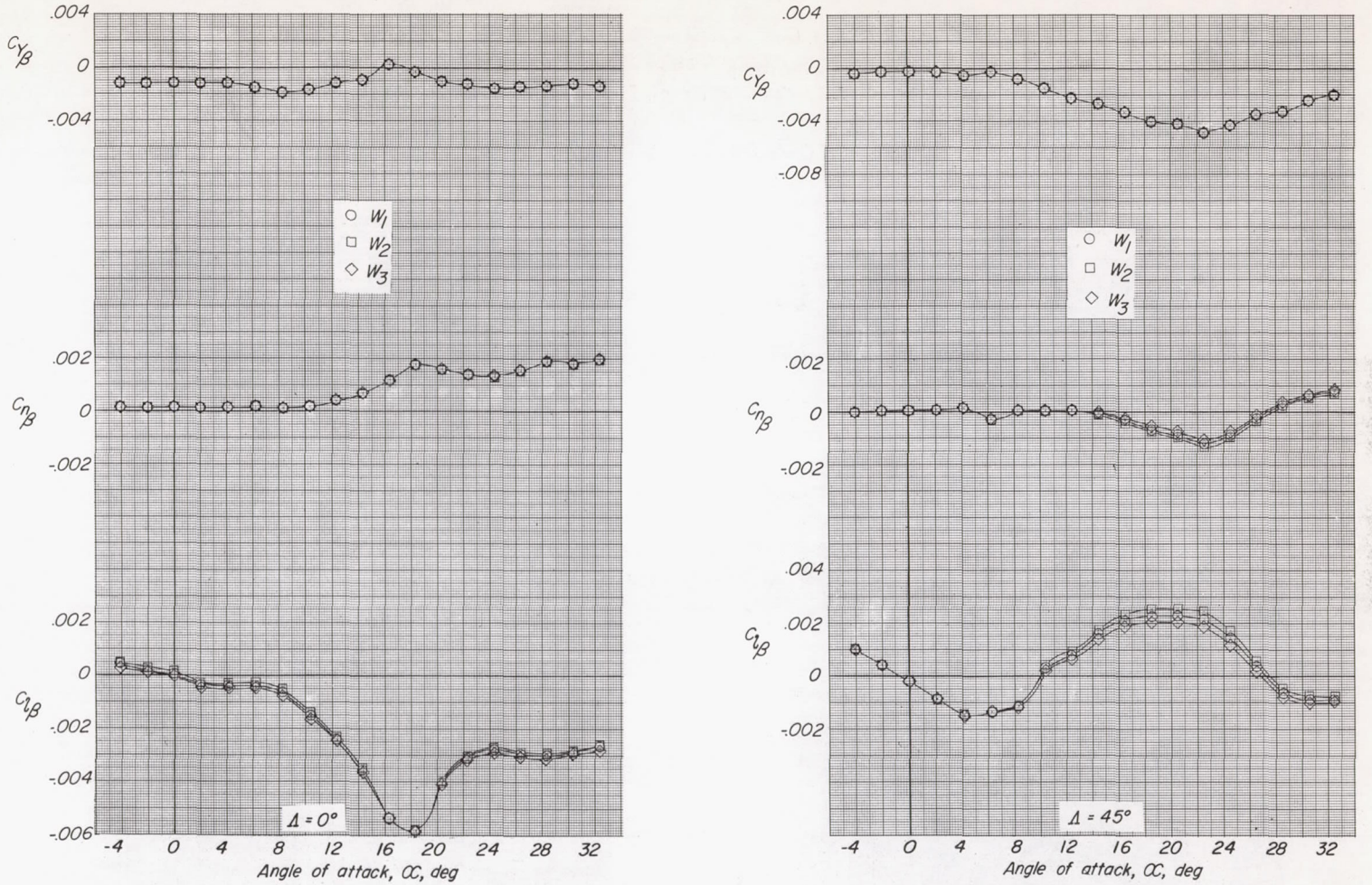
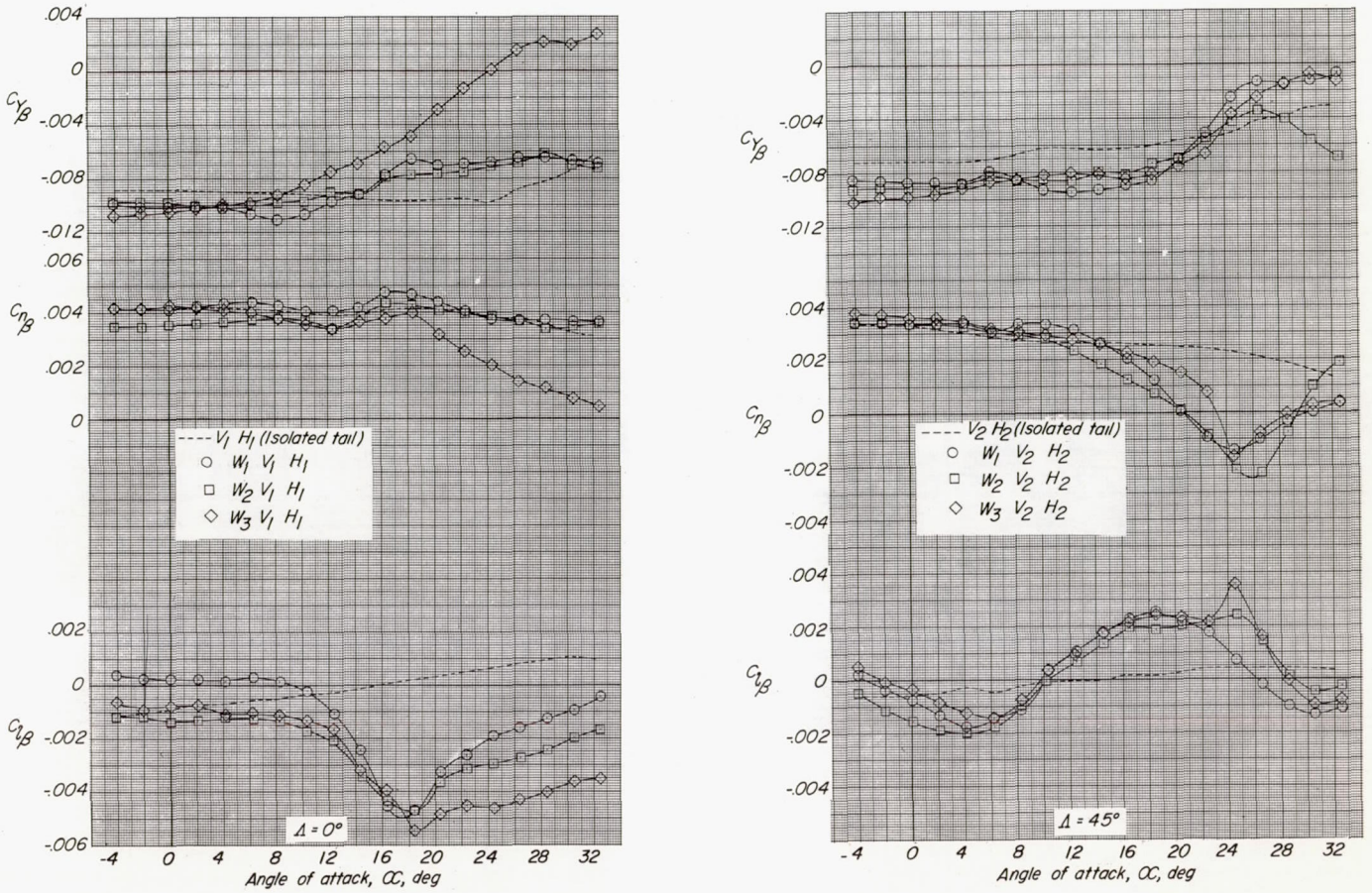
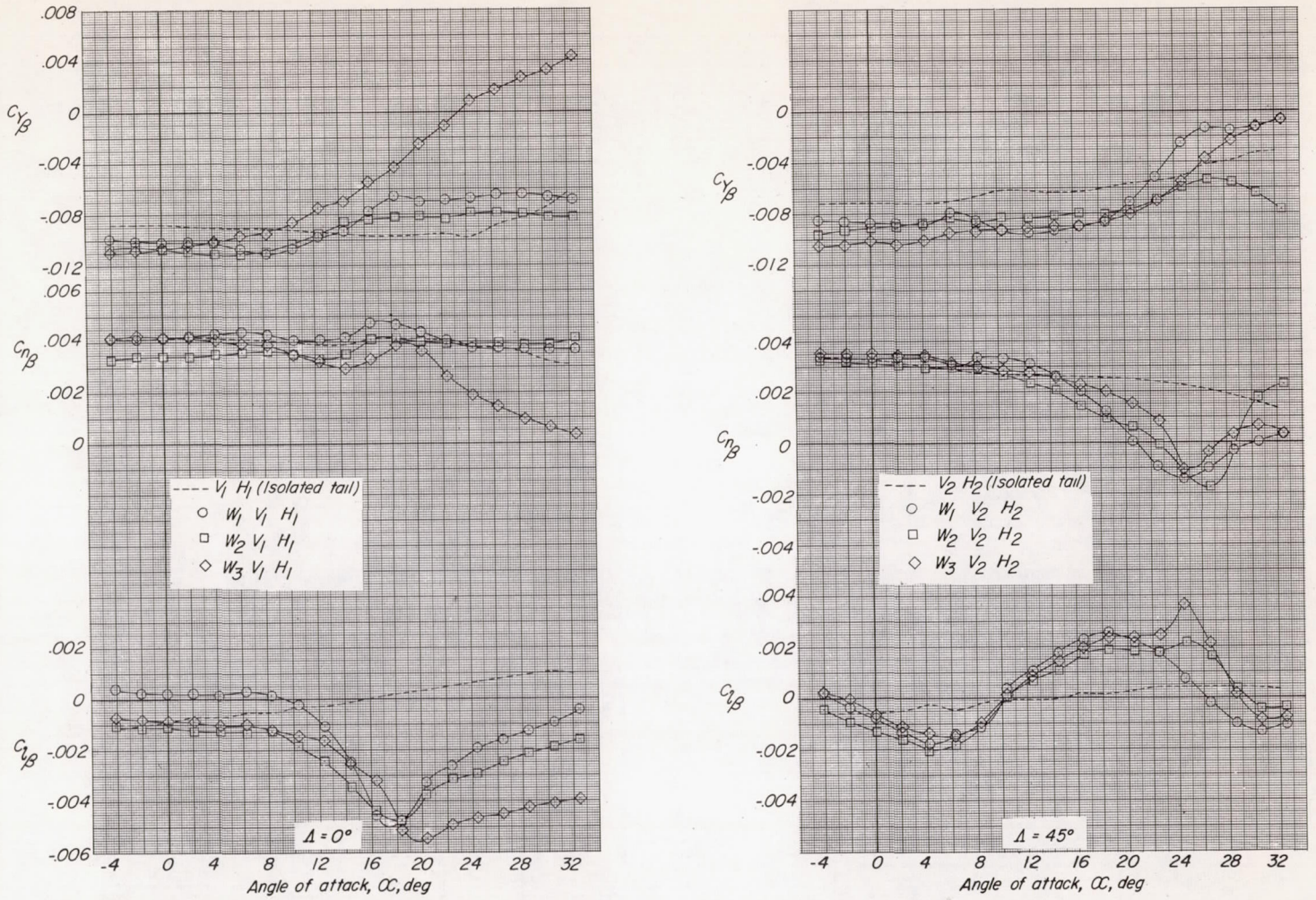


Figure 25.- Static lateral stability characteristics of the unswept and 45° sweptback wings. Wings located on balance center and at $\Delta h/b = 0.0672$ above and below balance center.



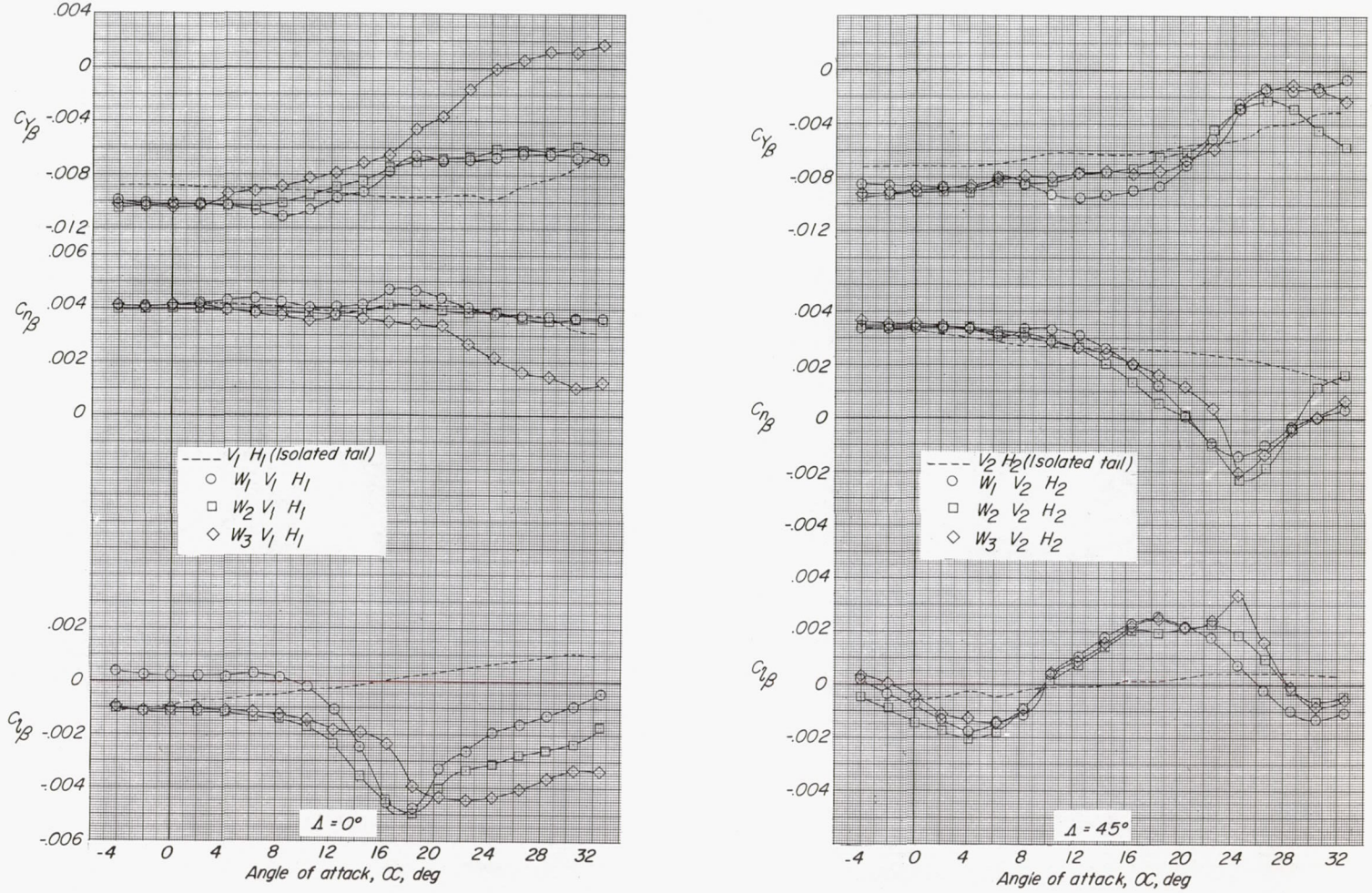
(a) $\Delta h/b = 0$ and ± 0.050.

Figure 26.- Static lateral stability characteristics of several unswept and 45° sweptback wing-tail and isolated-tail configurations. Wings located on balance center and at $\Delta h/b = 0.037$, 0.050, and 0.0672 above and below balance center.



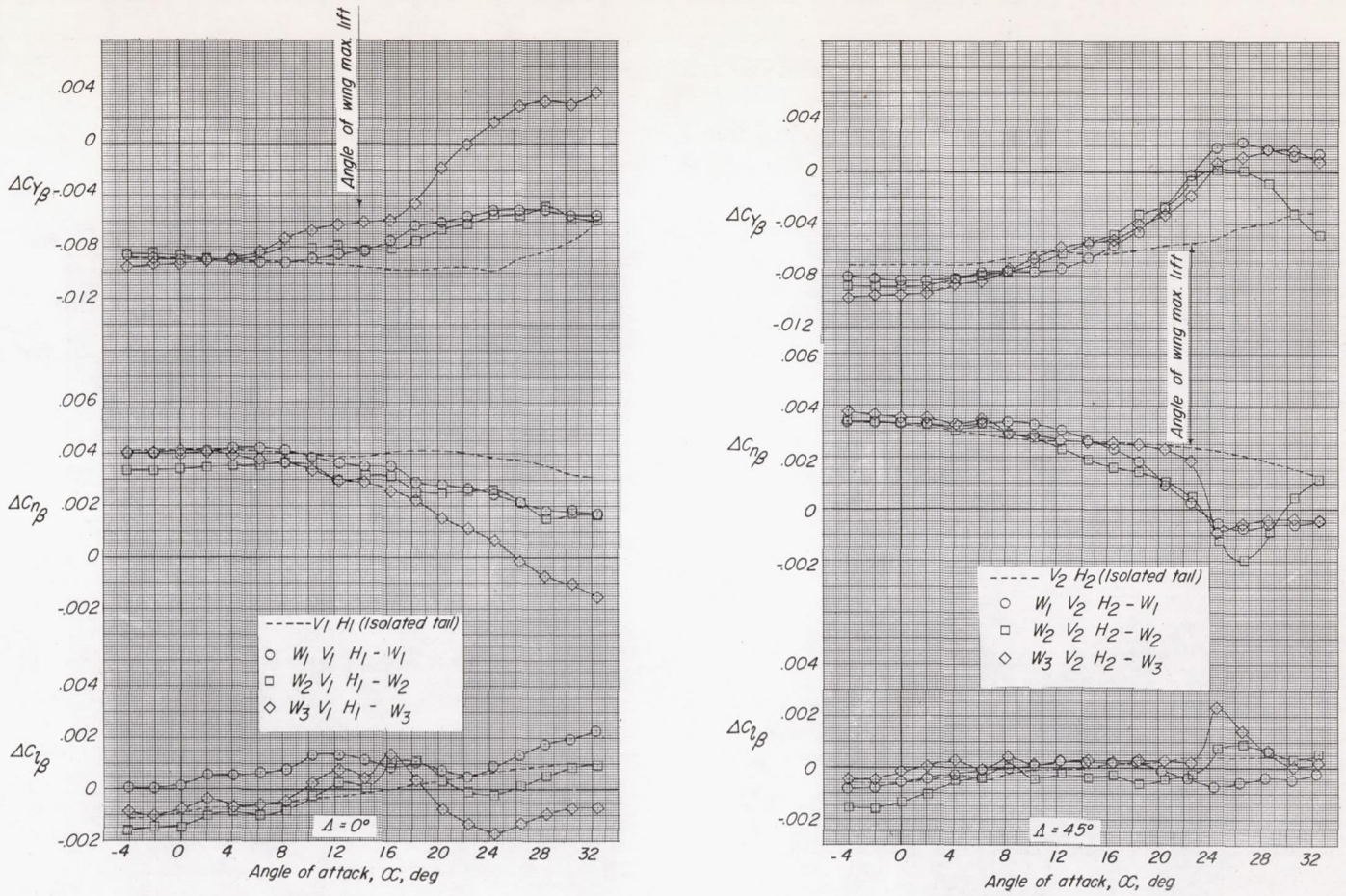
(b) $\Delta h/b = 0$ and ± 0.0672.

Figure 26.- Continued.



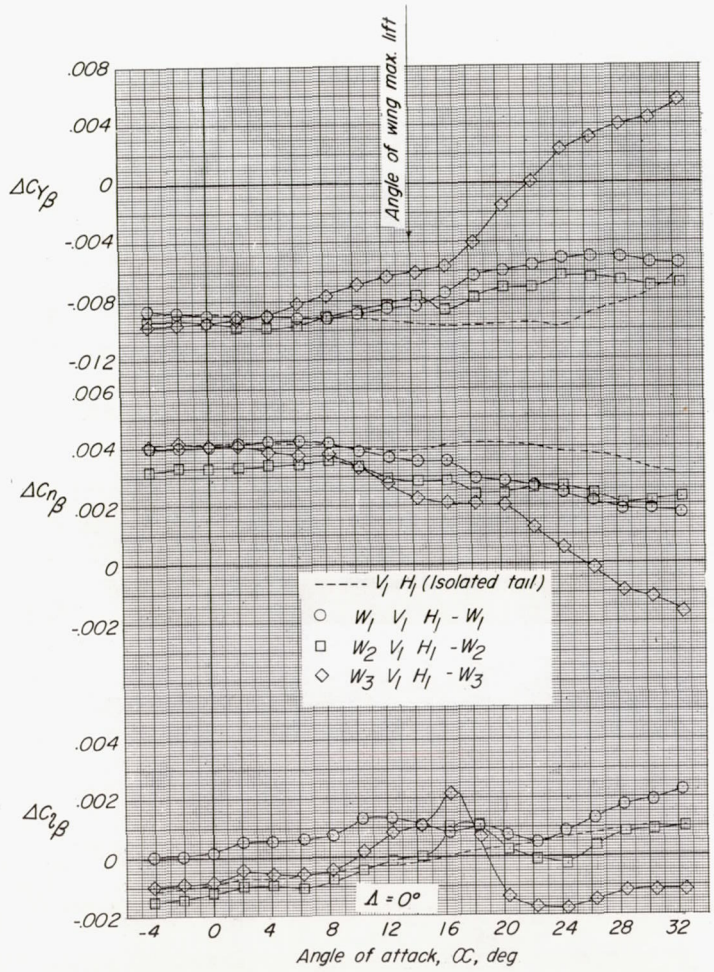
(c) $\Delta h/b = 0$ and ± 0.037.

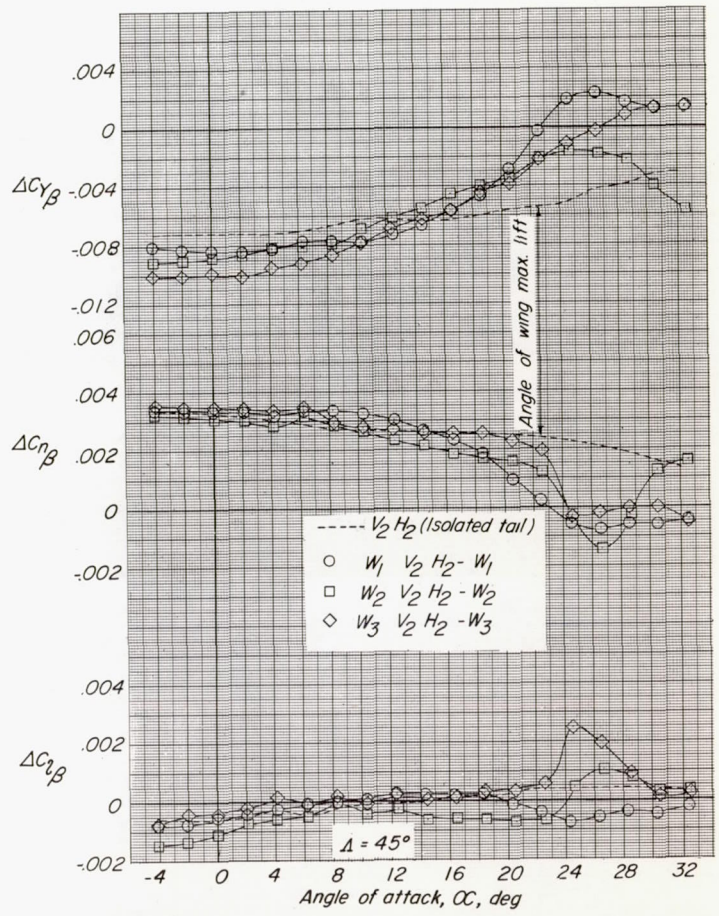
Figure 26.- Concluded.



(a) $\Delta h/b = 0$ and ± 0.050.

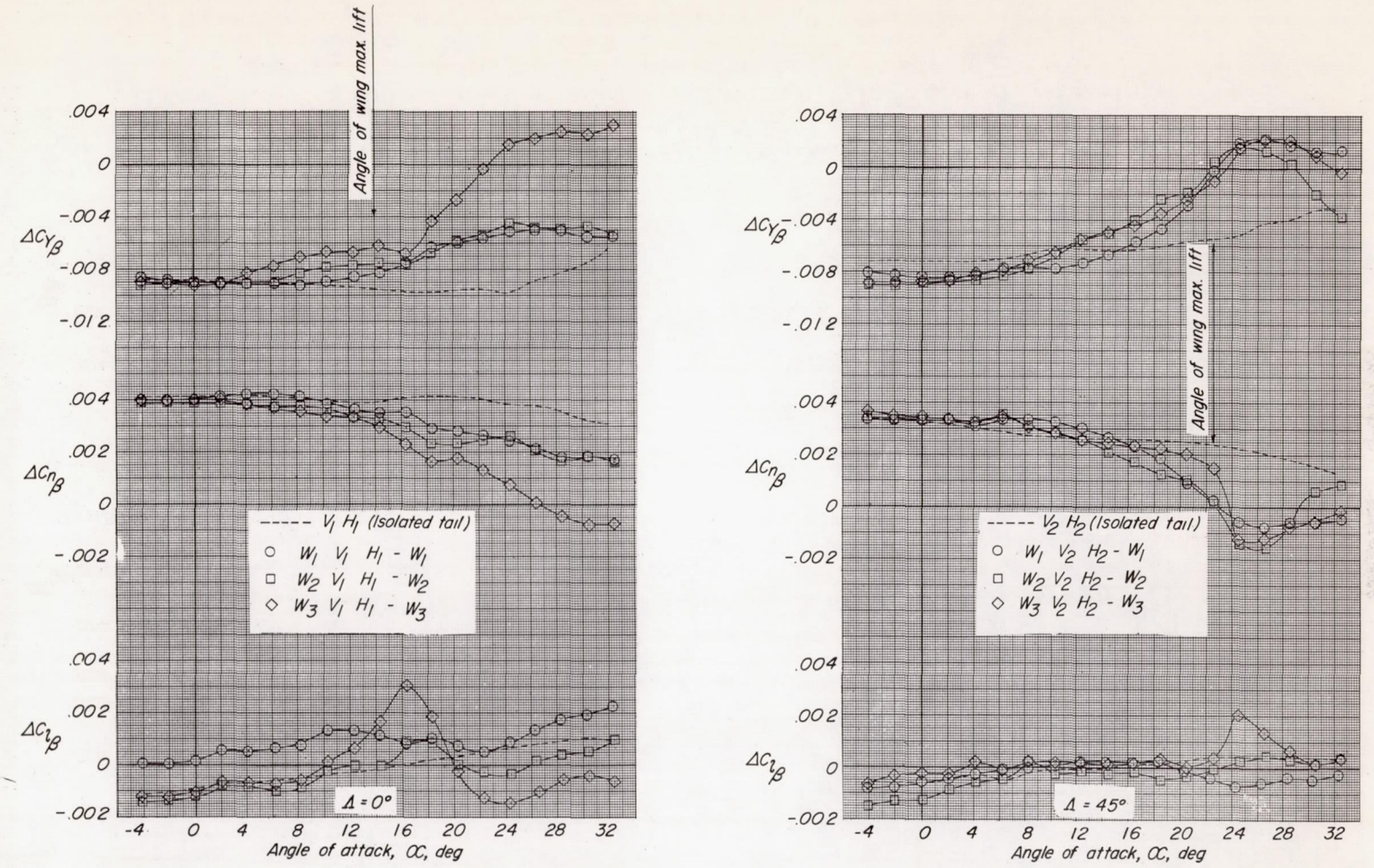
Figure 27.- Effect of wing position on the tail contribution to C_{Y_β}, C_{n_β}, and C_{l_β} of several unswept and 45° sweptback wing-tail configurations.





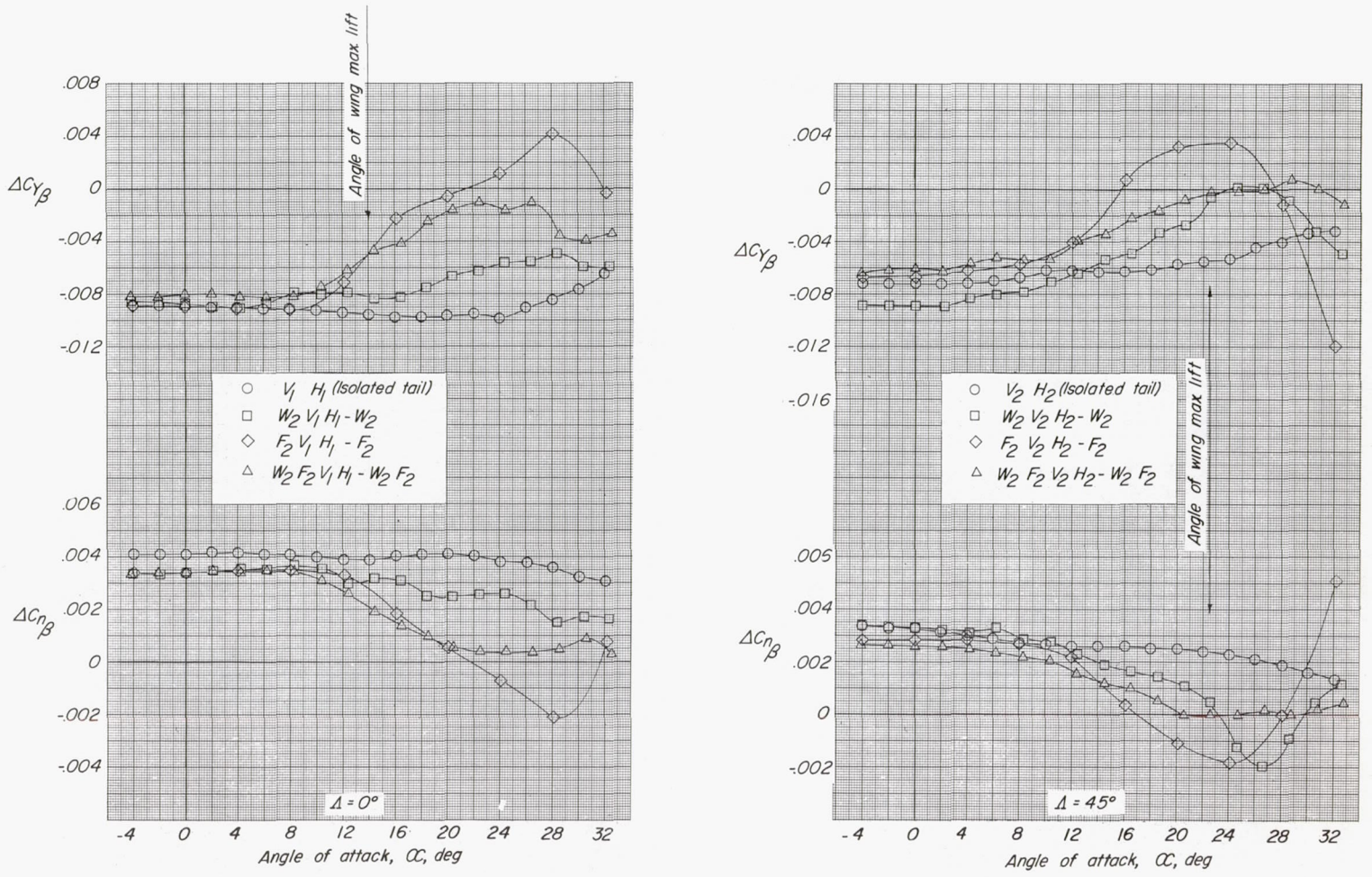
(b) $\Delta h/b = 0$ and ± 0.0672.

Figure 27.- Continued.



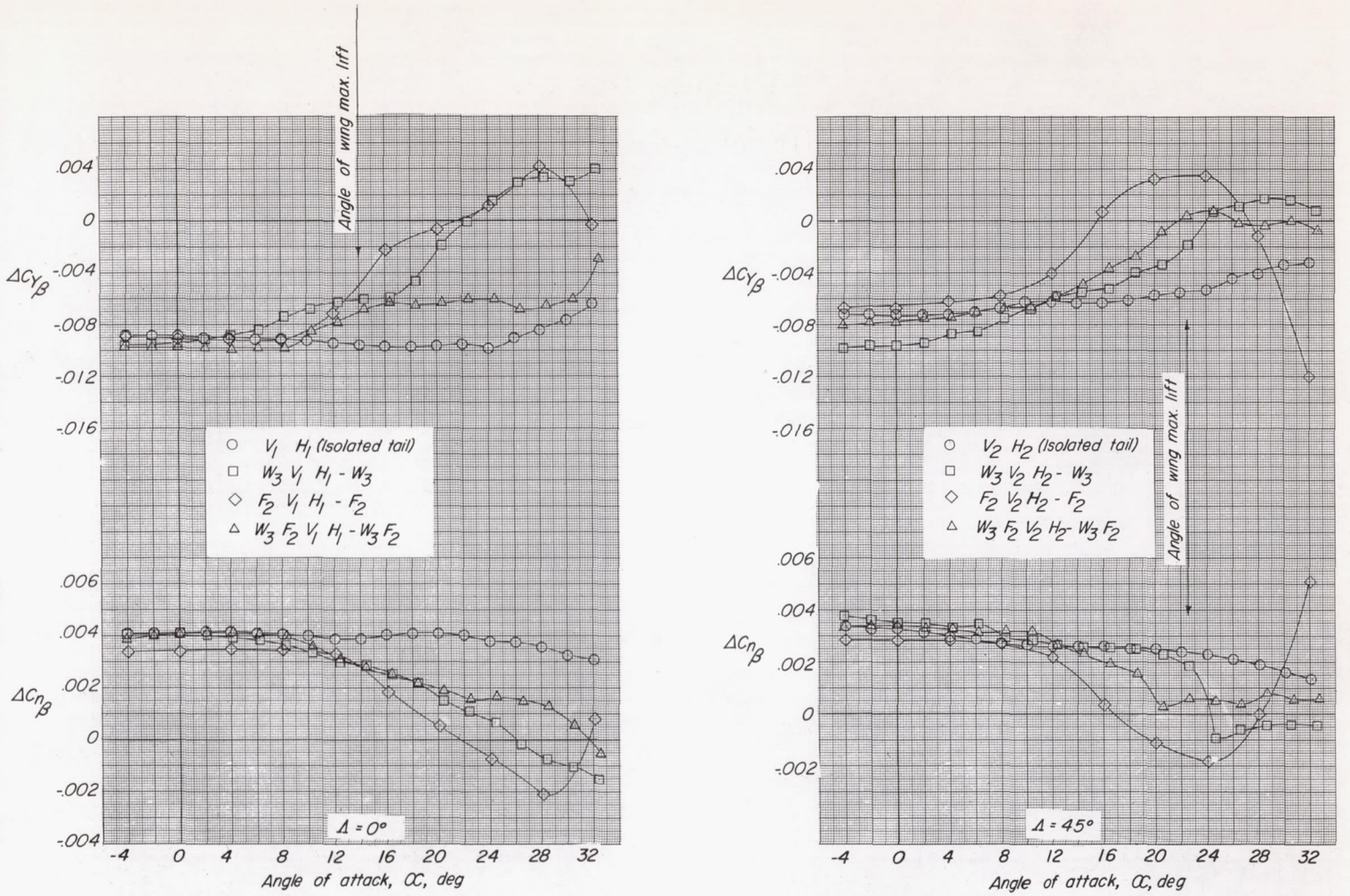
(c) $\Delta h/b = 0$ and ± 0.037.

Figure 27.- Concluded.



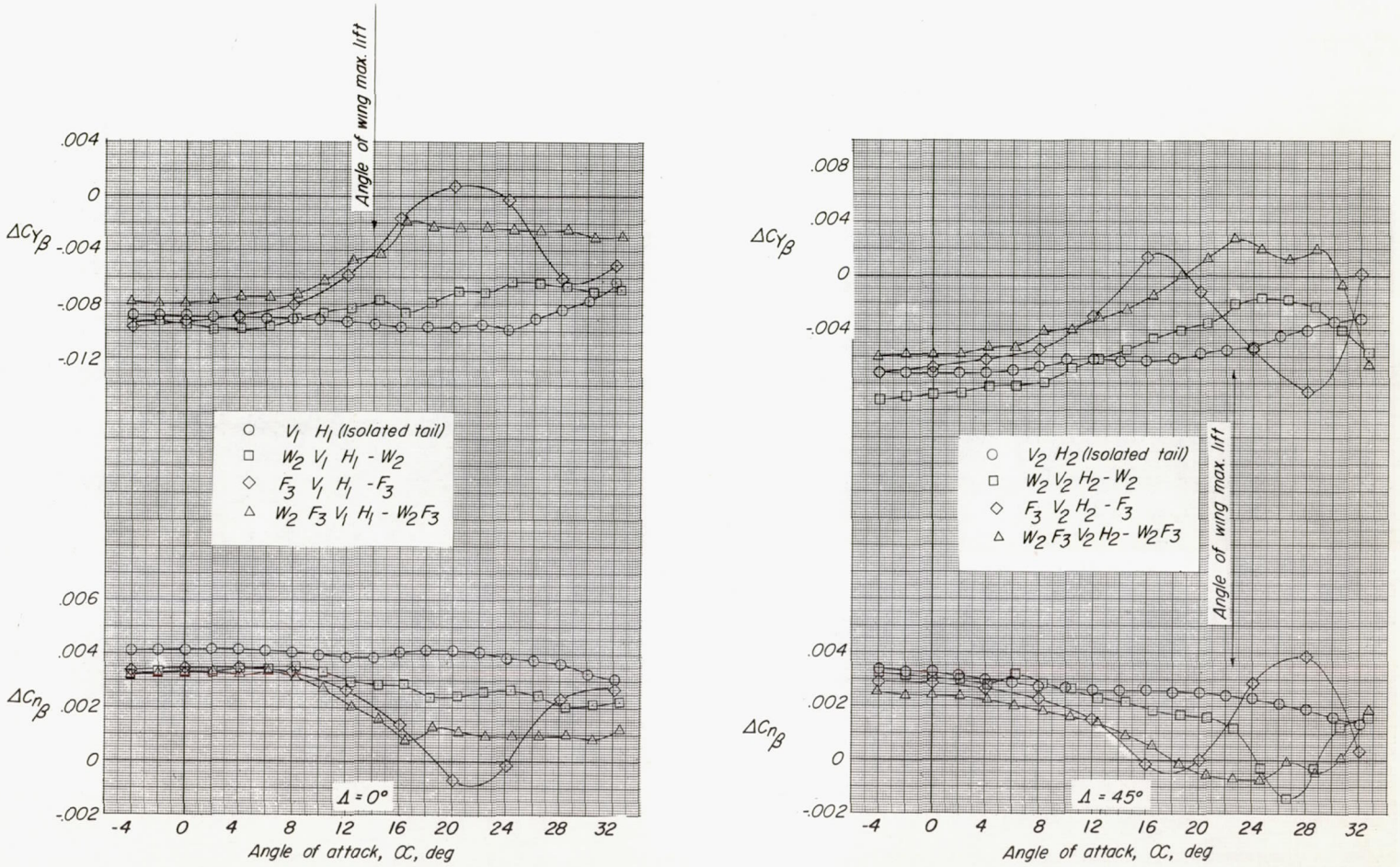
(a) Fuselage 2. Wing in high position.

Figure 28.- Comparison of the effect of fuselage, wing, and wing-fuselage combination on the tail contribution to C_{Y_β} and C_{n_β}.



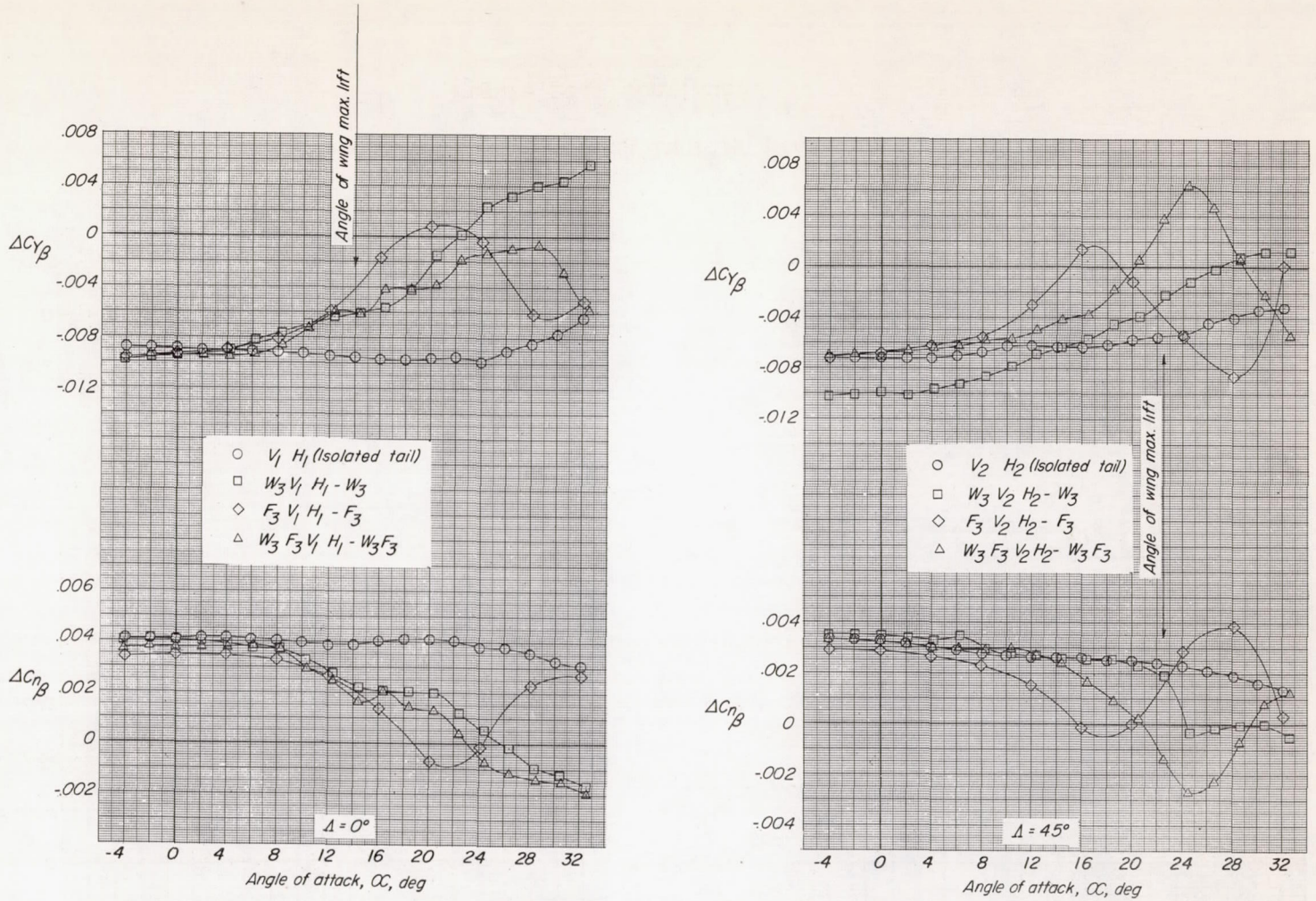
(b) Fuselage 2. Wing in low position.

Figure 28.- Continued.



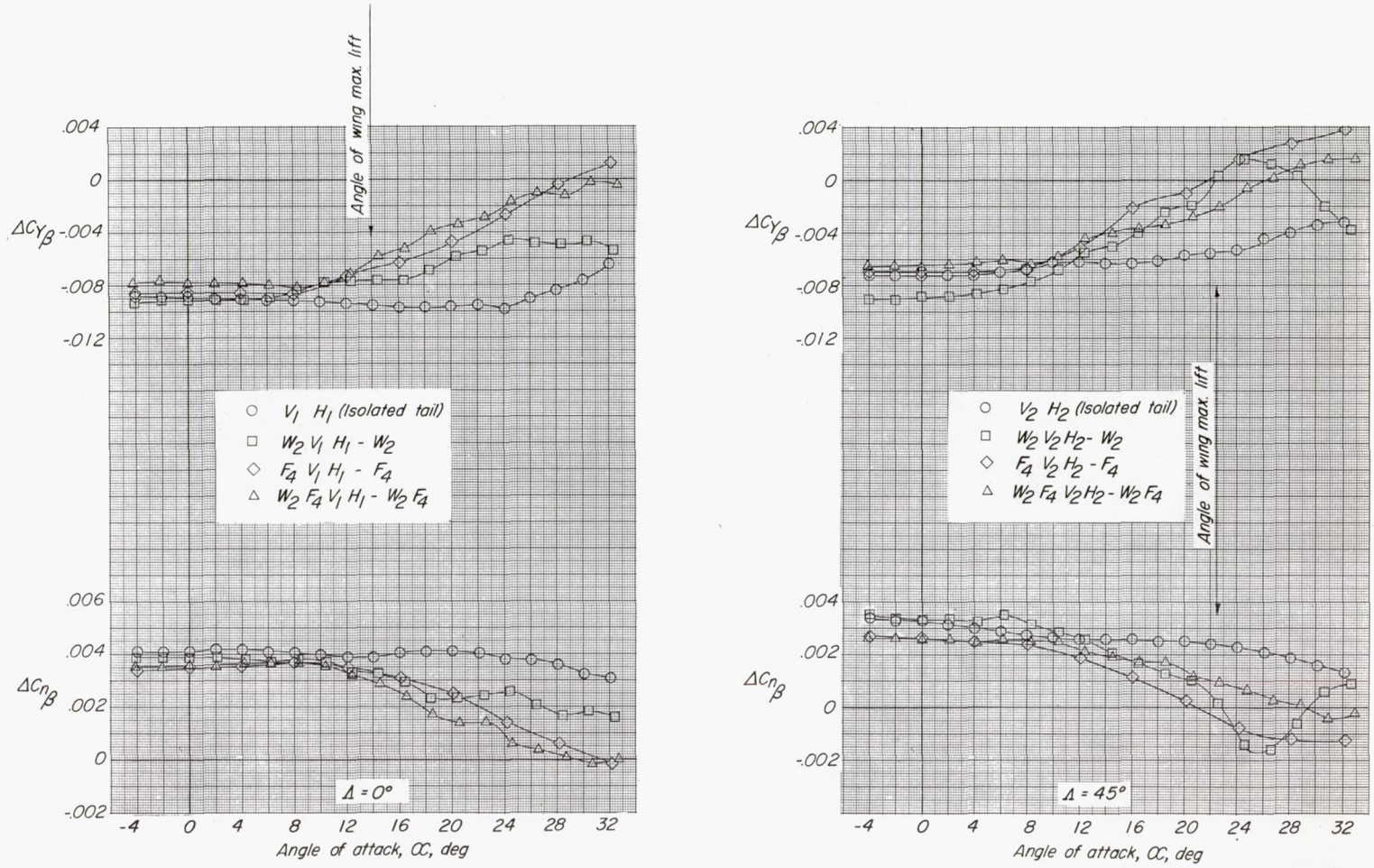
(c) Fuselage 3. Wing in high position.

Figure 28.- Continued.



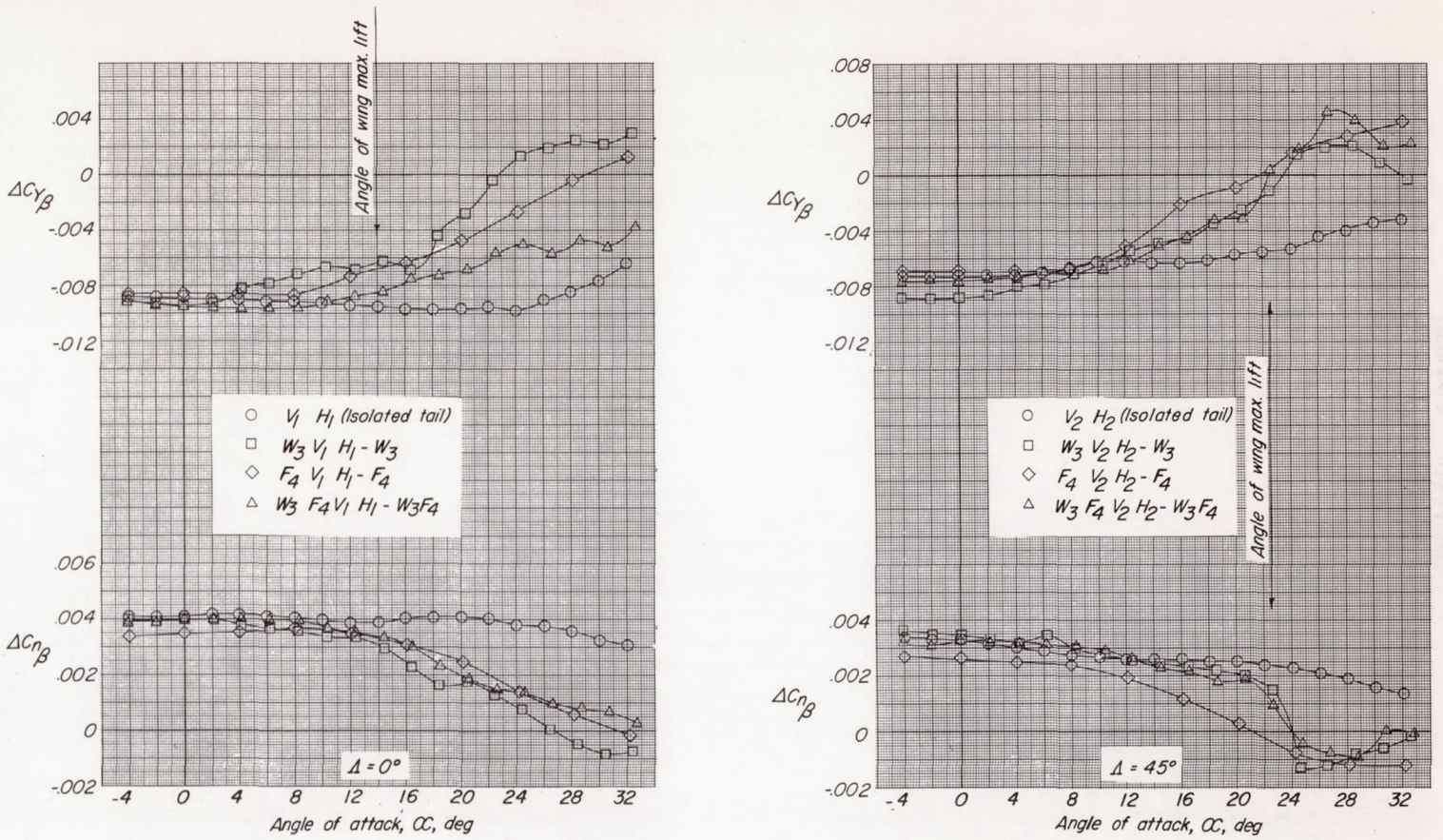
(d) Fuselage 3. Wing in low position.

Figure 28.- Continued.



(e) Fuselage 4. Wing in high position.

Figure 28.- Continued.



(f) Fuselage 4. Wing in low position.

Figure 28.- Concluded.